


1-1-2018

# Engineering Hyaluronic Acid Carbon Nanotube Nanofibers: A Peripheral Nerve Interface To Electrically Stimulate Regeneration

Elisabeth M. Steel  
*Wayne State University,*

Follow this and additional works at: [https://digitalcommons.wayne.edu/oa\\_dissertations](https://digitalcommons.wayne.edu/oa_dissertations)

 Part of the [Biomechanics Commons](#), [Biomedical Engineering and Bioengineering Commons](#), and the [Materials Science and Engineering Commons](#)

---

## Recommended Citation

Steel, Elisabeth M., "Engineering Hyaluronic Acid Carbon Nanotube Nanofibers: A Peripheral Nerve Interface To Electrically Stimulate Regeneration" (2018). *Wayne State University Dissertations*. 2074.  
[https://digitalcommons.wayne.edu/oa\\_dissertations/2074](https://digitalcommons.wayne.edu/oa_dissertations/2074)

This Open Access Embargo is brought to you for free and open access by DigitalCommons@WayneState. It has been accepted for inclusion in Wayne State University Dissertations by an authorized administrator of DigitalCommons@WayneState.

**ENGINEERING HYALURONIC ACID-CARBON NANOTUBE NANOFIBERS:  
A PERIPHERAL NERVE INTERFACE TO ELECTRICALLY STIMULATE REGENERATION**

by

**ELISABETH MARIE STEEL**

**DISSERTATION**

Submitted to the Graduate School

of Wayne State University,

Detroit, Michigan

in partial fulfillment of the requirements

for the degree of

DOCTOR OF PHILOSOPHY

2018

MAJOR: BIOMEDICAL ENGINEERING

Approved By:

---

Harini G. Sundararaghavan, Ph.D. Date

---

Howard W.T. Matthew, Ph.D. Date

---

Wei-Ping Ren, Ph.D. Date

---

Mark Ming-Cheng Cheng, Ph.D. Date

**© COPYRIGHT BY  
ELISABETH MARIE STEEL  
2018  
All Rights Reserved**

**DEDICATION**

*To Ian, Gavin, and Kevin:  
Live your way into the answers in your hearts,  
as you have been the answers in mine.*

*The Circle of Mercy is Timeless*

## ACKNOWLEDGEMENTS

**Dr. Harini G. Sundararaghavan's impact is unparalleled**, as exemplified by her patient discernment to ask the frustratingly simple question. "Beth, you are running yourself in circles. Just start at a low amplitude. You know the literature, pick a reasonable voltage, repeat the experiment at least 4 times, step up from there, repeat, step, repeat." I owe a deep gratitude for my advisor's character, for her willingness to manage my ego by ignoring it, and her gentle, firm resolve to teach me focus by not fueling my intensity.

**Thank you to Dr. Wei-Ping Ren** for being a mainstay, my earliest WSU BME advocate when I was still a MS student and working at HFHS. Your encouragement to join the Society of Biomaterials and submit my work to World Biomaterials Congress 2016 was a game changer. Your attention to detail in the context of the bigger picture gives me the light I needed for my path.

**Thank you to Dr. Howard Matthew** for embracing my rebellious nature with a smile, my love for family and friends; equally important is your dismissal of poorly chosen boundary constraints and ability to distinguish the diamonds from the rough in both data and life.

**Thank you to Dr. Mark Ming-Cheng Cheng.** I was reticent to accept your open-door policy because I too am that person quick to drop a sandwich for the opportunity to run to the lab and troubleshoot on a dime. Thank you for your genuine capacity to encourage hard work by enabling access to the necessary tools.

**Thank you to Tonya Jo Whitehead** for teaching me the art of following directions with a foulard flair.

**Thank you to Melissa Renee Wrobel** for teaching me to relent to love to endure the vastness.

**Thank you to Lizzy Mays** for rolling a druid, skilled in engineering and improv.

**Thank you to Jean-Yves Azar and Mallak Taleb**, you let me Avenge with passion, teach by doing, and be agile by asking questions so that you could act with purpose.

Here we are, finally. This surreal M.C. Escher demonstration of a cell's response to its microenvironment to permit growth to its full potential, juxtaposed to a woman hellbent on finding the mathematical underpinnings for why she responds so strongly to the energy of her environment. That life's mystery is not nature v. nurture, it's not *versus* anything, it's a state of being. It's feeling accepted and trusted to be.

It takes an environment like Wayne State University, and the mish mosh wonderfully diverse existence that nurtures the hustle and soul that thrives in Detroit. Detroit Music and people are instrumental to my transformation from a pinball to a wizard.

~~~

**Thank you to Allen P. Liu**, University of Michigan, your scientific training and example led me to refine my analytical and relationship building skills, which resulted in flipping the sign on my correlation coefficient relating success to hard work.

**Thank you to Clifford M. Les** for teaching me how to hop clods without becoming a clod hopper. I might not always get it right the first time, but thank you for teaching me the difference between right and first. Thank you for teaching me statistics and Latin, reinforcing experiential learning, and most of all, teaching me patience through Rainer Maria Rilke. By extension, thank you for bringing me to HFHS where I made lifelong relationships with some wonderful people.

**Thank you to the University of Toledo**, UT College of Engineering and UTEC, the Department of Bioengineering, CCUP, and Theta Tau for shining true gold and blue.

**Thank you to our family and friends in Michigan** who have made this geographical place resonate with the frequency of my heart, spirit, and mind.

**Thank you to Alice J. Michels**, your unconditional love emboldens my vivacity for life. Your guidance and insistence on being a whole person inspires me to work to be a whole person.

**Thank you to Brittany Michels** for being the sunshine even on the darkest of Easter mornings and the downpour from miles 19-24. Thank you for guiding us to push our limits and toe the line with joy.

**Thank you to Fina** for being a paladin and bard by nature, acting with truth and inspired by love, committing to act with purpose, and empowering the soul by merging the heart and mind with music.

**Thank you to Joe Gampfer** for being the rock in whitewater rapids. You have shown me what a real Purdue University engineer looks like, how a real baller acts, and the meaning of a family blessing.

**Thank you to the Bross Family** for nurturing a family that never quits, never accepts the status quo, and leads with courage, thoughtfulness, and a quick wit.

**Thank you to the Michels Family** for teaching me to balance joy and grit, to accept grief and pain with love, and that Family is First no matter what.

**Thank you to the Steel and Volz families** for embracing me with love and imbuing me with courage.

**Thank you to my MMHS and TSB Circles** for exhibiting a charisma of social justice, equality, hospitality, compassion, and Trust bounded only by game theory. My friends look out for me on a 5-year plan.

**Thank you to Kevin Steel**, who has walked beside me, behind me, and ahead of me on this journey. You are the catalyst for this incredible experiment that is our life. You empowered me to reconcile my past, focus on a future of my choosing, while grounding me in the present.

Kevin Thomas, you are the ultimate ranger, my *Strijder*—  
my warrior, my defender activist, my Heart of Hearts.

You are the servant leader, the sounder of the *oliphant* when celebration is at hand, and  
the salve to a weary soul at waypoints along the journey.

Woe to anyone who comes in conflict with any of those.

Ian Michael, my inspiration and my guardian,  
Gavin Everett, my white hawk and knight that bounds over mountains,  
experiencing the beauty and wonder of the world through your eyes  
has brought my focus to where my feet alight on my path.

Together,  
our passage will be safe, in darkness and in light.  
Goodness and kindness follow in our wake,  
As our intents are grounded in love,  
nurtured with wholesome food,  
our path will continue beside still water

## TABLE OF CONTENTS

|                                                                                                                                                                |     |
|----------------------------------------------------------------------------------------------------------------------------------------------------------------|-----|
| DEDICATION .....                                                                                                                                               | ii  |
| ACKNOWLEDGEMENTS.....                                                                                                                                          | iii |
| LIST OF TABLES.....                                                                                                                                            | x   |
| LIST OF FIGURES .....                                                                                                                                          | xi  |
| Chapter 1 : An Electroactive Materials-Based Repair Strategy for Neural Tissue Engineering with Hyaluronic Acid-Carbon Nanotube Nanofibers.....                | 1   |
| Problem and Significance .....                                                                                                                                 | 1   |
| Nervous system response to injury.....                                                                                                                         | 2   |
| Current Treatments and Shortcomings.....                                                                                                                       | 4   |
| Tissue Engineering and Regenerative Medicine for PNI .....                                                                                                     | 5   |
| Conductive Biomaterials.....                                                                                                                                   | 7   |
| Examples from the Literature.....                                                                                                                              | 7   |
| Carbon Nanotubes.....                                                                                                                                          | 7   |
| Electrical Stimulation and CNTs for tissue regeneration .....                                                                                                  | 8   |
| Material Design Constraints .....                                                                                                                              | 10  |
| Predicted Challenges .....                                                                                                                                     | 12  |
| Proposed Solution .....                                                                                                                                        | 13  |
| Rationale, Hypothesis, and Specific Aims.....                                                                                                                  | 17  |
| Rationale.....                                                                                                                                                 | 17  |
| Central Hypothesis .....                                                                                                                                       | 17  |
| Specific Aims and Hypotheses.....                                                                                                                              | 18  |
| Specific Aim 1.....                                                                                                                                            | 18  |
| Specific Aim 2.....                                                                                                                                            | 18  |
| Specific Aim 3.....                                                                                                                                            | 18  |
| Chapter 2 : Fabrication and Material Characterization Of Conductive Hyaluronic Acid-Carbon Nanotube Nanofibers For Neural Tissue Engineering Applications..... | 20  |

|                                                  |    |
|--------------------------------------------------|----|
| Introduction .....                               | 20 |
| Experimental Methods .....                       | 22 |
| Methacrylated Hyaluronic Acid Synthesis .....    | 22 |
| Scaffold Fabrication .....                       | 23 |
| Generation 1 HA-CNT Fabrication .....            | 23 |
| MWCNT Functionalization .....                    | 23 |
| Generation 2 HA-CNT Fabrication .....            | 24 |
| Generation 3 HA-CNT Fabrication .....            | 24 |
| Material Characterization.....                   | 25 |
| Generation 1 HA-CNT .....                        | 25 |
| Chemical Functionalization Characterization..... | 25 |
| Topographical Characterization .....             | 25 |
| Electrical Characterization .....                | 25 |
| Generation 2 HA-CNT .....                        | 25 |
| Topographical Characterization .....             | 25 |
| Electrical Characterization .....                | 26 |
| Generation 3 HA-CNT .....                        | 26 |
| Topographical Characterization .....             | 26 |
| Electrical Characterization .....                | 26 |
| Surface Characterization .....                   | 27 |
| Mechanical Characterization .....                | 27 |
| Bulk Mechanical Testing .....                    | 27 |
| Local Modulus Mapping .....                      | 27 |
| Statistical Analysis .....                       | 28 |
| Results .....                                    | 28 |
| Generation 1 HA-CNT .....                        | 28 |
| Chemical Functionalization Characterization..... | 28 |



|                                                                                                                       |    |
|-----------------------------------------------------------------------------------------------------------------------|----|
| Topographical Characterization .....                                                                                  | 29 |
| Electrical Characterization .....                                                                                     | 30 |
| Generation 2 HA-CNT .....                                                                                             | 33 |
| Topographical Characterization .....                                                                                  | 33 |
| Electrical Characterization .....                                                                                     | 34 |
| Generation 3 HA-CNT .....                                                                                             | 34 |
| Topographical Characterization .....                                                                                  | 34 |
| Electrical Characterization .....                                                                                     | 37 |
| Mechanical Characterization .....                                                                                     | 39 |
| Bulk tensile testing .....                                                                                            | 39 |
| Local Modulus Mapping .....                                                                                           | 39 |
| Contact Angle .....                                                                                                   | 42 |
| Discussion .....                                                                                                      | 42 |
| Conclusions .....                                                                                                     | 48 |
| Chapter 3 : HA-CNT Nanofibrous Scaffolds Exhibit L-929 Fibroblast Biocompatibility and Support Neurite Outgrowth..... | 49 |
| Introduction .....                                                                                                    | 49 |
| Experimental Methods .....                                                                                            | 51 |
| General Procedures .....                                                                                              | 51 |
| Scaffold Fabrication .....                                                                                            | 51 |
| "Generation 1" HA-CNT <i>in vitro</i> Neuron Attachment.....                                                          | 52 |
| "Generation 2" HA-CNT <i>in vitro</i> Neuron Attachment.....                                                          | 52 |
| "Generation 3" HA-CNT.....                                                                                            | 54 |
| Nanofiber Fabrication.....                                                                                            | 54 |
| L-929 Fibroblast Attachment.....                                                                                      | 54 |
| <i>in vitro</i> Neuron Attachment .....                                                                               | 55 |
| Results .....                                                                                                         | 56 |

|                                                                                                 |    |
|-------------------------------------------------------------------------------------------------|----|
| “Generation 1” HA-CNT .....                                                                     | 56 |
| in vitro Neuron Attachment .....                                                                | 56 |
| “Generation 2” HA-CNT .....                                                                     | 57 |
| in vitro Neuron Attachment .....                                                                | 57 |
| “Generation 3” HA-CNT .....                                                                     | 58 |
| L-929 Fibroblast Attachment.....                                                                | 58 |
| HA-CNT (0.01%, 0.02%, 0.3%) in vitro Neuron Attachment.....                                     | 59 |
| HA-CNT (0.01%) in vitro Neuron Attachment.....                                                  | 61 |
| Discussion .....                                                                                | 63 |
| “Generation 1” HA-CNT <i>in vitro</i> Neuron Attachment.....                                    | 63 |
| “Generation 2” HA-CNT <i>in vitro</i> Neuron Attachment.....                                    | 63 |
| “Generation 3” HA-CNT .....                                                                     | 63 |
| L-929 Fibroblast Attachment.....                                                                | 63 |
| HA-CNT (0.01%, 0.02%, 0.3%) in vitro Neuron Attachment.....                                     | 63 |
| HA-CNT (0.01%) in vitro Neuron Attachment.....                                                  | 64 |
| Biocompatibility of HA-CNT Nanofibers .....                                                     | 65 |
| Conclusions .....                                                                               | 67 |
| Chapter 4 : Electrical Stimuli Delivered Through HA-CNT Nanofibers Enhances Neuron Growth ..... | 69 |
| Introduction .....                                                                              | 69 |
| Experimental Methods .....                                                                      | 73 |
| Custom Electrical Stimulation Chambers .....                                                    | 73 |
| Electrical Stimulation <i>in vitro</i> Assays.....                                              | 76 |
| L929 Cytotoxicity Assays with Electrical Stimulation .....                                      | 76 |
| Electrical Stimulation Assays with Dissociated Dorsal Root Ganglia .....                        | 78 |
| Mechanistic Studies .....                                                                       | 80 |
| Rationale.....                                                                                  | 80 |

|                                                                       |     |
|-----------------------------------------------------------------------|-----|
| Mechanistic Experimental Method .....                                 | 81  |
| Experimental Results .....                                            | 83  |
| L929 Cytotoxicity Assays with Electrical Stimulation .....            | 83  |
| Calcium Imaging and Electrical Stimulation Assay Results .....        | 87  |
| Discussion.....                                                       | 90  |
| Conclusion.....                                                       | 94  |
| Chapter 5 : Successful Biomaterials Engineering Requires Failure..... | 95  |
| Portions of this chapter are contained in the publication:.....       | 95  |
| Design Iteration for Biomaterial Development.....                     | 95  |
| Study Strengths: in vitro neuron model .....                          | 97  |
| Future Directions.....                                                | 98  |
| Electrical Stimulation: Incomplete Mechanistic Evidence.....          | 100 |
| Conclusion.....                                                       | 105 |
| APPENDIX A .....                                                      | 108 |
| REFERENCES .....                                                      | 113 |
| ABSTRACT.....                                                         | 134 |
| AUTOBIOGRAPHICAL STATEMENT .....                                      | 136 |

**LIST OF TABLES**

Table 2-1. "Generation 1" Topographical Characterization. .... 30

Table 2-2. "Generation 3" Electrical Characterization Summary..... 37

Table 2-3. "Generation 3" Topographical and Mechanical Characterization Summary. .... 40

## LIST OF FIGURES

|                                                                                                                       |    |
|-----------------------------------------------------------------------------------------------------------------------|----|
| Figure 1-1. Directed cell behavior from cues in the microenvironment.....                                             | 5  |
| Figure 1-2. Proposed molecular pathways affected by electrical stimulation associated with neuronal regeneration..... | 6  |
| Figure 1-3. Illustration of Multi-Walled Carbon Nanotubes (MWCNTs). ....                                              | 13 |
| Figure 1-4. TEM micrograph of a MWCNT-PMMA nanofiber.....                                                             | 15 |
| Figure 2-1. COOH-CNT Functionalization .....                                                                          | 29 |
| Figure 2-2. Transmission Electron Micrographs of MWCNTs and COOH-MWCNTs.....                                          | 30 |
| Figure 2-3. Scanning Electron Micrographs of MWCNTs, HA and HA-CNT "Generation 1" Nanofiber Scaffolds. ....           | 31 |
| Figure 2-4. Scanning Electron Micrographs of "Generation 1" Aligned HA-CNT Nanofibers..                               | 32 |
| Figure 2-5. Scanning Electron and Transmission Electron Micrographs of "Generation 2" Nanofibers.....                 | 33 |
| Figure 2-6. "Generation 2" 0.5% HA-CNT Nanofiber Impedance. ....                                                      | 34 |
| Figure 2-7. Scanning Electron Micrographs of "Generation 3" HA-CNT Nanofibers. ....                                   | 35 |
| Figure 2-8. Transmission Electron Micrographs of "Generation 3" HA-CNT Nanofibers. ....                               | 36 |
| Figure 2-9. Electrical Characterization of "Generation 3" Nanofibers.....                                             | 38 |
| Figure 2-10. Tensile testing of hydrated "Generation 3" Nanofibers. ....                                              | 39 |
| Figure 2-11. Young's Modulus from AFM Force Mapping of Nanofibers.....                                                | 40 |
| Figure 2-12. Quantitative Nanomechanical Mapping by Atomic Force Microscopy. ....                                     | 41 |
| Figure 2-13. Representative contact angle measurements for "Generation 3" HA and 0.01% HA-CNT nanofibers. ....        | 42 |
| Figure 3-1. "Generation 1" Neuron Attachment. ....                                                                    | 56 |
| Figure 3-2. "Generation 2" Dissociated DRG 48 Attachment.....                                                         | 57 |
| Figure 3-3. L929 Alamar Blue 24h Attachment Assay.....                                                                | 58 |
| Figure 3-4. "Generation 3" DRG Neuron 24h Attachment 0.01%, 0.02%, 0.3% HA-CNT Nanofibers.....                        | 60 |

Figure 3-5. "Generation 3" 0.01% HA-CNT Neuron Attachment. .... 61

Figure 3-6. "Generation 3" 0.01% HA-CNT Neuron Length and Number. .... 62

Figure 4-1. Custom Electrical Stimulation Culture Dish. .... 74

Figure 4-2. Cytotoxicity Testing with L-929. .... 83

Figure 4-3. Cell Attachment with L-929. .... 84

Figure 4-4. Electrical Stimulation of Neurons Cultured on HA and 0.01% HA-CNT nanofibers.  
..... 87

Figure 4-5. Relative Intracellular Calcium Changes in Neurons Upon Electrical Stimulation. 89

## **Chapter 1 : An Electroactive Materials-Based Repair Strategy for Neural Tissue Engineering with Hyaluronic Acid-Carbon Nanotube Nanofibers**

Portions of this chapter are contained within the publication:

Steel E.M., Sundararaghavan H.G. (2016) Electrically Conductive Materials for Nerve Regeneration. In: Zhang L., Kaplan D. (eds) Neural Engineering. Springer, Cham.

### **Problem and Significance**

Peripheral nerve injuries (PNI) annually affect upwards of 250,000 people in the United States and 300,000 in Europe (Mokarram et al., 2017; Seil and Webster, 2010). Patient quality of life is impacted when functional loss occurs following when a nerve transection or crush injuries caused by trauma or surgical complications (Mukhatyar). Coaptation (surgical term for suturing two segments together) is employed to connect nerve defects of less than 20 mm (Bellamkonda, 2006). The current gold standard for repair of long gap PNI (defects greater than 30 mm in humans) is to autograft the sural nerve due to the ease of access and the low donor site morbidity at the second surgical site (Bellamkonda, 2006; Kawamura et al., 2010). Currently, autografts only successfully restore useful function in 40% of patients treated for long gap PNI (>30 mm) (Mokarram et al., 2017). The research conducted in this thesis sought to develop a biomaterial for neural tissue engineering therapies to improve upon insufficient patient outcomes following repair using gold standard autografting techniques.

Nerve guide conduits (NGC) offer an alternative strategy for repair of PNI. Currently, natural and synthetic biomaterials used in FDA-approved NGCs range from degradable materials such as Type I Collagen, polyglycolic acid, poly(caprolactone) to those that do not degrade such as elastomer hydrogels (Seil and Webster, 2010). While tubular guidance channels have been successful in repairing human PNI that are less than 30 mm, there is a clear unmet clinical need for NGC design that leverages the inherent regenerative capacity of the peripheral nervous system to promote and accelerate functional tissue regeneration in long gap PNI (>30 mm) (Wrobel and Sundararaghavan, 2014). In recent years, a materials based repair strategy to control cues in the injury microenvironment has been investigated

to augment NGCs for improving patient functional outcomes (Wrobel and Sundararaghavan, 2014).

Cells are magnificent integration centers, responding to cues in their microenvironment through a variety of signaling mechanisms. Increasing evidence has established that mechanics (Anderson et al., 2015; Koch, 2012) and topography (Jang et al., 2010; Kim; Whitehead et al., 2018) of a cell's microenvironment influences neuron regeneration. Additionally, several groups have demonstrated that exogenous electrical cues (either through extracellular fluid or through a conductive substrate) activate intracellular signaling pathways favorable towards regenerative behavior. Such behavior in the realm of neural tissue includes Schwann cells releasing NGF (Koppes et al., 2014a; Koppes et al., 2011; Koppes et al., 2014c) and neurons increasing BDNF expression (Wenjin et al., 2011; Zheng et al., 2011) which has then been correlated to increased neurite/axonal outgrowth. The goal of the research reported in this thesis was to design a conductive nanofibrous biomaterial to augment current NGC repair strategies through a multi-combinatorial approach using topographical, mechanical, and electrical cues.

### **Nervous system response to injury**

The peripheral nervous system (PNS) inherently employs systematic repair processes to regenerate axotomized nerves (Mukhatyar). Within hours following peripheral nerve injury, the impacted axons undergo the process of Wallerian degeneration during which Schwann cells (SCs) breakdown myelin by secreting phospholipases and recruit macrophages by releasing cytokines (Chan et al., 2014). Within 2 days of injury, SCs revert to a proliferative phenotype in response to neurotrophins, axon-derived calcitonin gene-related peptide, neuregulin, and IL-1 $\alpha/\beta$ . SCs migrate and align to form the Bands of Büngner which support and guide regenerating axons (Chan et al., 2014). SCs release growth factors within the first few weeks which influence damaged neurons to regenerate. Under conditions permissive to regeneration, neurons increase the expression of tubulin, actin, and growth-associated



protein 43 (GAP43) at the growth cone front which extends out in filopodia to probe the microenvironment (Chan et al., 2014).

Several molecular pathways are involved in peripheral nerve regeneration. The tropomyosin related kinase (Trk) receptor expressed by neurons bind nerve growth factor (NGF) secreted by SCs which activates the phosphatidylinositol-3 kinase (PI3K)-Akt pathway that inhibits apoptosis and promotes neurite outgrowth (Chan et al., 2014). Neurite outgrowth and neuron survival is also promoted by neurotrophins binding to Trk to activate the extracellular signal-regulated kinase (ERK) pathway (Kaplan and Miller, 2000). The second messenger cyclic AMP (cAMP) is involved in the promotion of axon elongation through the upregulation of cytoskeletal protein synthesis as well as the secretion of polyamines that serve to reduce the inhibitory effects of myelin and myelin associated glycoproteins (Gao et al., 2004; Hannila and Filbin, 2008). The Rho-ROCK signaling pathway is activated following nerve injury and is involved in mediating growth cone interactions with its microenvironment serving to inhibit axon outgrowth; inhibiting ROCK has been shown to increase neurite outgrowth.(Cheng et al., 2008) In addition to NGF, the neurotrophins NT-3 and NT-4 as well as brain-derived neurotrophic factor (BDNF) have been established in promoting neuron survival (Varma et al., 2013).

For short injuries less than 10 mm, the oriented fibrin matrix Bands of Büngner forms within the injury microenvironment directing Schwann cells and fibroblasts to migrate, multiply, and differentiate to support and guide neuron regrowth and axonal targeting (Mokarram et al., 2017) (Seil and Webster, 2010). Once Schwann cells and fibroblasts migrate across the injury gap, axons from the proximal nerve segment can bridge the injury gap and reconnect with target tissue at the distal end of the nerve injury. For injuries longer than 30 mm, the fibrin matrix cable responsible for directing support cell infiltration to guide axonal targeting fails to form resulting in incomplete bridging of nerve defects (Bellamkonda, 2006). The failure of natural PNS repair processes to effectively bridge critical injury gaps reduces functional reinnervation of target tissues (Kawamura et al., 2010). Neuron axonal elongation

rates have been measured to be 0.5-1mm per day *in vitro* (Seil and Webster, 2010). However, bridging long nerve defects requires weeks to traverse the harsh *in vivo* microenvironment causing clinical concern for motor endplate degeneration before the axonal front can reconnect (Kawamura et al., 2010; Seil and Webster, 2010).

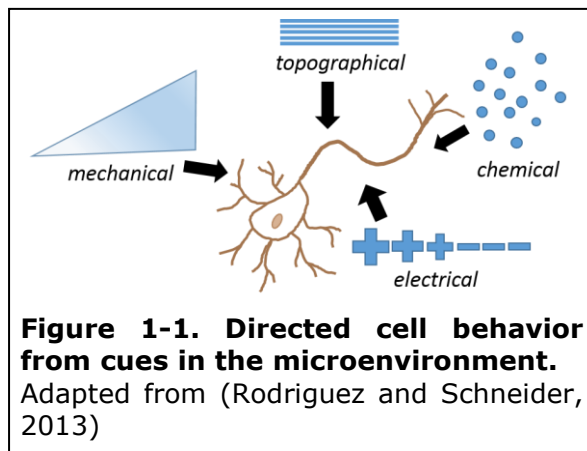
### **Current Treatments and Shortcomings**

The current treatments available for peripheral nerve injuries depend on the size of the injury gap. Coaptation by suturing two segments together is employed to connect nerve defects of less than 20 mm (Bellamkonda, 2006). The current gold standard for peripheral nerve repair for defects greater than 20 mm is to autologous nerve grafting (Bellamkonda, 2006; Kawamura et al., 2010). The disadvantages to autologous nerve grafts are the need for a second surgery to obtain graft tissue, loss of function from the donor site, and difference in tissue size and structure (Li et al., 2014). The use of allografts is hampered by the need for immunosuppressive therapy, but is sometimes necessary in cases when the required graft length exceeds the length available from an autograft (Kehoe et al., 2012; Li et al., 2014). An FDA approved acellular human nerve allograft called Avance® Nerve Graft restored between 77-89% meaningful recovery of function for sensory, motor, and mixed peripheral nerve injuries between 5-50 mm in length in patients in clinical trials between 2007-2010 (Brooks et al., 2012). FDA approved synthetic and natural materials have been available commercially as grafting options in the form of nerve guide conduits by which the severed nerve is joined by entubulation (Li et al., 2014). The collagen conduit NeuroGen has been shown to be equally as effective as coaptation for short gap peripheral nerve repair (<20 mm).(Kehoe et al., 2012) Polyglycolic acid (PGA) and poly D,L lactide-co-ε-caprolactone (PCL) conduits, Neurotube and Neurolac respectively, have demonstrated comparable efficacy to autografts for 20 mm defects (Kehoe et al., 2012). The limitations to PGA conduits are the high degradation rate and acidic degradation products. PCL conduits are extremely rigid, complicating the surgical procedure, and resulted in some cases of severe foreign body reactions that led to neuroma formations (Kehoe et al., 2012). The field of neural tissue

engineering (NTE) has the potential to advance NGC design by developing biomaterials which surmount size and immunogenicity constraints of autografts and allografts while engineering the microenvironment with permissive cues for modulating regenerative cell behavior.

### **Tissue Engineering and Regenerative Medicine for PNI**

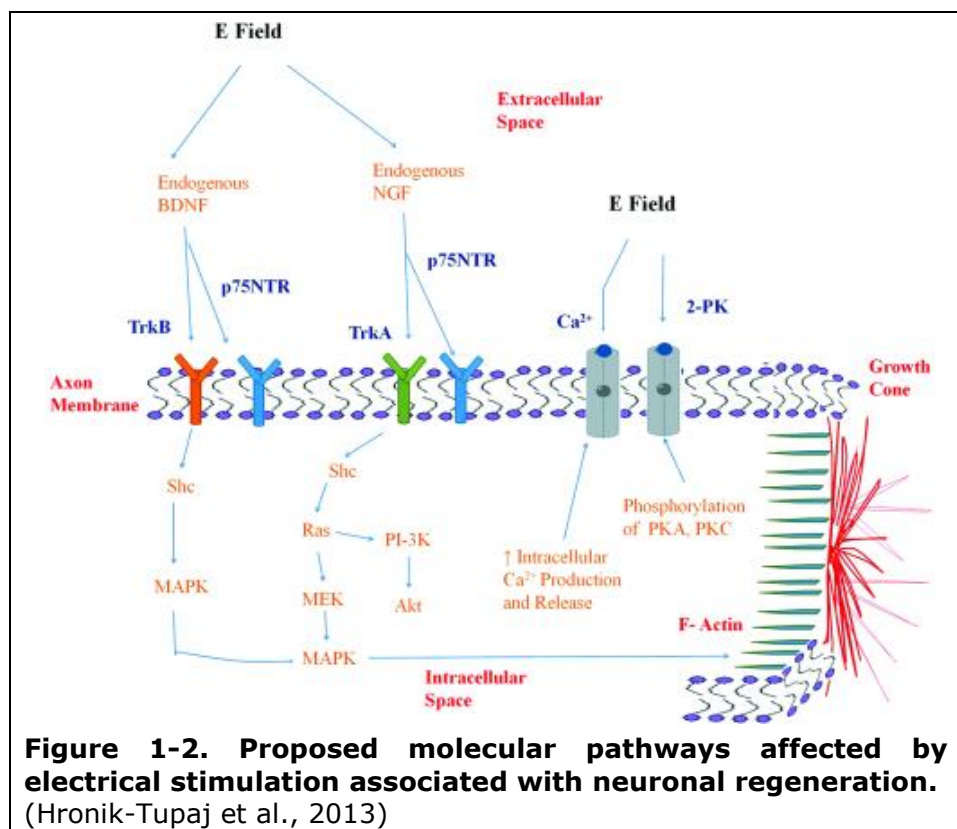
To achieve complete functional recovery that fails to occur with current conventional treatments, tissue engineering approaches seek to incorporate a combination of biomaterials, cells, and/or growth factors to accelerate nerve regrowth. Biomaterials can be tailored with customized cues to mimic a favorable microenvironment that stimulates the processes of cell migration and axonal elongation and targeting that are required for complete repair. These processes can be influenced by topographical, chemical, mechanical, and electrical cues from the microenvironment (Figure 1-1) (Rodriguez and Schneider, 2013; Wrobel and Sundararaghavan, 2014).



The prominent role of bioelectricity in the body makes it an attractive factor to manipulate to accelerate wound healing. Bioelectricity plays its most notable role in the body in the form of electrical signals throughout tissues in the nervous system, influencing a wide variety of active and passive biological functions ranging from movement and thinking to sensory

perception and respiration. External electric fields can influence ion influx through ionic membrane channels to affect intracellular signal transduction pathways through second messengers such as cAMP and  $\text{Ca}^{2+}$  which can in turn affect enzyme phosphorylation and alter gene expression (Brushart et al., 2002). Application of a range of voltages from 15.6  $\mu\text{V}/\text{mm}$  to 300  $\text{mV}/\text{mm}$  using both AC and DC currents have successfully elicited neurite outgrowth in various cell types including dorsal root ganglia neurons, spinal cord neurons and neural stem cells with Feng calculating a threshold to be 16 $\text{mV}/\text{mm}$  (Feng et al., 2012; Graves et al.,

2011; Royo-Gascon et al., 2013; Seil and Webster, 2010; Wrobel and Sundararaghavan, 2014). Electrical stimulation has been shown to accelerate and enhance expression of regeneration-associated genes such as GAP-43 (associated with motoneuron growth), the factor BDNF and its receptor trk-B, and the cytoskeleton proteins tubulin and actin (Al-Majed et al., 2004; Hronik-Tupaj et al., 2013). Calcium channels and two pore domain potassium (2-PK) channels can be influenced by electrical stimulation serving to activate neurite outgrowth through cytoskeletal protein synthesis (Huang et al., 2012; Mathie et al., 2003). Electric field stimulation may regulate protein kinase A and C phosphorylation which mediate the activation of the 2-PK channel (Mathie et al., 2003). Two groups have demonstrated that electrical stimulation of Schwann cells activates T-type voltage gated calcium channels leading to increased intracellular calcium production resulting in calcium-dependent exocytosis of NGF (Huang et al., 2010; Koppes et al., 2014a). Figure 1-2 provides a summary of the molecular mechanisms influenced by electrical stimulation to increase regeneration. Topographical,



chemical, mechanical, and electrical cues have all separately (and in limited combination) been shown to guide and direct these behaviors (Wrobel M, 2013). Ideally, multiple cues could be presented spatially and temporally during the regeneration process. Many groups have demonstrated biocompatibility of a variety of materials as candidates for treatment of traumatic injury in the nervous system.

## **Conductive Biomaterials**

### **Examples from the Literature**

Several groups have delivered electrical cues to neuronal cells through a conductive material scaffold. Common conductive polymers used are polypyrrole (PPy) or polyaniline (PANI). PPy and its composites are brittle, nonbiodegradable, and can undergo spontaneous oxidation/reduction reactions with environmental  $H^+/OH^-$  and metal ions resulting in irreversible degradation affecting the polymer's composition, structure, and ability to conduct charge (Maksymiuk, 2006; Zhang et al., 2007b). PPy is a poor choice for biochemical modification for bioactive molecule delivery because covalent modification techniques change the polymer structure leading to decreased conductivity (Lee et al., 2009). PPy also lacks functional groups making it poorly adhesive to cells (Lee, 2013). Although electrical stimulation through nanofibrous PANi/PCL/gelatin scaffolds have improved neurite outgrowth *in vitro*, (Ghasemi-Mobarakeh et al., 2009) PANi is inherently brittle, nonbiodegradable, and is poor in processibility due to its insolubility in many organic solvents (Valipour et al., 2012). In addition to electrically conductive polymers, piezoelectric materials have also been investigated. Polyvinylidene fluoride (PVDF) films have been shown to enhance spinal cord neurons outgrowth when stimulated at 50 Hz using a custom vibration platform (Royo-Gascon et al., 2013). Though this system has potential in accelerating growth *in vitro*, PVDF is not biodegradable and electrical conductivity would be difficult to control *in vivo*.

### **Carbon Nanotubes**

Carbon nanotubes exhibit unique properties with diverse potential for clever modifications and applications in biomaterials for tissue engineering (Steel and

Sundararaghavan, 2016). Not only do CNT networks possess conductivity ranging from  $10^{-1}$  to  $10^3$  S/cm, they possess high tensile strength and thermal and chemical stability (Steel and Sundararaghavan, 2016). These qualities make them an attractive constituent for a conductive NGC composite material engineered to span a critical gap length of >30 mm and deliver a stable electrical stimulus without causing a concomitant increase in tissue temperature (Steel and Sundararaghavan, 2016). Electrical current passing through resistive tissue can generate heat that denatures proteins, and should thus be considered during material selection. Another consideration for electrode material choice is to limit the potential for electrochemical injury. By carefully considering the environment in which the electrode will be used, unwanted effects like electroconformational protein denaturation, electroporation of the cell membrane, and neurotoxicity can be avoided (Meng S, 2011).

### **Electrical Stimulation and CNTs for tissue regeneration**

One study systematically reviewed the effect of MWCNT surface charge on neurite outgrowth from rat hippocampal neurons (Hu et al., 2004). Hu *et. al.* prepared a series of MWCNTs with various charges via chemical functionalization to assess neurite growth and branching. MWCNTs were either functionalized with carboxylic groups to carry a negative charge (MWCNT-COOH), poly-*m*-aminobenzene sulfonic acid to carry a zwitterionic charge (+/-, MWCNT-PABS), or ethylenediamine to carry a positive charge (MWCNT-EN). Number of neurons, growth cones and neurites, neurite length, and neurite branching were quantified by fluorescence microscopy using calcein for viability or the neuron-specific FITC-conjugated C fragment of tetanus toxin. All three functionalized MWCNTs supported neuronal growth as assessed by positive uptake of calcein. Growth cone number and neurite length were greatest for the positively charged MWCNT-EN compared to MWCNT-PABS and MWCNT-COOH. Hu et al concluded that the negatively charged MWCNT-COOH (deprotonated at pH = 7.35) are not as effective in promoting initiation of growth cones, whereas the amine groups of the MWCNT-EN are positively charged (Hu et al., 2004).

Results of several studies support the incorporation of MWCNTs in electroactive scaffolds. Cho and Borgens developed MWCNTs/collagen composite films by dispersing HCl-treated MWCNTs in a 1% w/v collagen solution (Cho and Borgens, 2010). SEM analysis demonstrated that composites containing 5% CNT resulted in composites with CNTs tangled within the collagen matrix and dispersed on the surface compared to the 0.1% CNT composite in which the CNTs did not appear at the surface. The uniform dispersion of the 5% CNT composite resulted in increased conductivity and lower resistivity ( $10^5 \Omega\text{cm}$ ), measured by cyclic voltammetry and four-point probe method. The cyclic voltammograms for CNT/collagen composite films indicated the collagen/CNT composite's ability to transfer electrons to the working electrode surface compared to collagen only, characterized by increased peak current. Higher CNT concentration decreased PC12 metabolic activity, regardless of the exposure to 100 mV DC for 6 hours. Although 5% CNT/collagen composites exhibited significantly less viability compared to the 100% collagen control, it did not appear that the CNT concentration had a deleterious effect at concentrations of 10% CNT and below. PC12 cells cultured on 5% CNT/collagen composites and stimulated with 100mV for 6 hours revealed an increase in neurite extension versus unstimulated cells. (Cho and Borgens, 2010)

Aligned electrospun poly (L-lactic acid-co-caprolactone) (PLCL) nanofibers have been coated with MWCNTs following anionic modification with potassium sodium tartrate (Jin et al., 2011a, b). SEM analysis revealed MWCNT coated PLCL fibers to be generally rougher than the PLCL fibers alone; diameters were measured to be between 1.3-1.5  $\mu\text{m}$ . Jin *et. al.* assessed neurite outgrowth of rat dorsal root ganglia neurons cultured on aligned MWCNT-coated PLCL fibers for up to 9 days by fluorescence microscopy after staining with Phalloidin to visualize actin filaments. Compared to control aligned PLCL fibers, PC12 neurite length on aligned MWCNT-coated PLCL fibers was significantly greater. Notably, PC12 FAK expression, indicative of integrin-mediated signal transduction involved in neurite outgrowth, was assessed on the MWCNT-coated PLCL fibers by western blot band intensity and found to be higher compared to the control (Jin et al., 2011b).

The limitations to using carbon nanotubes in biomaterials can be classified as manufacturing and quality and toxicological concerns (Serrano et al., 2014). Toxicity concerns are minimized by eliminating the catalyst impurities remnant from fabrication, selecting an aspect ratio of  $\geq 1000$ , reducing aggregation, and making chemical modifications to increase hydrophilicity (Arora et al., 2015). Toxicological studies investigating the immune response to carbon nanotubes *in vivo* reported that hydrophilic CNTs do not cause acute toxicity *in vivo* and observed biodistribution led to accumulations in the liver and spleen (Firme Iii and Bandaru, 2010).

### **Material Design Constraints**

We used the example application of a long gap traumatic peripheral nerve injury as a frame of reference for developing a conductive nanofibrous biomaterial for a material-based repair strategy utilizing electrical stimulation to elicit neuron regeneration. We simplified the application of a traumatic long gap PNI to be modeled as a "black box" with an input of an electrical stimulus to the neural injury microenvironment with the resulting output of increased neurite growth. Motivated by the goal to translate the material developed in this thesis to augment a commercially available NGC conduit for enhanced PNI repair, Kehoe et al. (2012) provides factors in the PNI microenvironment that substantiates it as an advantageous model for "first application" in the clinic:

- (i) clearly defined cell phenotypes, physiology, and tissue structure with well-documented inherent regenerative capacity
- (ii) literature- and evidence-based *in vitro* and *in vivo* models
- (iii) opportunity for new treatment methods due to clear, unmet clinical need for long gap nerve repair (>30 mm)(Mokarram et al., 2017)
- (iv) defined regulatory pathway and reimbursement procedures

The barriers identified in clinical translation of an electroactive materials-based strategy for long-gap peripheral nerve repair include:

- (i) lack of a clearly defined target molecular mechanism for electrical signal input



(ii) disagreement and inconsistency in the literature for electrical stimulus parameters, including the strength and applied duration of DC, AC, pulsatile electrical signals. Moreover, cell response varies according to the properties of a time-dependent signal such as frequency, duty cycle, pulse train parameters.

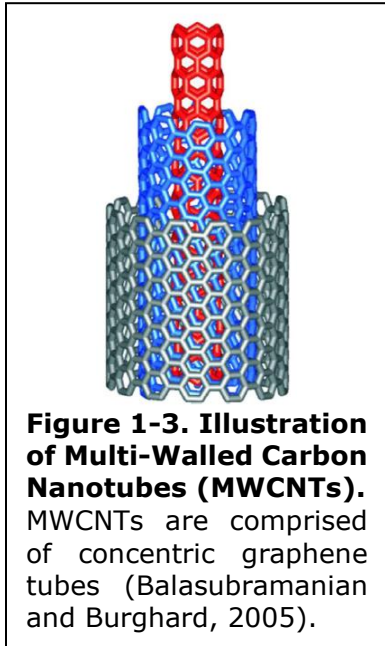
Main design criteria were to demonstrate the ability to transfer electrical conduction to ionic conduction while maintaining topographical and mechanical properties relevant to the peripheral nerve microenvironment. Physical guidance of regenerating axons can be achieved by aligned fibers of nanoscale diameter. The ideal mechanical and electrical properties would be to match native peripheral nerve tissue. The Young's moduli of acellular rat sciatic nerves were measured to be approximately between 0.5 MPa – 1 MPa during studies investigating acellular nerve tissue as a potential autograft substitute (Borschel et al., 2003).

Our electrical conductivity target for our composite HA-CNT nanofibrous substrate was 10,000 Ohm/cm<sup>2</sup>, the resistance of a typical patch of passive membrane.(Donnelly, 1994; Gutkin et al., 2003) The actual resistance of any given passive neuron could be estimated by its area and modeling it as a simple RC-circuit; for example, in the simple case of a sphere with an area of 20 microns, the membrane resistance for the cell is close to 200 MOhms (Gutkin et al., 2003). The purpose of our material is to initiate a functional response from the cell by causing local membrane potential change in the cell membrane when an electrical stimulus is passed through the substrate. Measuring the electrical impedance of a monopolar and dipolar electrode inserted into pork submersed in a cerebrospinal fluid substitute resulted in the ability to differentiate nerve tissue (6 kOhms) from other tissues along the distance of the probe (Sharp et al., 2017). Elsewhere desirable electroactive material properties have been described to be mimic "tissue as a liquid" such that the material interface function can transition between solid and wet as an ion permeable network (Cui et al., 2001; Richardson-Burns et al., 2007). Material properties describing electrical properties in an electrolyte solution can be characterized using electrochemical techniques (Liu et al., 2011). Conductivity can be measured through electrical impedance spectroscopy and capacitance can be qualified

through cyclic voltammetry (Cui et al., 2001). The goal is for the scaffold to allow for delivery of 200  $\mu\text{A}$  and an electric field on the order of 15  $\mu\text{V}/\text{mm}$  based from a study that observed similar directed neurite outgrowth from 1k Hz AC and DC stimuli of these voltage and amperage magnitudes (Graves et al., 2011).

### **Predicted Challenges**

The main challenge in observing cell-matrix responses to electrical stimulation passed through the substrate is to convert electron conductivity from metallic electrodes to ionic conductivity in the electrolyte without inducing a confounding factor of current passing through the media. A sophisticated review of the role of bioelectricity in embryogenesis and wound repair describes traditional experimental methods like the use of salt bridges (McCaig et al., 2005). Using these concepts as a foundation along with designs (Durgam et al., 2010; Xia et al., 2007) published and validated for ES studies with sample replicates, we designed a reproducible and stable *in vitro* electrical stimulation chamber from common and readily available materials and equipment that allow for separating the power source from the culture medium. The long-term goal would be to test the composite material in animal model for nerve regeneration and thus considered techniques that would merge a rat sciatic nerve model (Daly et al., 2013). The electrical stimulus parameters of an oscillating charge-balanced AC waveform (Borgens, 2000) with 200  $\mu\text{A}$  amplitude (Graves et al., 2011) square pulses at 20 Hz for 1 h has been reported in a series of studies to enhance regeneration and reinnervation (Al-Majed et al., 2000a; Al-Majed et al., 2000b; Al-Majed et al., 2004; Brushart et al., 2005; Geremia et al., 2007; Vivo et al., 2008). Additionally, the primary mode of conduction in the salt bridge technique is through the media which can be problematic when salt leeches from the bridges by Fickian diffusion causing an inhomogeneous culture medium. Our prediction is that electrical stimulation activates Voltage-Gated Calcium Channels in the cell membrane permitting calcium influx. Calcium, known as a second messenger, is a potent mediator of cellular pathways controlling cytoskeletal organization via the calcium/calmodulin signaling pathway (McCaig et al., 2002) as well as BDNF production in neurons (Wenjin et al., 2011;



Zheng et al., 2011) and release from Schwann cells (Luo et al., 2014). Thus, it is important to maintain a homogenous culture medium with known quantities of each ionic component (Meng S, 2011).

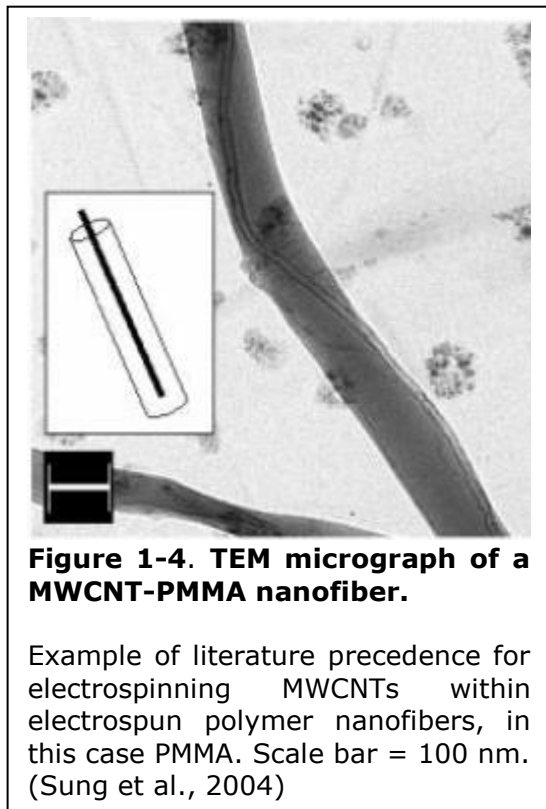
### **Proposed Solution**

The critical barrier currently in the field of nerve regeneration is that no approach achieves complete functional recovery or accelerates nerve regeneration enough to avoid target muscle loss. The current project seeks to implement neural tissue engineering therapies to overcome these barriers by accelerating regrowth and improving axonal targeting through electrical and topographical cues delivered by a conductive biopolymer composite scaffold. The strategy of this study proposes to achieve a conductive biopolymer composite by incorporating carboxylated multi-walled carbon nanotubes (COOH-MWCNTs) as the conductive constituents into a hyaluronic acid (HA) based nanofibrous scaffold (HA-CNT). It is hypothesized that scaffold conductance is achieved via charge hopping from one MWCNT to the next, similar to electrical conductance achieved in thin polymer films containing carbon nanotubes (CNTs) (Liu et al., 2009). HA, one of the primary components of neural tissue extracellular matrix, is a naturally derived biocompatible biopolymer that is biodegradable, promotes cell attachment, and possesses the capability to be biochemically modified to fine tune stiffness and degradation properties (Prestwich et al., 1998; Suri and Schmidt, 2010).

MWCNTs synthesized by chemical vapor deposition comprise multiple sheets of graphene rolled into cylindrical nanostructures nesting within one another (Figure 1-3) (Balasubramanian and Burghard, 2005; Sung et al., 2004). Due to the innate electrical and mechanical properties of MWCNTs based on their chemical stability and electronic structure, incorporating MWCNTs within a polymer composite improves electrical conductivity and mechanical strength compared to the pristine polymer (Sung et al., 2004). CNT size, shape,

functionalization, and concentration have been characterized as influential factors in affecting cytotoxicity and biocompatibility on a cell type dependent basis (Hopley et al., 2014). Carbon nanotube, carbon nanofiber, and graphene film substrates have been cultured with neurons, Schwann cells, microglia and astrocytes to investigate cellular response. Functionalizing carbon nanotubes with carboxyl groups improves hydrophilicity and supports neuronal growth evidenced by neurite length, number, and branching (Balasubramanian and Burghard, 2005; Hu et al., 2004). Electrically stimulated CNT rope structures induced differentiation of neural stem cells and increased neurite outgrowth (Huang et al., 2012). Schwann cells cultured on carbon nanofibers displayed statistically similar viability, proliferation, and intracellular levels of reactive oxygen species (ROS) compared to SCs cultured on tissue culture plastic (Jain et al., 2013). Astrocytes cultured on CNT-PEG films and microglia cultured on 2D graphene did not exhibit significant evidence of inflammation (Gottipati et al., 2014; Song et al., 2014).

Although previous efforts have combined CNTs with synthetic materials such as poly(L-lactic-acid-co-caprolactone) (PLCL) and poly(methyl methacrylate) (PMMA) to achieve conductivity, (Jin et al., 2011b; Sung et al., 2004) directing cell behavior by electrical stimulation cues through these composite materials has not been investigated. The PMMA/CNT composite study by Sung demonstrated the feasibility of electrospinning CNTs within a polymer; however, the low conductivity ( $\sim 10^{-10}$  S/cm) regardless of CNT concentration made the mechanically stronger composite ill-suited for its intended application for battery electrodes or electronic devices (Sung et al., 2004). In the study using CNT-coated PLCL fibers, PC-12 neuron-like cells expressed the focal adhesion kinase, FAK, at significantly higher levels in comparison to PLCL controls (Jin et al., 2011b). The Jin group attributed the observed increases in neurite length to the increased FAK expression for its role in integrin-mediated signal transduction (Jin et al., 2011b). Yu et al. (2014) incorporated MWCNTs into electrospun collagen/PCL nanofibers to form nerve guide conduits to study treatment efficacy as well as the biocompatibility and toxicology of MWCNTs in an *in vivo* rat sciatic nerve injury model. The Yu study demonstrated the MWCNT-Col/PCL composite did not elicit infection,



rejection, or toxicity. Cho et. al. fabricated a conductive composite by combining collagen and 5% w/w CNTs to achieve a resistivity of  $10^5 \Omega\text{cm}$ ; while PC-12 neuronal-like cells maintained good viability, DC electrical stimulation with 100 mV for 6 h did not produce significantly enhanced neurite outgrowth (Cho and Borgens, 2010). A few studies have described incorporating MWCNTs into hydrogels whether to increase mechanical strength or to enhance electrical conductivity. One of the few studies to investigate CNT/HA composites combined carboxylated single-walled CNTs into HA hydrogels to enhance mechanical properties

(Bhattacharyya et al., 2008b). The researchers attributed a 300% increase in storage modulus to CNT networks that formed between the hydrogel cross-linker divinyl sulfone (DVS) and the hydroxyl groups on the carboxylated CNTs (Bhattacharyya et al., 2008b). The rheological properties of the CNT/HA solution were unaffected without the addition of DVS highlighting the contribution of the cross-linking method on mechanical properties (Bhattacharyya et al., 2008b). Luo et al. (2010) fabricated poly(methacrylic acid) (PMAA) and MWCNT composite hydrogels with improved compressive strength, swelling, and cytocompatibility compared to pure PMAA hydrogels. Arslantunali et al. (2014) incorporated MWCNTs into poly(2-hydroxyethyl methacrylate) (pHEMA) hydrogels to improve electrical conductivity to  $8 \times 10^{-2} \Omega^{-1} \cdot \text{cm}^{-1}$ , an improvement over 10-fold relative to native pHEMA hydrogels. Neuroblastoma viability was improved in cultures grown on pHEMA/MWCNT composite compared to pHEMA hydrogels following 10 minutes of 1 or 2V electrical stimulation every hour for 12 hours (Arslantunali et al., 2014). The combined results of these studies

establish the potential for MWCNT polymer composites to support and improve neuronal growth for regenerative applications when using optimized electrical stimulation parameters.

The proposed study is the first to incorporate COOH-MWCNTs within a methacrylated hyaluronic acid nanofibrous composite as a means to deliver electrical stimulation to manipulate cell behavior. The proposed material is the first to combine MWCNTs and hyaluronic acid in the effort to achieve a degradable, conductive, nanofibrous biopolymer scaffold. It is hypothesized that aligning MWCNTs within aligned nanofibers will provide a directed electrical signal cue. Several groups have demonstrated the feasibility of aligning MWCNTs within nanofibers by electrospinning using PMMA and PLGA (Figure 1-4) (Sung et al., 2004; Zhang, 2011). Most research studies found during our literature investigation about electrically mediated neural regeneration uses DC stimulation reported in V/mm across the culture area. This type of stimulation would result in an electrical field gradient as the voltage drops across any material, especially in a resistive polymer scaffold. To avoid this issue, this study proposes to use an alternating current (AC) to deliver electrical stimulation. Graves demonstrated that average neurite length of *Xenopus* neurons were statistically similar for AC- and DC-stimulated cells with preferential growth towards the cathode (Graves et al., 2011).

The advantage of using the proposed material is that the CNTs serve as the conductive constituent within the biopolymer HA that can adjust stiffness through crosslinking and to be modified with bioactive molecules through Michael addition reactions. Electrical conductance can be tuned by varying the concentration of CNTs (Liu et al., 2009). It is hypothesized that scaffold conductance is achieved via charge hopping of electrons trapped in the CNTs; a biomaterial for tissue engineering is the first application of its kind for this phenomenon which also has been observed with molecular wires and disordered semiconductors (Ambegaokar et al., 1971; Berlin et al., 2003). The proposed HA-CNT degradable material boasts the ability to deliver topographical, mechanical, and electrical cues to enhance and accelerate tissue regeneration.

## **Rationale, Hypothesis, and Specific Aims**

### **Rationale**

Delivery of electrical stimulation through the proposed conductive HA-CNT material will be investigated using two scaffold types, nanofibers and hydrogels. The conductive, aligned HA-CNT nanofibers could support robust neurite outgrowth by providing the topographical benefits of mimicking native extracellular matrix in size and structure and the ability to deliver an electrical cue to direct outgrowth in comparison to the hydrogels. Functionalizing pristine MWCNTs with carboxylic acid groups will facilitate dispersion (Ding et al., 2014) of the MWCNTs in the aqueous hyaluronic acid polymer solution, allowing for homogenous distribution of MWCNTs within the resulting nanofibrous or hydrogel constructs. Aligned HA-CNT nanofibers will be fabricated by electrospinning. The nanotopography of the fibers mimic the extracellular matrix while the fiber alignment has been previously demonstrated to direct and guide neurite growth (Chow et al., 2007; Corey et al., 2007; Patel et al., 2007; Schnell et al., 2007). Electrical and topographical cues have been shown to synergistically increase and direct neurite growth on a PPy nanofibrous scaffold (Xie et al., 2009b). Hyaluronic acid based hydrogels have been demonstrated to improve motor neuron survival as well as sensory neurite outgrowth both *in vitro* and *in vivo* (Jin et al., 2013; Schizas et al., 2014). Electrical stimulation has not only improved neuron growth but has also been shown to influence glial cell behavior by increasing Schwann cell secretion of nerve growth factor. Exposure of glial cells to carbon nanotube substrates have demonstrated a reduction in inflammation. Culture of astrocytes on carbon nanotube films reduced astrocyte activation indicated by a decrease in GFAP expression (Gottipati et al., 2014). Electrical stimulation through a HA-CNT based scaffold is a promising modality by not only directing neuron growth but also enhancing support cell activity.

### **Central Hypothesis**

The driving hypothesis in this thesis is that electrical stimulation cues can be delivered through aligned hyaluronic acid-carbon nanotube (HA-CNT) nanofibrous scaffolds to control

nerve growth by increasing neurite length, viability, and production and delivery of neurotrophins.

To test this hypothesis, a series of specific questions were investigated to systematically determine (1) optimal material components and properties and (2) electrical stimulus parameters that would provide experimental evidence that electrical cues via a material-based repair strategy can activate regenerative cell behavior.

### **Specific Aims and Hypotheses**

Three specific aims were developed to investigate these research questions.

#### **Specific Aim 1**

**SA1:** To fabricate and characterize material properties of hyaluronic acid carbon nanotube (HA-CNT) composite nanofibrous scaffolds.

We hypothesize that carbon nanotubes embedded within HA nanofibers by the electrospinning technique will result in increased electroactivity as measured by electrical impedance and cyclic voltammetry.

We hypothesize that composite nanofibers will meet mechanical and topographical design criteria for the peripheral nerve environment.

#### **Specific Aim 2**

**SA2:** To characterize *in vitro* cell responses to HA-CNT nanofibrous scaffolds

We hypothesize that HA-CNT based scaffolds will not induce cytotoxicity assessed by an *in vitro* L929 fibroblast model.

We hypothesize that in the absence of electrical stimulation, attachment assays using an *in vitro* dissociated dorsal root ganglia model will establish that neurite outgrowth on HA-CNT nanofibers will be no different than that observed on HA nanofibers.

#### **Specific Aim 3**

**SA3:** To demonstrate an electrical stimulus can be delivered through HA-CNT nanofibers to increase and accelerate neuron growth as measured by neurite extension and neuron number.



We hypothesize that a stable electrical stimulation system will enable reproducible and repeatable experimental conditions to observe *in vitro* cell response to electrical stimuli delivered through a conductive nanofibrous biomaterial.

We hypothesize electrical stimulation delivered through the HA-CNT nanofibrous scaffold will result in significantly greater neurite length in chick dissociated dorsal root ganglia neurons.

## **Chapter 2 : Fabrication and Material Characterization Of Conductive Hyaluronic Acid-Carbon Nanotube Nanofibers For Neural Tissue Engineering Applications**

### **Introduction**

The field of bio-inspired electroactive materials is experiencing a resurgence for their potential in delivering electrical stimulation in neural tissue engineering and electroceutical medical device applications (Anderson et al., 2015; Fairfield, 2017; Steel and Sundararaghavan, 2016). Modulating neuronal activity via electrical stimuli has been successful in the clinical treatment of an array of neurological disorders (Fairfield, 2017). Historically, the most commonly known and successful neuromodulation device to sense, stimulate and suppress neurological activity is the cochlear implant. Deep brain and spinal stimulators are electrical devices used to treat medical disorders. These electroceutical devices have been developed for the clinical treatment of Parkinson's disease, epilepsy, depression, pain and incontinence (Fairfield, 2017). However, there remain outstanding concerns surrounding the long-term safety and efficacy of electroactive biomaterials due to a lack of clarity in the molecular pathways responsible for observed cell behavior. In an ideal, simplified system based on circuit logic, a defined input of an electrical stimulus is delivered to the cell to initiate predictable outputs. Depending on the input, an output could encompass the resulting action from cascades initiated by cell-matrix and/or cell-cell signaling pathways. We sought to design a versatile electroactive nanofibrous biomaterial by building on existing knowledge at the interface of biology, chemistry, neuroscience, and electrical engineering. Robust and reproducible evidence of molecular mechanisms can be elucidated once a physiologically relevant extracellular matrix mimic (in terms of size scale, mechanics, and ionic conduction) is developed that is capable of interfacing with a metal electrode.

The focus of our study was to develop a biomaterial that incorporated electrical cues into existing peripheral nerve guide conduit approaches, while also maintaining modification potential for applications across other organ systems. Whether presented to the cell individually or in combination, topography, mechanics, and electrical properties can impact

neuron outgrowth and viability. Recognizing challenges facing other electrical stimulation modalities, such as the reduced signal-to-noise ratio and efficacy of chronic electrodes caused by the foreign body response to topography and mechanical mismatch, we sought to design an extracellular mimic in terms of topography and mechanics, while increasing material conductivity.

Main design criteria were to demonstrate the ability to transfer electrical conduction to ionic conduction while maintaining topographical and mechanical properties relevant to the peripheral nerve microenvironment. Physical guidance of regenerating axons can be achieved by aligned fibers of nanoscale diameter. The ideal mechanical and electrical properties would be to match native peripheral nerve tissue. The mechanical property benchmark for bulk Young's Modulus is between 0.5 – 1 MPa, the stiffness native to the *in vivo* peripheral nerve environment. Rat sciatic nerve was measured to be approximately 500 kPa during studies comparing the effects of acellularization processing on nerve mechanical properties (Borschel et al., 2003). Local mechanical properties influence neuron function and regeneration. Dorsal root ganglion (DRG) neurons exhibited maximal outgrowth on substrates with a Young's Modulus around ~1000 Pa (Koch, 2012). The Young's Modulus of myelinated axons from murine sciatic nerves have been measured by atomic force microscopy force mapping to be between 100 – 300 kPa (Heredia et al., 2007). The electrical conductivity target for composite HA-CNT nanofibrous substrate was 10,000 Ohm/cm<sup>2</sup>, the resistance of a typical patch of passive membrane (Donnelly, 1994; Gutkin et al., 2003).

We hypothesized that we could achieve target topographical, mechanical, and electrical characteristics by embedding carbon nanotubes within electrospun hyaluronic acid nanofibers. One of the primary motivations of this strategy was to expand upon our previously well characterized nanofibrous platform comprised of hyaluronic acid nanofibers electrospun out of an aqueous solution (Sundararaghavan and Burdick, 2011; Whitehead et al., 2018; Wrobel 2017). Not only do aqueous formulations eliminate the need to use organic solvents, but also are more conducive to maintaining bioactivity of molecules if the adoption of a

chemical cue is desired. Carboxylated multi-walled carbon nanotubes (CNTs) were chosen to serve as the conductive constituent of the composite based on their excellent electrical properties and minimal toxicological issues due to favorable chemical functionalization and an aspect ratio of 1000 (Kim, 2011). We utilized methacrylated hyaluronic acid (MeHA) for its tunable properties - stiffness and degradation rates can be adjusted through photocrosslinking, and covalent immobilization of bioactive molecules. Electrical conductance can be tuned by varying the concentration and dispersion of CNTs (Liu et al., 2009). The hyaluronic acid-carbon nanotube (HA-CNT) composite boasts the ability to deliver electrical, mechanical, and topographical cues to enhance and accelerate tissue regeneration.

To complete Aim 1, hyaluronic acid-carbon nanotube (HA-CNT) composite nanofibrous scaffolds were fabricated and material properties were characterized for concentrations of 0.01%, 0.02%, 0.03%, 0.5%, and 1% w/w CNT to HA polymer solution. We hypothesized that carbon nanotubes embedded within HA nanofibers by the electrospinning technique would result in increased electroactivity as measured by electrical impedance and cyclic voltammetry. We hypothesized that composite nanofibers will meet mechanical and topographical design criteria for the peripheral nerve environment.

## **Experimental Methods**

### **Methacrylated Hyaluronic Acid Synthesis**

Methacrylated hyaluronic acid (MeHA) was synthesized as previously described such that 60% of the HA hydroxyl groups will be modified with methacrylate groups (Marklein and Burdick, 2010; Smeds and Grinstaff, 2001). Briefly, a 1 wt% solution of sodium hyaluronate (HA, 66 kDA, ECM Science, Detroit, MI) in DI H<sub>2</sub>O will be reacted with methacrylic anhydride (2.22 mL per gram of HA, Sigma), adjusted to pH 8 with 5N NaOH, on ice for ~24 hours. The resulting macromer solution will be purified by dialysis against water for 48 hours and lyophilized to recover the final product.

## **Scaffold Fabrication**

Nanofibrous scaffolds were fabricated using an electrospinning technique previously described (Whitehead, 2017; Wrobel 2017). Briefly, HA nanofibers were electrospun onto 12-mm diameter cover glass adhered to a rotating mandrel from an aqueous solution, ejected from a blunt 18G needle, containing 2% methacrylated hyaluronic acid (HA), 2% polyethylene oxide (PEO, 900kDa), and 0.05% I2959 photo-initiator for controls (HA). Variations in formulation and methods for HA-CNT nanofibers are denoted as "Generation 1," "Generation 2," and "Generation 3." Nanofibrous scaffolds were cross-linked under a long wave UV light for 30 minutes and stored in a desiccator cabinet until use.

We performed an optimization of our HA-CNT electrospinning formulation to achieve aligned composite nanofibers by electrospinning. This optimization was achieved by implementing an iterative design and revision approach to achieve target material characteristics.

### **Generation 1 HA-CNT Fabrication**

#### *MWCNT Functionalization*

Pristine MWCNTs were fabricated by members of Dr. Ming-Cheng Cheng's laboratory using the Wayne State University nanofabrication facility and the Chemical Vapor Deposition technique. MWCNTs were functionalized with carboxylic acid groups to render them hydrophilic to facilitate homogeneous dispersion in the HA polymer solution during scaffold fabrication. Carboxylic acid groups form on the surface of MWCNTs by acid surface treatment due to the free oxygen atoms released by strong acids reacting with unstable carbon atoms (Kar and Choudhury, 2013). To prepare COOH-MWCNTs, pristine MWCNTs were suspended in a 3:1 v/v mixture of concentrated H<sub>2</sub>SO<sub>4</sub> and HNO<sub>3</sub>, sonicated in a water bath for 2 hours, then refluxed at 90°C for 18 hours while stirring. The COOH-MWCNTs and acid mixture were diluted in deionized (DI) water, neutralized to pH 7.4 using NaOH, and centrifuged at 5000 rpm for 45 minutes. The MWCNTs were resuspended in DI water then dialyzed for 48 hours using a 12-14 kDa MWCO membrane to remove salts. Water was removed via lyophilization.

HA-CNT electrospinning solution containing 1% (w/w) CNT was electrospun onto a mandrel rotating at 10 m/s to obtain randomly oriented nanofibers or at 18 m/s to obtain aligned nanofibers. Electrospinning solution was ejected at a flow rate of 150  $\mu$ /h.

### **Generation 2 HA-CNT Fabrication**

Generation 2 scaffolds were fabricated with the formulation described above with the several optimized parameters. Carboxylated multi-walled carbon nanotubes were sourced from an external supplier (Cheaptubes.com), with similar specifications to the in-house fabricated CNTs used in Generation 1 (20-30 nm diameter, 20-30  $\mu$ m length). HA-CNT electrospinning solution containing 0.5% (w/w) CNT was dispersed within an aqueous solution containing 1% bovine serum albumin (BSA) in 0.85% physiological saline (1% BSA saline) and sonicated for 10 minutes using a standard ultrasonic cleaner bath (35kHz, 48W, VWR) adapting a technique reported in 2011 in Archives in Toxicology (Kim, 2011). CNT dispersion was suspended to form a working electrospinning solution with final concentrations (w/w) 2% HA, 2% PEO and 0.05% I2959 photo-initiator. Generation 2 formulation was electrospun onto a mandrel rotating at 18 m/s and using a flow rate of 900  $\mu$ l/h resulting in aligned nanofibers.

### **Generation 3 HA-CNT Fabrication**

COOH-MWCNTs (Cheaptubes.com, 20-30 nm diameter, 20-30  $\mu$ m length) were dispersed in 1% BSA physiological saline using a bath sonicator (40 kW) at a concentration of either 0.01% w/w, 0.02% w/w, or 0.3% w/w. Hyaluronic acid (40 kDa, ECM Science, Detroit, MI) was dissolved in deionized water and methacrylated to approximately 30% methacrylation by adding methacrylic anhydride (Sigma) dropwise while maintaining a basic pH using NaOH. Nanofibers were electrospun at 24kV ejected at a 1.7 ml/hr flow rate from an 18G blunt needle at an 11 cm distance onto a rotating mandrel (21.25 m/s) using an aqueous mixture of the dispersed CNT solution (1/3 v/v), 2% w/w MeHA, and 2% w/w PEO. Control hyaluronic acid nanofibers were electrospun using the same formulation but with deionized water in place of the CNT dispersion solution.

## **Material Characterization**

### *Generation 1 HA-CNT*

#### *Chemical Functionalization Characterization*

Successful functionalization of MWCNTs with carboxylic acid groups was confirmed by Fourier transform IR-attenuated total reflectance (FTIR-ATR) spectroscopy. Spectra were collected in a frequency range between 400 and 4000  $\text{cm}^{-1}$  under nitrogen with a spectral resolution of 4  $\text{cm}^{-1}$  and averaged over 75 scans for pristine carbon nanotubes, carboxylated carbon nanotubes, HA nanofibers, and HA-CNT nanofibers using a Nicolet 8700 FT-IR (ThermoFisher Scientific, Waltham, MA). The autobaseline function was used within the SpectraMax software following spectra acquisition.

#### *Topographical Characterization*

Scanning electron microscopy (SEM) and scanning transmission electron microscopy (TEM) was performed on HA and CNT-HA nanofibers electrospun onto either glass coverslips and Au-sputter coated or onto copper TEM sample grids.

#### *Electrical Characterization*

A four-point probe instrument was used to measure scaffold conductivity. The probes were connected to the material surface through silver paste point contacts patterned on the material surface. A known current was passed through the two outer probes (referred to as source and drain) while voltage was measured through the two inner probes to calculate resistance using Ohm's Law.

### *Generation 2 HA-CNT*

#### *Topographical Characterization*

Scanning electron microscopy (SEM) and scanning transmission electron microscopy (TEM) was performed on HA and CNT-HA nanofibers electrospun onto either glass coverslips and Au-sputter coated or onto copper TEM sample grids.

### *Electrical Characterization*

A 3-electrode cell was employed for electrochemical impedance spectroscopy (EIS, HP 4284 impedance analyzer) in phosphate buffered saline (PBS) at room temperature, where 28.3 mm<sup>2</sup> nanofibrous substrates served as the working electrode, platinum as the auxiliary electrode, and Ag/AgCl electrode as the reference.

### *Generation 3 HA-CNT*

Topographical and electrical characterization was performed on HA and 0.01%, 0.02% and 0.3% HA-CNT nanofibers. Surface and mechanical characterization was performed only on HA and 0.01% HA-CNT nanofibers once it was determined that optimal topography and electrical parameters were achieved with the 0.01% HA-CNT electrospinning formulation.

### *Topographical Characterization*

Scanning electron microscopy (SEM) and scanning transmission electron microscopy (TEM) was performed on HA and CNT-HA nanofibers electrospun onto either glass coverslips and Au-sputter coated or onto copper TEM sample grids.

### *Electrical Characterization*

A 3-electrode cell was employed for electrochemical impedance spectroscopy (EIS, HP 4284 impedance analyzer) and cyclic voltammetry (CV, Gamry PC4 potentiostat) in PBS at room temperature, where 28.3 mm<sup>2</sup> nanofibrous substrates served as the working electrode, Pt as the auxiliary electrode, and Ag/AgCl electrode as the reference. CV data collected with a -0.8 to 0.8 V potential range and 50mV/s scan rate with 2 mV step. EIS applied a 10 mV AC signal in a frequency sweep from 0.20 Hz-150 kHz. EIS results are reported as impedance magnitude as obtained from the Gamry Analysis software. CV results were calculated as interfacial capacitance calculated by using a custom MatLAB script to integrate the area under the CV curve between the scan voltage limits then divided by the geometric area for specific capacitance.



### *Surface Characterization*

Droplets of phosphate buffered saline (PBS, 6  $\mu$ l) on the surface of the nanofibrous scaffolds were imaged from three locations on each of three nanofibrous samples of HA and HA-CNT to determine wettability by quantifying the droplet contact angle. One set of images were taken with the camera angle perpendicular to fiber alignment, a second set of images were taken with the camera angle parallel to fiber alignment. Contact angle images were acquired using a goniometer (SI-CAM2000) and analyzed using the Contact Angle ImageJ plug-in.

### *Mechanical Characterization*

#### *Bulk Mechanical Testing*

Tensile properties of hydrated nanofibrous samples for both HA and HA-CNT ( $n = 5$ ) were measured at a strain rate of 1%  $\text{min}^{-1}$  (10 cm gauge length, Instron 3342, 50N load cell). Prior to testing, scaffolds were immersed in PBS for 24 h then the gauge length, width and thickness of each sample was recorded. Instron Bluehill 3 software was used to record the stress-strain curves; raw data was analyzed in Microsoft Excel. The slope of the linear portion of the stress-strain curve was calculated to be the Young's modulus; the maximum stress recorded for each curve was the ultimate stress.

#### *Local Modulus Mapping*

Nanofibrous samples were immersed in PBS 24 h prior to imaging, then secured to double-sided tape in a 35mm culture dish and imaged using the Quantitative Nanomechanical Mapping (QNM) mode in fluid (PBS) using a Bruker Bioscope Catalyst Atomic Force Microscope (AFM). Prior to imaging the nanofibrous samples, the silicon nitride DNP-D cantilever (0.06 N/m nominal spring constant, nominal spring constant 18kHz) was calibrated in air according to Bruker absolute calibration documentation using a series of standards (fused silica standard for deflection sensitivity, thermal tuning, then titanium roughness and 2.5 MPa PDMS standards for tip radius). To ensure deformation of the 2.5 MPa PDMS standard during tip radius calibration, a peak force setpoint of 8 nN was employed. Prior to imaging the

nanofibrous samples in fluid, the thermal tune was repeated for fluid condition. The PeakForce settings employed were 0.25 kHz PeakForce frequency and 1000 nm PeakForce amplitude with 1200 nm lift height.

Scans with the dimensions of 10 x 10 nm, 128x128 lines were acquired with PeakForce Capture enabled such that a force curve was acquired at each point. Using Nanoscope Analysis 1.5, force curves were analyzed and fit to a Sneddon model to calculate Young's Modulus, Young's modulus (Oyen and Cook, 2009).

### **Statistical Analysis**

All data is reported as mean  $\pm$  standard error. Microsoft Excel was used to calculate descriptive statistics. Microsoft Excel Data Analysis Add-in was employed for F-test and Student's *t*-tests. For *p* value < 0.05 for the F-Test Two-Sample for Variances, the Student's *t* test assuming unequal variances was applied; otherwise, the Student's *t* test assuming equal variances was used. Statistical significance was accepted at  $\alpha = 0.05$ .

## **Results**

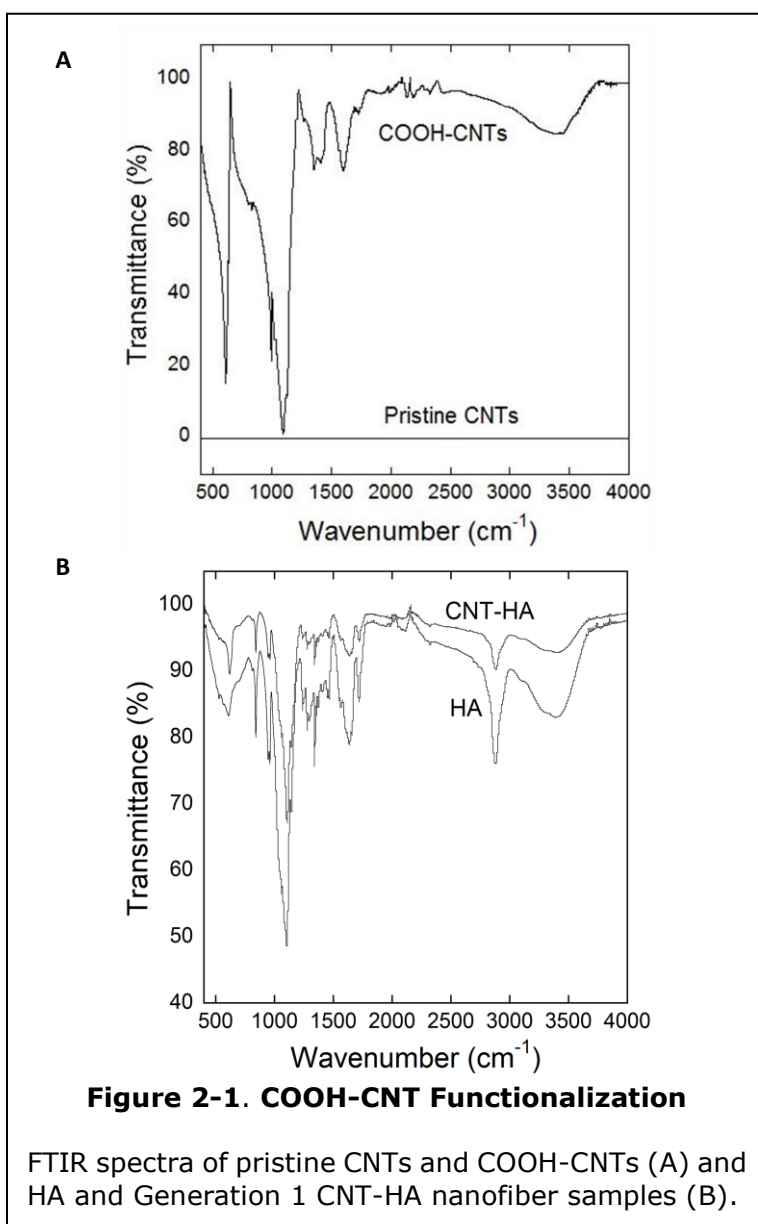
### **Generation 1 HA-CNT**

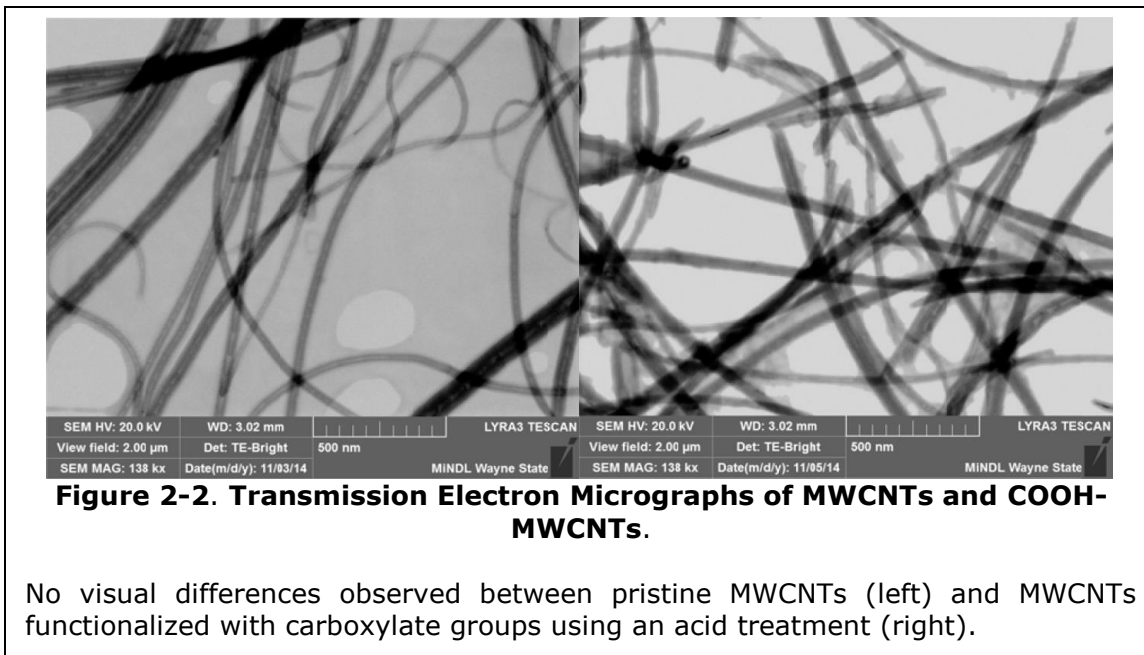
#### *Chemical Functionalization Characterization*

Successful functionalization of MWCNTs with carboxylic acid groups was confirmed by Fourier transform IR-attenuated total reflectance (FTIR-ATR) spectroscopy. The spectra in Figure 2-1 (A) reveals bands near 1600, 1356, and 1092  $\text{cm}^{-1}$  which correspond to  $-\text{COOH}$  group stretching vibrations (Kar and Choudhury, 2013). The broad band around 3400  $\text{cm}^{-1}$  denotes the O-H stretching in the terminal carboxyl group (Kar and Choudhury, 2013). Due to the presence of carboxylic acid moieties in hyaluronic acid, it is difficult to distinguish differences between the COOH-CNT, HA, and CNT-HA samples. The bands at 936 and 1492  $\text{cm}^{-1}$  in Figure 2-1 (B) distinguish the methacrylate carbon double bonds in the HA and CNT-HA nanofibers sample spectra.

### Topographical Characterization

Scanning transmission electron microscopy (TEM) was performed on pristine MWCNTs and COOH-MWCNTs to qualitatively review morphology before and after acid treatment. Figure 2-2 provides visual evidence that there was no change in MWCNT morphology before and after  $-COOH$  functionalization, respectively. SEM was performed to observe nanofiber topography (Figure 2-3, random and Figure 2-4, aligned) and quantify nanotube and





| <b>Table 2-1. "Generation 1" Topographical Characterization.</b>              |                          |                      |                             |
|-------------------------------------------------------------------------------|--------------------------|----------------------|-----------------------------|
| Mean diameter and alignment for CNTs, HA nanofibers, and 1% HA-CNT nanofibers |                          |                      |                             |
| <b>Condition</b>                                                              | <b>MeanDiameter (nm)</b> | <b>Alignment (%)</b> | <b>Number of fibers (n)</b> |
| <b>Pristine CNTs</b>                                                          | 29.4 ± 7.4               | n/a                  | 100                         |
| <b>HA-CNT</b>                                                                 | 104.4 ± 24.2             | 9.6 ± 1.3            | 135                         |
| <b>HA Control</b>                                                             | 130.0 ± 30.8             | 12.6 ± 4.6           | 135                         |

nanofiber morphology (Figure 2-3 panel D, Table 2-1). Generation 1 Results tabulated in Table 2-1.

#### *Electrical Characterization*

Dry 1% HA-CNT nanofibrous mats were measured using four-point probe. Scaffolds 50 μm thick resulted in a sheet resistance of 34 MΩ.

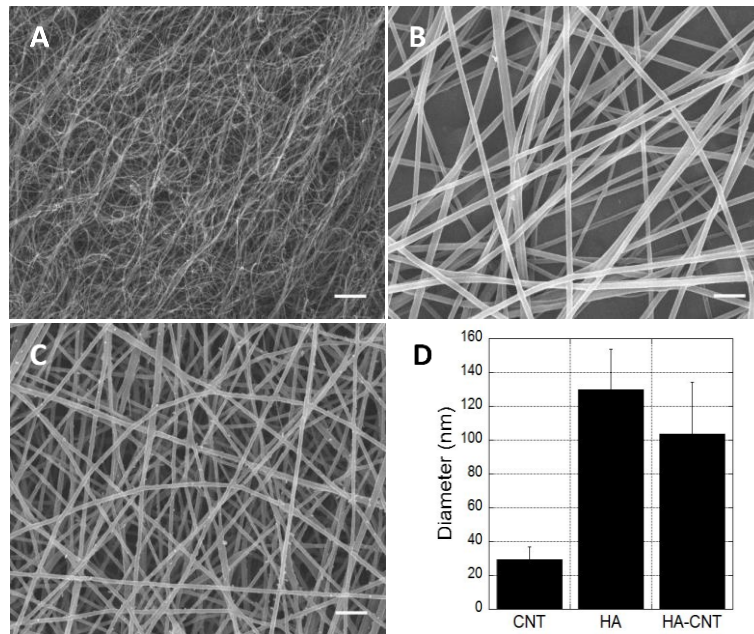


**Figure 2-3. Scanning Electron Micrographs of MWCNTs, HA and HA-CNT "Generation 1" Nanofiber Scaffolds.**

Scanning electron micrographs depict the topography of (A) pristine MWCNTs (B) HA nanofibers and (C) Generation 1 HA-CNT nanofibers with 1% CNT (w/w). (scale bar 1 μm) (D) Quantification of nanotube and nanofiber diameter confirms the average diameter of CNTs relative to HA and HA-CNT nanofibers are significantly smaller. The average diameter of HA and HA-CNT nanofibers are no different.

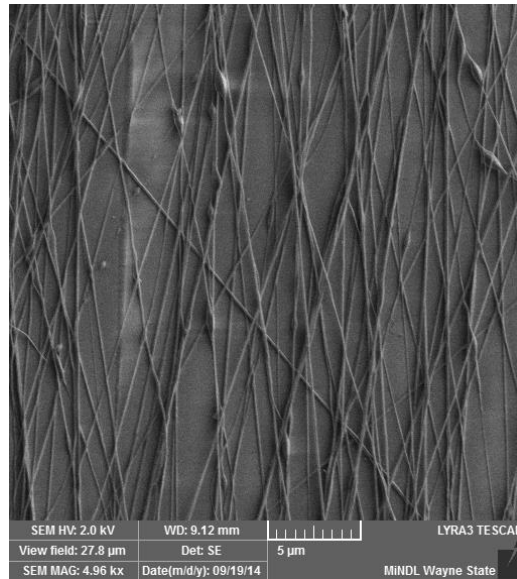


**Figure 2-4. Scanning Electron Micrographs of "Generation 1" Aligned HA-CNT Nanofibers.**

Increasing mandrel speed during electrospinning resulted in Generation 1 HA-CNT nanofibers with an aligned topography (scale bar 5 μm).

## Generation 2 HA-CNT

### *Topographical Characterization*

Nanofiber topography was characterized by scanning electron and transmission electron microscopy (Figure 2-5). SEM images revealed smooth nanofiber topography between the HA and HA-CNT conditions. The 0.5% HA-CNT nanofibers display rough patches in several areas where the CNTs disrupt the nanofiber surface. In the TEM images, aligned bundles of CNTs are visualized within the HA nanofibers.

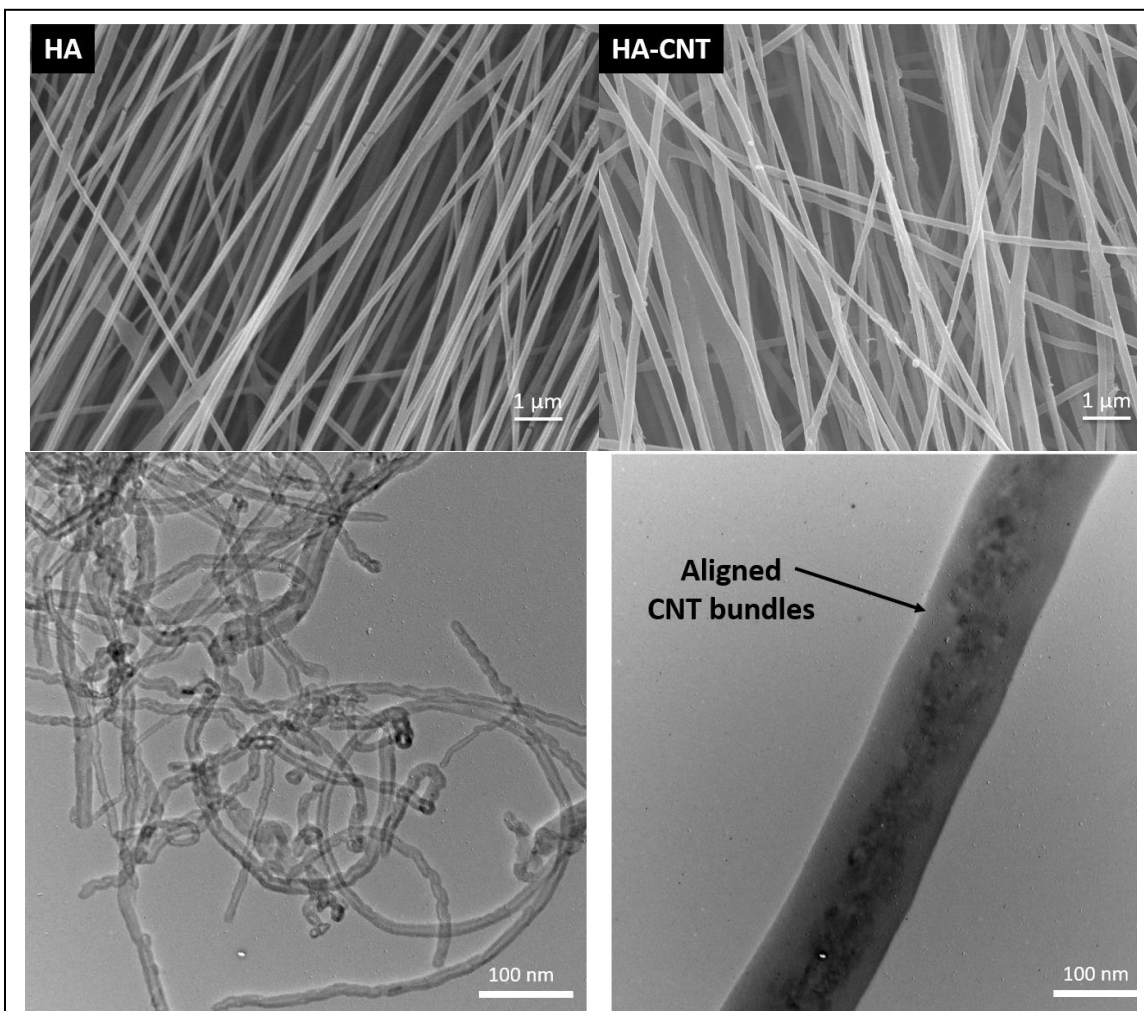
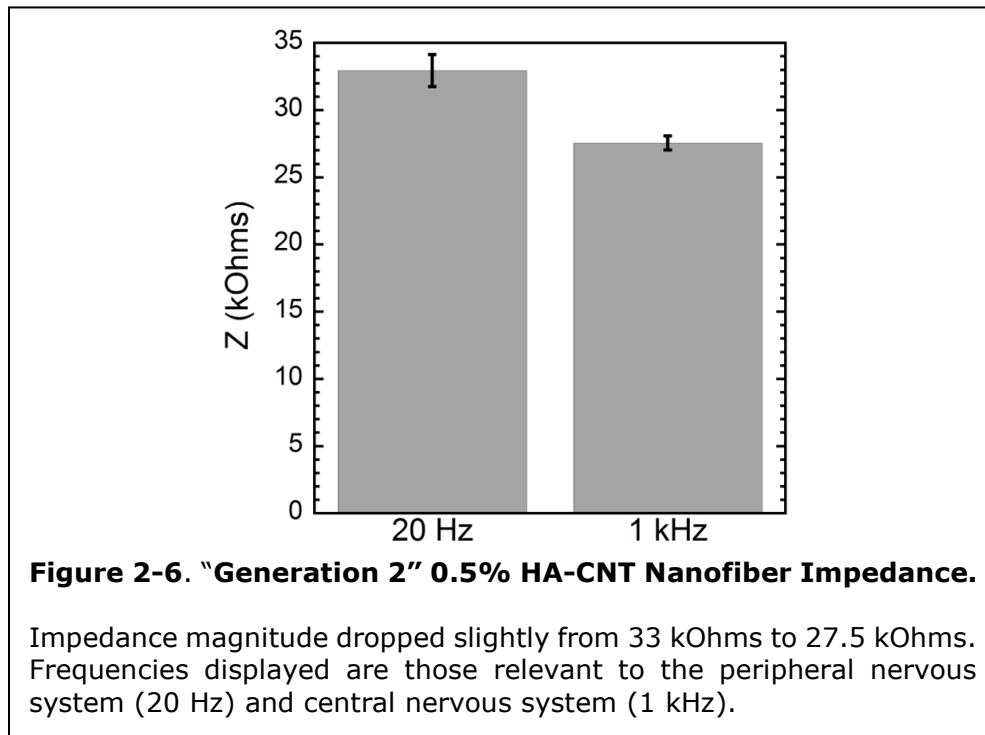


**Figure 2-5. Scanning Electron and Transmission Electron Micrographs of "Generation 2" Nanofibers.**

Top row: SEM micrographs of HA (left) and 0.5% HA-CNT (right).  
 Bottom row: TEM micrograph of supplier sourced COOH-MWCNTs (left) and aligned CNT bundle within HA nanofiber (right).

### Electrical Characterization

Electrical impedance results from Generation 2 HA-CNT nanofibers (0.5%) is displayed in Figure 2-6. Impedance was observed to decrease with increasing frequency.



### Generation 3 HA-CNT

Topographical and electrical characterization was performed on HA and 0.01%, 0.02% and 0.3% HA-CNT nanofibers. Surface and mechanical characterization was performed only on HA and 0.01% HA-CNT nanofibers once it was determined that optimal topography and electrical parameters were achieved with the 0.01% HA-CNT electrospinning formulation.

#### Topographical Characterization

The 0.01% CNT dispersion resulted in nanofibers with a smooth uniform surface, visually no different than the HA control nanofibers. Conversely, SEM revealed rough bumps on the surface of the 0.02% and 0.3% CNT nanofibers (Figure 2-7). These bumps were measured to be on the same size scale ( $\sim 120$  nm) as the agglomerates that breached the surface of the nanofibers imaged by TEM (Figure 2-8). Although there was a difference in fiber diameter calculated from SEM measurements ( $n = 100$  nanofibers) between HA ( $137.4 \pm 11.7$



nm) and 0.01% CNT ( $201.3 \pm 2.8$ ), there was no statistical difference in between percent alignment. Our transmission electron micrographs are consistent with TEM images of PEO/CNT (Dror et al., 2003) and PCL/silk fibroin/CNT nanofibers (Wu et al., 2017) demonstrating CNTs embedded within the nanofiber and aligned along the fiber axis. In Figure 2-8, the CNTs visualized in Panel A can be seen dispersed as bundles within the nanofiber in Panel B. Figure 2-8 panels C and D show that a poorly dispersed solution of CNT concentrations of 0.02% result in CNT aggregates protruding from the nanofiber surface. The protruding CNT aggregate in Figure 2-8 Panel C measures to be 129 nm in diameter parallel to the nanofiber axis. Measurements of rough features in 0.02% HA-CNT nanofibers like those in Figure 2-7 are approximately 114 nm.

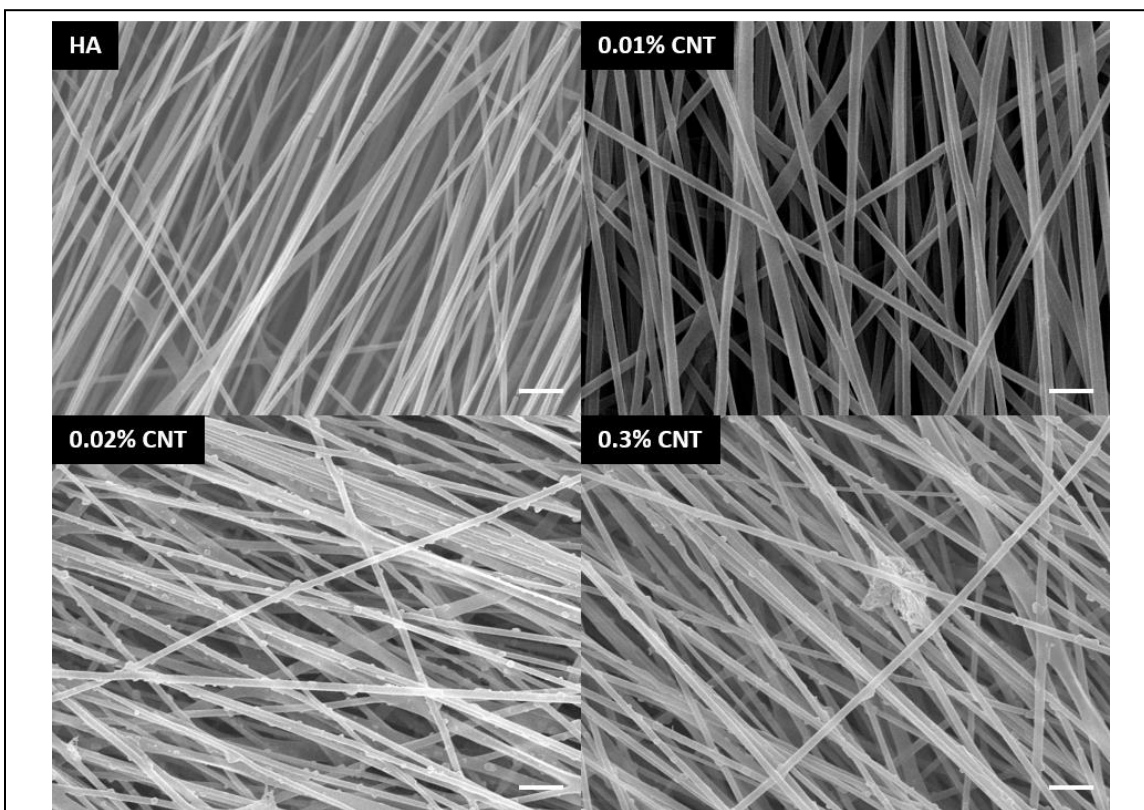


**Figure 2-7. Scanning Electron Micrographs of “Generation 3” HA-CNT Nanofibers.**

SEM micrographs of varying w/v concentrations of CNTs electrospun into HA nanofibers (scale bar = 1  $\mu\text{m}$ ). HA (upper left), 0.01% CNT (upper right), 0.02% CNT (bottom left) and 0.3% CNT (bottom right).

Three SEM micrographs (10,000 magnification) were analyzed to determine nanofiber diameter and alignment. A significant difference was found between fiber diameter but no significant alignment for HA and HA-CNT nanofibers (Table 2-3). HA nanofibers overall

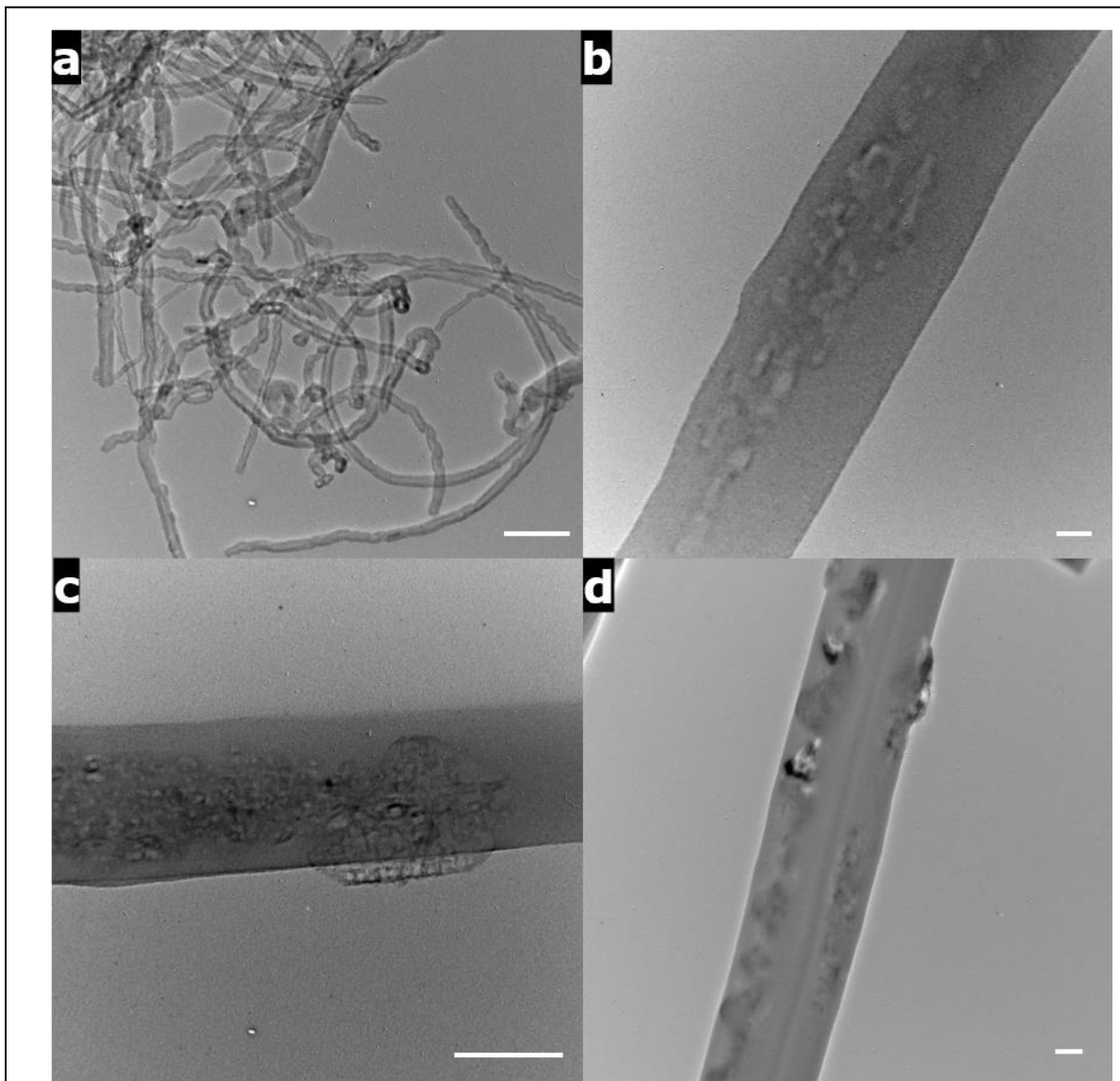


**Figure 2-8. Transmission Electron Micrographs of "Generation 3" HA-CNT Nanofibers.**

TEM micrographs of (a) COOH-MWCNTs (scale bar = 100 nm, Cheaptubes.org), (b) 0.01% HA-CNT nanofibers (scale bar = 20 nm). TEM micrographs in (c) and (d) are representative of nanofibers spun from formulations with higher concentrations of CNTs (scale bars = 100 nm). Nanofiber morphology at this size scale is consistent with the surface roughness observed in SEM at lower magnifications. TEM shows clear evidence of CNT agglomerates hanging out of the fiber.

exhibited a 75% alignment while the HA-CNT were measured to be 63%. Diameters were on the nanoscale with measurements of  $137 \pm 12$  and  $201 \pm 38$  for HA and HA-CNT, respectively.

#### *Electrical Characterization*

HA and HA-CNT (0.01%, 0.02%, and 0.3%) HA-CNT nanofibers were characterized for their resistance to passing current (impedance) and ability to store charge (CV). Graphical results are depicted in Figure 2-9. EIS results indicate that the agglomerations present in the TEM/SEM images for the 0.02% and 0.3% CNT HA-composites increase the impedance of the nanofibers. The 0.01% HA-CNT composite indicates the lowest impedance across the frequency scan, while there is some overlap amongst the other groups at frequencies 100 Hz and lower. Relevant frequencies for the nervous system are 20 Hz (peripheral) and 100 Hz (central). Relative to HA, the 0.01% HA-CNT composite exhibits a modest decrease in impedance by a factor of 1.7 at 20 Hz and 1.2 at 1000 Hz. Analysis of the cyclic voltammetry data was performed to quantify relative specific capacitance values to HA using a method previously described (Yi et al., 2015). CV results reveal that the specific capacitance of the 0.01% HA-CNT material doubles over HA (results tabulated in Table 2-2). Notably, the nanofibers fabricated from the 0.02% and 0.3% CNT dispersion solutions exhibited poor electrical properties as evidenced by increased impedance and decreased specific capacitance. CNT aggregation at higher concentrations decreased CSC and increased impedance compared to well-dispersed formulations.

**Table 2-2. "Generation 3" Electrical Characterization Summary.**

| Sample          | Impedance (k $\Omega$ )<br>at 20 Hz | Impedance (k $\Omega$ )<br>at 1 kHz | Specific<br>Capacitance<br>(mF/cm <sup>2</sup> ) |
|-----------------|-------------------------------------|-------------------------------------|--------------------------------------------------|
| HA              | 17.5                                | 6.3                                 | 15.3                                             |
| 0.01%<br>HA-CNT | 10.3                                | 5.2                                 | 32.3                                             |
| 0.02%<br>HA-CNT | 17.6                                | 9.1                                 | 13.5                                             |
| 0.3%<br>HA-CNT  | 22.4                                | 11.2                                | 8.9                                              |

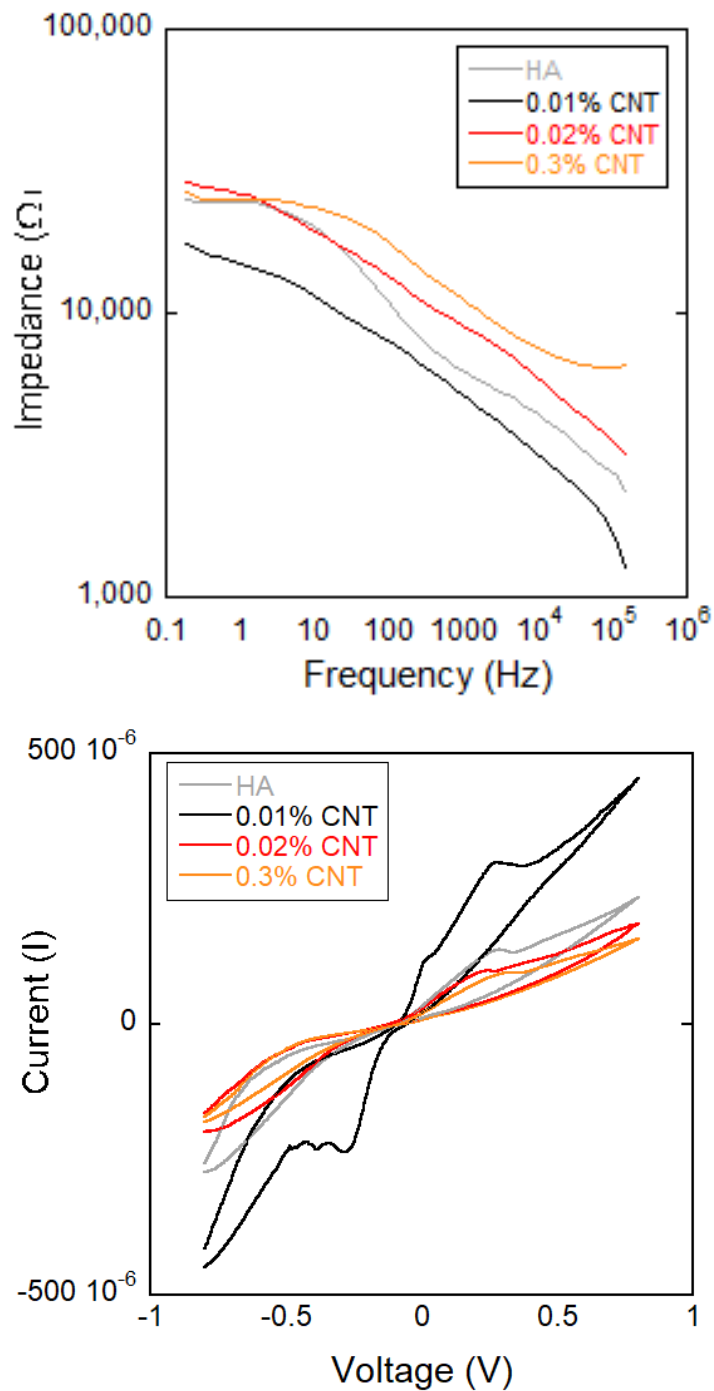


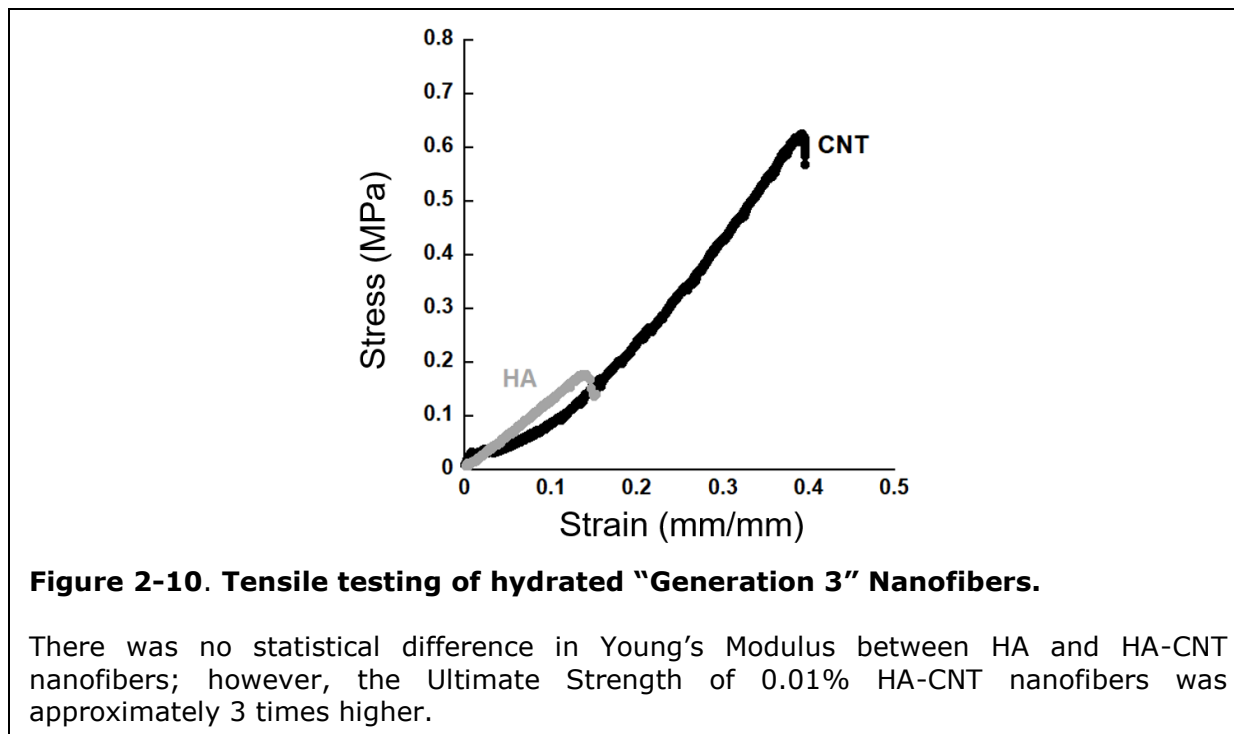
**Figure 2-9. Electrical Characterization of "Generation 3" Nanofibers.**

Electrochemical behavior of HA and HA-CNT (0.01%, 0.02%, 0.3%) nanofibers was characterized by impedance spectroscopy (top panel, impedance magnitude) and cyclic voltammetry (bottom panel). Impedance decreased by a factor of 1.7 at 20 Hz and 1.2 at 1k Hz (top) and charge storage capacity (CSC) doubled in 0.01% CNT versus HA nanofibers (bottom).

## Mechanical Characterization

### Bulk tensile testing

The Young's modulus for bulk mechanical testing was not statistically different between HA and HA-CNT nanofibers (Table 2-3). The ultimate strength of the HA-CNT nanofibers was three times higher than the HA nanofibers. Typical stress-strain curves are shown in Figure 2-10.



### Local Modulus Mapping

PeakForce QNM mode in fluid (Bruker Bioscope Catalyst) was utilized to measure local modulus values of hydrated HA and HA-CNT nanofibers. Absolute calibration of Bruker DNP-D tips (nominal spring constant 0.06 N/m) was conducted using the Bruker Standard fused silica, titanium roughness, and 2.5 MPa PDMS samples to determine deflection sensitivity, tip half angle, and tip radius. Thermal tune was conducted in fluid prior to imaging nanofiber samples fully hydrated to equilibrium in PBS. Additional parameters were set with Poisson's ratio as 0.30, PeakFrequency 250 Hz, PeakForce amplitude 1000 nm, lift height 300 nm, Sync Distance QNM ~600 nm, and PeakForce setpoint at 2-4.25 nN.

The Young's Modulus was calculated by applying the Sneddon model using first the Baseline Correction and then Indentation Analysis functions in the Bruker NanoScope Analysis 1.5 software package. Figure 2-11 displays the average Young's Modulus obtained from averaging 10 force curves obtained from N = 3 PeakForce Capture scans of HA and HA-CNT nanofiber samples (10 nm x 10 nm, such as those in Figure 2-11 panels E, F). Figure 2-12 displays AFM QNM PeakForce Capture images hydrated HA nanofibers (panels A, C, E) and hydrated HA nanofibers (panels B, D, F). Mechanical characterization results are summarized in Table 2-3.

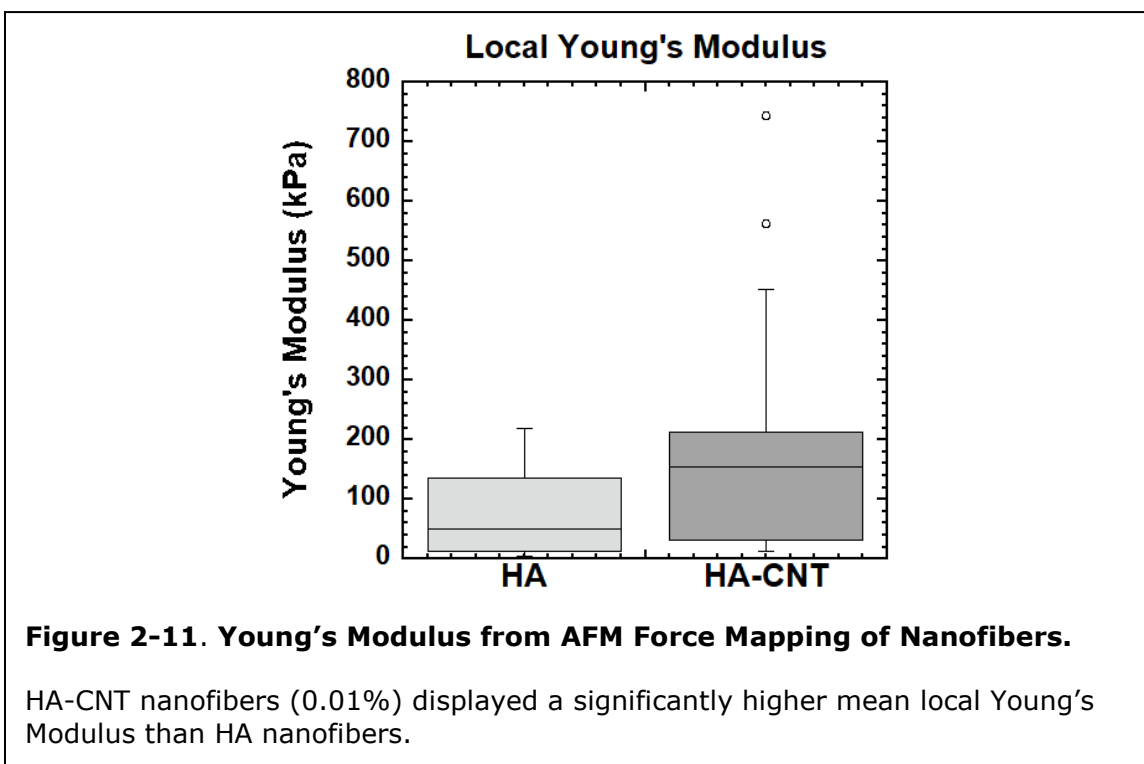


**Table 2-3. "Generation 3" Topographical and Mechanical Characterization Summary.**

| Fiber Type | Fiber Diameter (nm) | Fiber Alignment (%) | Contact Angle* (°) | Bulk Modulus (MPa) | Ultimate Strength* (MPa) | Local Modulus* (kPa) |
|------------|---------------------|---------------------|--------------------|--------------------|--------------------------|----------------------|
| HA         | 137 ± 12            | 75                  | 43.9 ± 2.5         | 1.471 ± 0.26       | 0.208 ± 0.04             | 74.93 ± 12.6         |
| HA-CNT     | 201 ± 38            | 67                  | 39.7 ± 4.3         | 1.769 ± 0.26       | 0.582 ± 0.08             | 174.85 ± 31.9        |

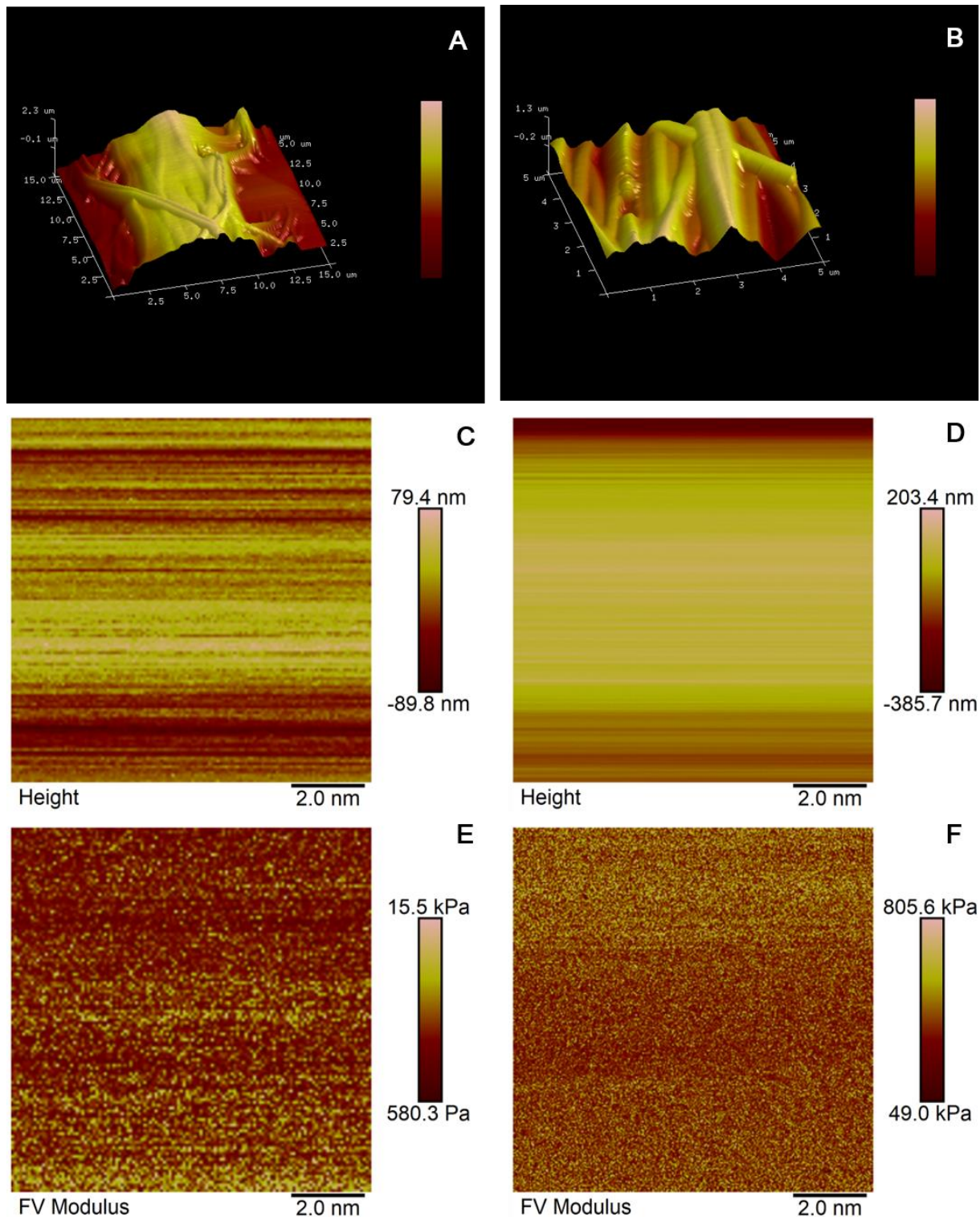


**Figure 2-12. Quantitative Nanomechanical Mapping by Atomic Force Microscopy.**

Fluid Imaging of hydrated nanofibers immersed in PBS (A) Hyaluronic acid nanofibers displayed swelling behavior that decreased distinct nanoscale topography relative to the morphology of (B) HA-CNT nanofibers. (C, D) Height images and (E, F) Force Volume images of 10 x 10 nm scan of the nanofiber samples displayed in (A,B). Local modulus determined by scanning with a calibrated tip with PeakForce Capture enabled and applying the Sneddon Model to fit force-displacement curves.

### Contact Angle

The surface of HA-CNT nanofiber substrates was measured to be more hydrophilic in the direction perpendicular to nanofiber orientation using a surface contact angle method and goniometer. The droplet volume was 3  $\mu$ l and experiments were conducted in an ambient environment. Contact angle was found to be higher for HA-CNT perpendicular to fiber orientation. There was no significant difference found when comparing the contact angle parallel to fiber orientation between HA and HA-CNT. Figure 2-13 provides representative sample images.



**Figure 2-13. Representative contact angle measurements for “Generation 3” HA and 0.01% HA-CNT nanofibers.**

### Discussion

The Generation 3 HA-CNT electrochemical characterization data taken in conjunction with the evidence of CNT agglomeration from SEM and TEM leads us to conclude that aggregated CNTs inhibit efficient electron flow. Highly aggregated and poorly dispersed CNTs throughout the nanofibers act as the equivalent of frayed wiring, effectively shorting out the ability of current to pass through the substrate. CNT agglomeration has been shown to decrease conductivity in composites with carbon nanofillers (J. et al., 2007; Sebastian et al., 2018). Increases in interfacial area of nanostructured surfaces are known to decrease material impedance (Cui et al., 2001; Yi et al., 2015). The primary factor influencing the decrease in impedance observed with the HA-CNT nanofibers versus HA is the increased interfacial area that would arise from well-formed, lesser swollen nanofibers. We observed increased swelling in the HA substrates during AFM fluid imaging.

Contact angle measurements indicate that the surface of the HA-CNT nanofibers may be more hydrophilic in the direction of the nanofiber alignment than the HA control nanofibers.



FTIR spectra qualify the presence of COOH- groups in the multi-walled carbon nanotubes used in both our Generation 1 and Generation 2/Generation 3 HA-CNT nanofibers. The main difference between COOH-MWCNTs in Generation 1 HA-CNT and Generation 2/3 was carbon nanotube supplier. The MWCNTs reported in Generation 1 were generously supplied by Wayne State University (WSU) Electrical Engineering Professor Mark Ming-Cheng Cheng and fabricated by Wenwen Yi during her Ph.D research. Dr. Yi and Dr. Cheng collaborated with the WSU BME department to demonstrate the application of an aligned MWCNT electrode interface with parylene to rat peripheral nerve stimulation and recordings (Yi et al., 2015). Once initial Generation 1 HA-CNT nanofibrous scaffold assays provided confirmation for the potential of the composite to promote neuron regeneration, COOH-MWCNTs were obtained from a commercial supplier that matched specifications discussed previously in terms aspect ratio, chemical functionalization. FTIR confirms the presence of -COOH moieties relative to pristine MWCNTs and COOH-MWCNTs, both those functionalized in-house by EM Steel by the standard strong acid method as well as those supplied by Cheaptubes.com. The as-received COOH-MWCNTs were not be stable long-term in deionized water or PBS solution, thus necessitating further investigation on methods to achieve a stable dispersion.

Extensive experimental data in the literature provides evidence that aligned nanofibers provide physical guidance to the extending neurites of regenerating neurons, including a synergistic effect on neurite length upon introduction of an electrical cue (Jin et al., 2011a, b; Jin et al., 2013; Jin et al., 2016; Koppes et al., 2014b; Xie et al., 2009a). Here, we provide clear quantified data supporting the ability to fabricate hydrophilic carbon nanotubes enclosed within hyaluronic acid by the electrospinning method. Unique to our formulation is the ability to achieve these material properties using an aqueous fabrication formulation with an ultra-low carbon nanotube weight percentage without the need for organic solvents. The differences in alignment as measured from dry samples imaged under vacuum are negligible under hydrated conditions. Observations with AFM height data (5  $\mu\text{m}$  scale) with HA-CNT versus (15  $\mu\text{m}$  scale) with HA to probe for distinguishing fiber characteristics provided qualitative

comparison that HA nanofiber topography is inconsistent and not reproducible upon reaching equilibrium swelling. Further, attempts to collect AFM height data at 5, 10, 15  $\mu\text{m}$  scales provided insight as to the effect the swelling behavior had on sample stability. Locally, nanofibers were not stably fixed to the underlying glass substrate resulting from apparent unpredictable and uncontrolled substrate morphology. During *in vitro* cell culture experiments, the pronounced HA nanofiber swelling observed over different culture times (24h versus 72h) could potentially account for some of the differences seen in neurite extension parameters measured. While substrate swelling and degradation rate were material properties not explicitly characterized in this body of work, the two parameters have been shown historically in the literature to be interconnected. Increased water retention within the hyaluronic acid supramolecular polymer matrix provides increased opportunity for hydrolytic degradation mechanisms. Proteolytic degradation by hyaluronidase is required for full breakdown of the polymer; degree of methacrylation provides a mechanism to control degradation further. Most instructive from the characterization described here in our composite polymer system is the theory that the CNTs physically entangled with HA molecules acting serving as a filler not only for electrical conduction but also as a mediator of nanofiber topography by reducing the amount of water molecules that could infiltrate between polysaccharide side groups as reported extensively in the molecular modeling literature through the 1990s (Haxaire et al., 2000).

Reports in literature regarding difficulty in engaging with the surface of low modulus biomaterial substrates corroborate with our difficulty in measuring local modulus properties for collagen, HA hydrogels, and HA nanofibers (Ouasti et al., 2011). Ouasti, et. al. switched to performing nanoindentation in "hydrated" state versus fluid immersion. In this body of work, we offer a method to map the nanomechanical properties of hydrated biopolymer nanofibers using AFM QNM in Fluid. While it is possible to obtain this data, it is critical to consider sample preparation and fixation to prevent micromotion during imaging, load amplitude and frequency (PeakForce closed loop mode), ramp amplitude (deformation control

mode), ramp rate, cantilever calibration and characterization. However, differences in moduli by mode of data collection (local versus bulk) may indicate that HA on the nanoscale responds to load in more viscoelastic behavior while in the bulk material indicates that HA nanofibers behave more elastic. This behavior is opposite in the composite, where the CNT clusters physically inhibiting adjacent movement of water molecules and reducing number of water molecules intercalated throughout the matrix results in a more plastic deformation on the nanoscale while on the bulk scale, there is a viscoelastic toe-in region observed.

The limitations of the mechanical characterization experiments and this interpretation is that the bulk tensile testing was performed using a 50N load cell with a load cell sensitivity (0.05 N) that was being operated toward the lower range of its sensitivity due to the low modulus of the hydrated nanofiber mats. Bulk testing was performed with a 1% strain following a pre-loading scheme that employed a 0.01% strain rate 0.02 N trigger value as measured by the load transducer. The trigger value of 0.02 N (the predictable and reproducible lower limit just above the noise threshold of the force sensor). Future bulk testing experimentation under physiological conditions could be successful using a 5N load cell. The other option would be to electrospin nanofiber mats 2-3x thicker (7 and 10 ml thicknesses were investigated, with the 10 ml thicknesses being reported here). We opted to forego this line of testing in the present body of work due to the amount of MeHA that would be required to fabricate the samples relative to the perceived value of data acquired from such a study (cost to benefit assessment of materials).

Pioneering work using biomacromolecules such as hyaluronic acid to modify and control the microenvironment with various cues to influence cell function provides background into the rheological behavior of HA hydrogels. Electrospun HA nanofibers are essentially hydrogels in a controlled cylindrical fiber structure. Control of mechanical properties using varying degrees of methacrylation, either in traditionally casted hydrogels (Burdick et al., 2005) or in nanofibrous mats (Sundararaghavan and Burdick, 2011). Mechanical property characterization techniques include measurement of rheological modulus (reduced modulus,

G\*) (Burdick et al., 2005), moduli from nanoindentation (Ouasti et al., 2011) or AFM (Sundararaghavan and Burdick, 2011), or bulk tensile modulus (Whitehead 2017). Limitations to comparing our local modulus values to the existing biomaterials literature requires the assumption of the Poisson's ratio; while we consulted the literature to arrive to this value, not all literature reports of mechanical data as measured by AFM enumerates the assumed Poisson's ratio which further complicates comparison. The data reported here assumes a value of 0.3 for the Poisson's ratio (Boudou et al., 2006; Fung, 1989; Lin, 2008; Mow et al., 1989) while elsewhere values from 0.45 - 0.5 are employed assuming a nearly incompressible material (Caliari and Burdick, 2016). A Poisson's ratio assumption can result in 10-20% difference in reported modulus. Seidlits et al reported spatial variations in local modulus over 70 x 70  $\mu\text{m}$  areas of methacrylated hyaluronic acid hydrogels, with an average of  $7.2 \pm 0.03$  kPa (Poisson's ratio not reported) (Seidlits et al., 2010). A hyaline cartilage structural biology study studying the effects of staining on the mechanics of the hyaluronic acid rich extracellular matrix used a Poisson's ratio of 0.35. These two example studies are consistent with our reports in achieving spatial variation in Young's Modulus. The hyaline cartilage study reported Young's moduli of  $265 \pm 53$  kPa for pericellular matrix (PCM) and  $636 \pm 123$  kPa for interterritorial matrix (ITM). Compositionally, PCM is high in hyaluronic acid and Type VI collagen whereas ITM contains high amounts of aggrecan and Type II collagen as well as Type IX and Type XI collagens and keratan sulfate. Comparatively, native peripheral nerve extracellular matrix secreted by Schwann Cells is high in type IV collagen, laminin, and type V collagen (Rutka, 1988). High concentrations of hyaluronic acid associated with GAGs are located at the nodes of Ranvier suggesting a role in homeostatic functions (Rutka, 1988). Recently, hyaluronic acid has been implicated in modulating synaptic calcium channel activity (Kochlamazashvili et al., 2010a). Our HA-CNT biopolymer ECM mimic matches both the topography and mechanics necessary for promoting nerve regeneration, while also offering a functionally relevant biological and biochemical interface to regenerating neurons.

Recently, catechol functionalized hyaluronic acid (HA-CA) hydrogels incorporated with 0.5 % single-walled carbon nanotubes were reported to have an impedance of 1.94 c at frequencies below 10 Hz as well as an Elastic Modulus on the order of 1.2 kPa (Shin et al., 2017). The HA-CA conjugate solution was reported to facilitate dispersion of SWCNTs whereas incorporation into traditional methacrylated hyaluronic acid (HA-ME) produced large agglomerates. Our dispersion technique using 1% BSA saline facilitated dispersion leading to successful nanofiber fabrication without CNT agglomeration for our 0.01% HA-CNT conditions using carboxylated carbon nanotubes. While Shin and colleagues achieved a lower impedance with their HA-CA CNT hydrogels, their CNT material was not functionalized. Carboxylation of CNTs can lead to lower conductivity, perhaps partially accounting for their 1.94 k $\Omega$  relative to our 10.3 k $\Omega$  impedance magnitude. The HA-CA CNT hydrogels also exhibited lower Elastic Modulus at  $\sim$ 1.2 kPa than our 1% HA-CNT nanofibers which were approximately 174 kPa. The lower conductivity and higher Elastic Modulus in our nanofibers may be a function of the nanofiber structure versus the bulk hydrogel structure.

Polymeric network mesh and porosity, monomer size, and extent of cross-linking affect not just mechanics and degradation of the material but also diffusion of ions throughout the polymer network (Bhattacharyya et al., 2008a; Peppas et al., 2000). Seidlits reported fluorescent dye diffusion that supports the concept that diffusion of molecules through methacrylated hydrogels can differ dependent on structure. HA and HA-CNT polymeric networks could be assessed in the future by time lapse microscopy to capture the diffusion rates of DAPI or toluidine blue to measure differences in crosslinking density, porosity, and CNT entanglement within the polymeric network in terms of barrier to ion diffusion (Allen and Mao, 2004; Seidlits et al., 2010). Toluidine blue strongly binds to electronegative moieties and is used commonly in orthopaedic histomorphology studies to ascertain extracellular matrix structure (Allen and Mao, 2004). Future investigation using simple methods to elucidate polymeric network and local electronegative side chain concentrations in turn may

provide functional insight into how current passes through HA and HA-CNT materials upon voltage application and thus activate voltage-gated ion channels.

## **Conclusions**

There are reports in the neuroscience literature successfully using conductive hyaluronic acid and carbon nanotube biomaterial composites to support neuronal growth, such as SWCNT-HA hydrogels (Shin et al., 2017; Thompson et al., 2009) and SWCNT-HA fiber microelectrodes (Lynam et al., 2009; Razal, 2008). These preceding reports of hyaluronic acid single-walled carbon nanotube composites exhibit higher conductivity than our SI converted conductivity of 68 mS/m, HA-SWCNT microfibers were measured to be  $1.86E07$  mS/m (Lynam et al., 2009) and 515 mS/m for HA-CA SWCNT hydrogels (Shin et al., 2017). Advantages of our HA-CNT material includes nanoscale topography, electrical conductivity, and  $<1$  MPa Elastic Modulus while the Lynam HA-CNT microfibers exhibited 5-8 GPa and the Shin hydrogels require cell encapsulation to achieve a 3D environment. Further, we are the first to report incorporation of MWCNTs into nanoscale diameter hyaluronic acid fibers using an aqueous formulation solution and the electrospinning fabrication technique.

Cumulatively considering the material characterization data, we have demonstrated the ability to fabricate conductive nanofibers by incorporating hydrophilic carbon nanotubes within aligned hyaluronic acid nanofibers with mechanical properties relevant to peripheral nerve ( $<1$  MPa) and fiber diameters on the nanoscale even when fully hydrated to equilibrium. Electroactivity as assessed by electrical impedance and charge storage capacity is significantly enhanced with the addition of an ultra-low concentration of well-dispersed COOH-MWCNTs.

Chapter 3 will explore the neuron cytocompatibility and fibroblast biocompatibility behavior observed when chick dorsal root ganglia are cultured on HA-CNT nanofibers in a series of attachment experiments on Generation 1, Generation 2, and Generation 3 scaffolds.

## **Chapter 3 : HA-CNT Nanofibrous Scaffolds Exhibit L-929 Fibroblast Biocompatibility and Support Neurite Outgrowth**

### **Introduction**

One of the clinical challenges in implementing medical treatments involving carbon nanotubes are the toxicological concerns. Chapter 1 introduced systemic toxicological evaluations that identified influential characteristics of carbon nanotubes (CNT)s that determine cytotoxicity and biocompatibility on a cell type dependent basis (Ahn et al., 2015; Arora et al., 2015; Firme Iii and Bandaru, 2010). These factors include CNT size, shape, functionalization, concentration, and agglomeration. have been characterized as influential factors in affecting cytotoxicity and biocompatibility on a cell type dependent basis (Arora et al., 2015; Firme Iii and Bandaru, 2010; Hopley et al., 2014). Chapter 2 described in detail the material characterization techniques employed to quantify the topographical, mechanical and electrochemical properties of hyaluronic acid-carbon nanotube (HA-CNT) nanofibers fabricated from an optimized formulation of 2% methacrylated hyaluronic acid and 2% polyethylene oxide (900,000 Da). Electrochemical characterization qualified the HA-CNT 0.02% and 0.3% wt. nanofibers as having higher impedance and lower charge storage capacity; these outcomes were attributed to the CNT agglomerations visualized in both tunneling and scanning electron microscopy. HA-CNT (0.01%) composite nanofibers were determined to have: (1) electrochemical properties of lower impedance and higher capacitance, (2) topographical properties of smooth nanofibers with reduced agglomeration, and (3) mechanical elastic modulus within the kPa range.

In Chapter 3, we will discuss the observations made during *in vitro* evaluation of HA-CNT nanofibers fabricated from three different formulations, termed as "Generation 1," "Generation 2," and "Generation 3." We provide evidence that 0.01% HA-CNT nanofibrous scaffolds are an appropriate material for a materials-based therapy for neural tissue engineering (NTE) through a series of *in vitro* cell characterization assays. The *in vitro* characterization methods described in this chapter are guided by the ASTM standard

“Standard Practice for Direct Contact Cell Culture Evaluation of Materials for Medical Devices,” also known as ASTM F813-07(2012). To translate a biomaterial to a specific biomedical application, it is necessary to follow guidelines like those outlined in ASTM F813 as a point of reference when determining whether a material is biocompatible.

First, we will present direct contact cell culture evaluation performed with 0.01% HA-CNT nanofibers using the L-929 cell line (ATCC, gift from Professor Olivia Merkel, Ludwig-Maximilians-Universität München). The L-929 cell line is well-characterized with demonstrated reproducibility for use in cytotoxicity testing as a first line evaluation for biomaterials which will have direct contact with cells and tissues in the body. Next, guided by ASTM F813, a second cell culture technique using a cell model relevant to the target tissue in which the material will be applied can demonstrate the compatibility of HA-CNT nanofibrous scaffolds to support neuron outgrowth. By establishing a reproducible *in vitro* neuron model relevant to the peripheral nervous system, we seek to demonstrate the cytocompatibility of HA-CNT nanofibers as a biomaterial for peripheral nerve regeneration.

Neuron behavior was evaluated by immunofluorescence analysis of cell morphology. Two significant outcomes result from the body of work presented in Chapter 3. First, we demonstrate a reproducible *in vitro* chick dorsal root ganglia (DRG) neuron model relevant to the peripheral nervous system. This *in vitro* neuron model protocol was optimized as we optimized the electrospinning formulation. We documented the advantages we observed from quantifying DRG single neuron morphology over DRG explant morphology. Secondly, we demonstrate the potential for HA-CNT nanofibers to be considered for the treatment of PNI as described in Chapter 1, by performing sequential assessment of proliferation of L-929 and cytocompatibility of dissociated DRG cultures on “Generation 3” HA-CNT.

To complete Aim 2, *in vitro* experiments were performed to determine cytocompatibility of L-929 fibroblasts and neurons behavior on HA-CNT nanofibers.



## **Experimental Methods**

### **General Procedures**

#### *Scaffold Fabrication*

Nanofibrous scaffolds were fabricated using the electrospinning techniques outlined in Chapter 2. Briefly, HA nanofibers were electrospun onto 12-mm diameter cover glass adhered to a rotating mandrel from an aqueous solution, ejected from a blunt 18G needle, containing 2% methacrylated hyaluronic acid (HA), 2% polyethylene oxide (PEO, 900kDa), and 0.05% I2959 photo-initiator for controls (HA). Variations in formulation and methods for HA-CNT nanofibers denoted as "Generation 1," "Generation 2," and "Generation 3" are discussed in detail in Chapter 2 and will be introduced briefly to provide context about the differences of CNT percent weight content. Nanofibrous scaffolds were cross-linked under a long wave UV light for 30 minutes and stored in a desiccator cabinet until use. For *in vitro* experiments, cover slips were transferred to a sterile cell culture plate under aseptic conditions and sterilized under long-wave UV for 20 minutes. Nanofibrous scaffolds were rinsed at least 3 times with sterile 1X PBS pH 7.4 prior to onset of culture experiments to remove PEO and allow MeHA to reach hydrated equilibrium (Burdick et al., 2005).

#### *Chick Dorsal Root Ganglia Neuron Cell Culture*

Dorsal root ganglia (DRG) were dissected from E9-E13 chick embryos. Eggs were incubated at 37 °C and ~60% humidity until dissection day. The egg plate was broken with EtOH sterilized forceps and the embryo was removed. The embryo head, internal organs, and skin were removed prior to plucking DRGs from the vertebral column with fine forceps. DRGs were transferred to ice cold HBSS until time of seeding for no more than 2 hours.

### **“Generation 1” HA-CNT *in vitro* Neuron Attachment**

Generation 1 scaffolds were fabricated with the formulation described above. Carboxylated multi-walled carbon nanotube source was produced in-house as described in Chapter 2, briefly pristine multi-walled carbon nanotubes were fabricated using chemical vapor deposition onto a silicon wafer, released, and underwent a strong acid treatment to remove iron oxide catalyst impurities and functionalize with –COOH groups following an established method optimized for our application (Kar and Choudhury, 2013). HA-CNT electrospinning solution containing 1% (w/w) CNT was electrospun onto a mandrel rotating at 10 m/s flow rate of 150  $\mu$ /h resulting in randomly oriented nanofibers. All other handling and standard culture techniques were the same as previously described.

A single intact DRG was dissected as described under the general procedures from E9-E11 embryos, then seeded in the center of each scaffold and allowed to adhere for up to 16 hours. The scaffold and DRG containing wells were then gently flooded with serum free media (SFM) composed of 1:1 v/v DMEM/Hams F-12 (Sigma), 2 mM L-glutamine, 50 U/mL penicillin/streptomycin (P/S, Sigma), 0.6% B27 supplement (Lonza, Allendale, NJ) and 50 ng/mL nerve growth factor (NGF, R&D systems, Minneapolis, MN) and cultured for 48h at 37°C at 5% CO<sub>2</sub>.

The FITC and DAPI channels were separated and then processed using a custom MatLab script which determined an automatic threshold from greyscale images, converted to binary, and summed pixels to quantify area. To measure relative growth, the FITC area was divided by the DAPI area to normalize for DRG body size. The major and minor axes of an ellipse fit to the peripheral DRG neurite area was used calculate aspect ratio, which is equal to the major axis divided by the minor axis.

### **“Generation 2” HA-CNT *in vitro* Neuron Attachment**

Generation 2 scaffolds were fabricated with the formulation described above with the several optimized parameters. Carboxylated multi-walled carbon nanotubes were sourced from an external supplier (Cheaptubes.com), with similar specifications to the in-house

fabricated CNTs used in Generation 1 (20-30 nm diameter, 20-30  $\mu\text{m}$  length). HA-CNT electrospinning solution containing 0.5% (w/w) CNT was dispersed within an aqueous solution containing 1% bovine serum albumin (BSA) in 0.85% physiological saline (1% BSA saline) and sonicated for 10 minutes using a standard ultrasonic cleaner bath (35kHz, 48W, VWR) adapting a technique reported in 2011 in Archives in Toxicology(Kim, 2011). CNT dispersion was suspended to form a working electrospinning solution with final (w/w) 2% HA, 2% PEO and 0.05% I2959 photo-initiator. Generation 2 formulation was electrospun onto a mandrel rotating at 18 m/s and using a flow rate of 900  $\mu\text{l/h}$  resulting in aligned nanofibers. All other handling and standard culture techniques were the same as previously described.

A single cell suspension of dissociated DRGs from intact DRGs dissected from E11 eggs were transferred from ice cold HBSS to 0.25% trypsin in a 15-ml conical tube and incubated at 37°C for 5 minutes followed by vortexing at maximum speed for 30 seconds. The tube was incubated at 37°C for 5 more minutes and vortexing was repeated. Trypsin was inactivated by adding 2 ml of DMEM with 10% FBS. The cell suspension was centrifuged for 3 minutes at 2000 rpm to isolate the cell pellet. The supernatant was discarded, and the pellet was triturated in 2 mL SFM. Dissociated neurons were counted using a hemacytometer and plated at a density of 6000-8000 cells/cm.<sup>2</sup> Cells were cultured under standard conditions for 48h.

At end of culture period, samples were gently rinsed with warmed 1X PBS pH 7.4 followed by fixation for 20 minutes with 4% paraformaldehyde and fluorescently labeled with a secondary goat anti-mouse FITC-conjugated Alexa Fluor 488 secondary antibody specific to an anti-mouse anti-neurofilament primary antibody. Nuclei were labeled with DAPI. Every neuron meeting exclusion criteria was imaged on each 12-mm dia. nanofibrous substrate cover glass using a 10X Short Path Length objective in each of 3 channels Bright Field, FITC, DAPI. Every neuron counted towards analysis was required to meet the following inclusion criteria: (1) single neuron with a (2) neurite extending at least twice in length of the diameter of the soma and (3) not contacting any other neuron. Assessment of inclusive cell morphology was cross-referenced between each of the BF, FITC, and DAPI channels. Statistical

significance was determined using F-test for sample variance and *Student's t-test* with  $\alpha = 0.05$  value considered for significance.

### **"Generation 3" HA-CNT**

#### *Nanofiber Fabrication*

Nanofibers were electrospun at 24kV ejected at a 1.7 ml/hr flow rate from an 18G blunt needle at 11 cm distance from a rotating mandrel (21.25 m/s) using an aqueous mixture of the dispersed CNT solution (1/3 v/v), 2% w/w MeHA, and 2% w/w PEO. Control hyaluronic acid nanofibers were electrospun using the same formulation but with deionized water in place of the CNT dispersion solution. Nanofibrous scaffolds were cross-linked under a long wave UV light for 30 minutes and stored in a desiccator cabinet until use. For *in vitro* experiments, cover slips were transferred to a sterile cell culture plate under aseptic conditions and sterilized under long-wave UV for 20 minutes. then rinsed at least 3 times with sterile 1X PBS pH 7.4 prior to onset of culture experiments to remove PEO and allow MeHA to reach hydrated equilibrium.

#### *L-929 Fibroblast Attachment*

L-929 were seeded onto scaffolds at a density of 25,000 cells/well in high glucose DMEM supplemented with 10% FBS and PenStrep and cultured at 37C, 5% CO<sub>2</sub> for 24h. Media supplemented with 10% Alamar Blue reagent (AB, Fisher) was replaced on cultures and incubated for 4 hours. Aliquots (100  $\mu$ l) were transferred to a flat-bottom 96 well plate using a spectrophotometer to measure absorbance following manufacturer's guidance. Experiment was repeated 3 times, each with  $n \geq 3$  culture samples (glass, HA, 0.01% HA-CNT) for each condition with AB assay performed in triplicate for each sample. A standard curve was generated from known seeding densities on glass coverslips cultured under same conditions within the same 24 well plate (0, 25k, 50k, 100k, 150k). Each treatment type (glass, HA, and HA-CNT) had a blank well in which media without cells served as a background reference for each cell culture sample. Statistical analysis was a one-way ANOVA with  $\alpha = 0.05$  for to determine significance.

### *in vitro* Neuron Attachment

In general, Generation 3 HA-CNT *in vitro* assays with neurons were conducted using lumbar dorsal root ganglia (DRG) dissected from E10-E13 chick embryos. Otherwise, dissociation and media formulation are the same as described in Generation 2 protocol. Two independent *in vitro* neuron attachment assays were performed. First, one trial of neurons from an E10 dissociation were seeded and cultured for 24h on HA and 0.01%, 0.02%, and 0.3% HA-CNT nanofibers (n = 3 culture samples of each nanofiber type). Second, 2 independent trials from E11 dissociations were seeded and cultured for each end-point time of 24h or 48h.

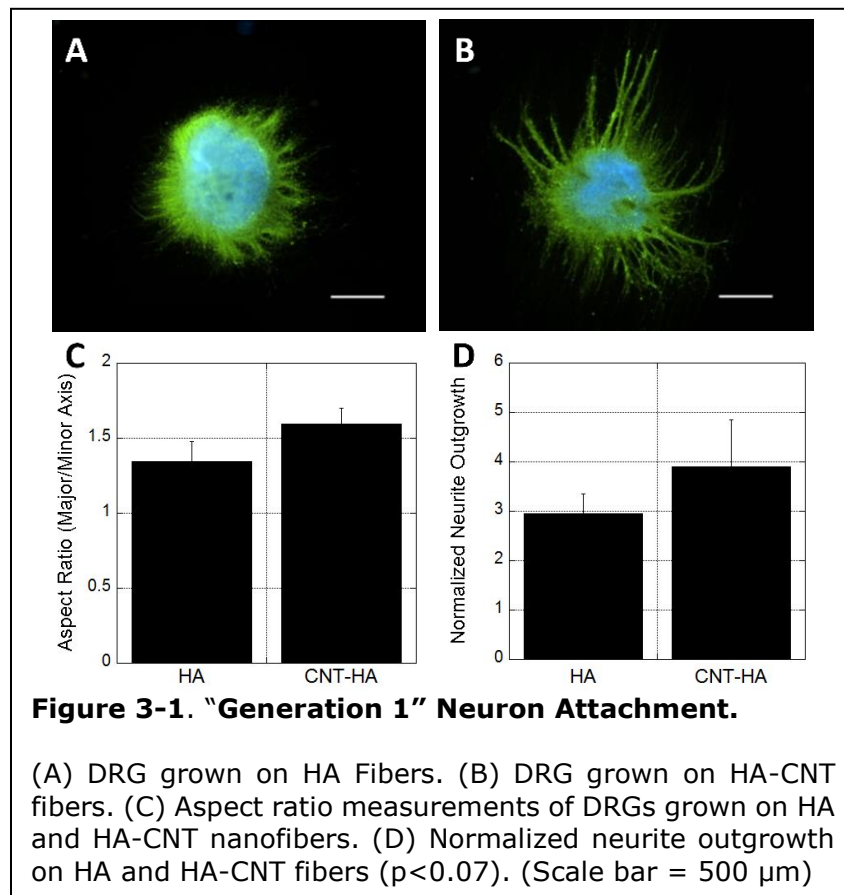
At end of culture period, samples were gently rinsed with warmed 1X PBS pH 7.4 followed by fixation for 20 minutes with 4% paraformaldehyde and fluorescently labeled with a secondary goat anti-mouse FITC-conjugated Alexa Fluor 488 secondary antibody specific to an anti-mouse anti-neurofilament primary antibody. Nuclei were labeled with DAPI. Every neuron meeting exclusion criteria was imaged on each 12-mm dia. nanofibrous substrate cover glass using a 10X Short Path Length objective in each of 3 channels Bright Field, FITC, DAPI. Every neuron counted towards analysis was required to meet the following inclusion criteria: (1) single neuron with a (2) neurite extending at least twice in length of the diameter of the soma and (3) not contacting any other neuron. Assessment of inclusive cell morphology was cross-referenced between each of the BF, FITC, and DAPI channels. Statistical significance was determined using F-test for sample variance and *Student's t-test* with  $\alpha = 0.05$  value considered for significance.

## Results

### “Generation 1” HA-CNT

#### *in vitro* Neuron Attachment

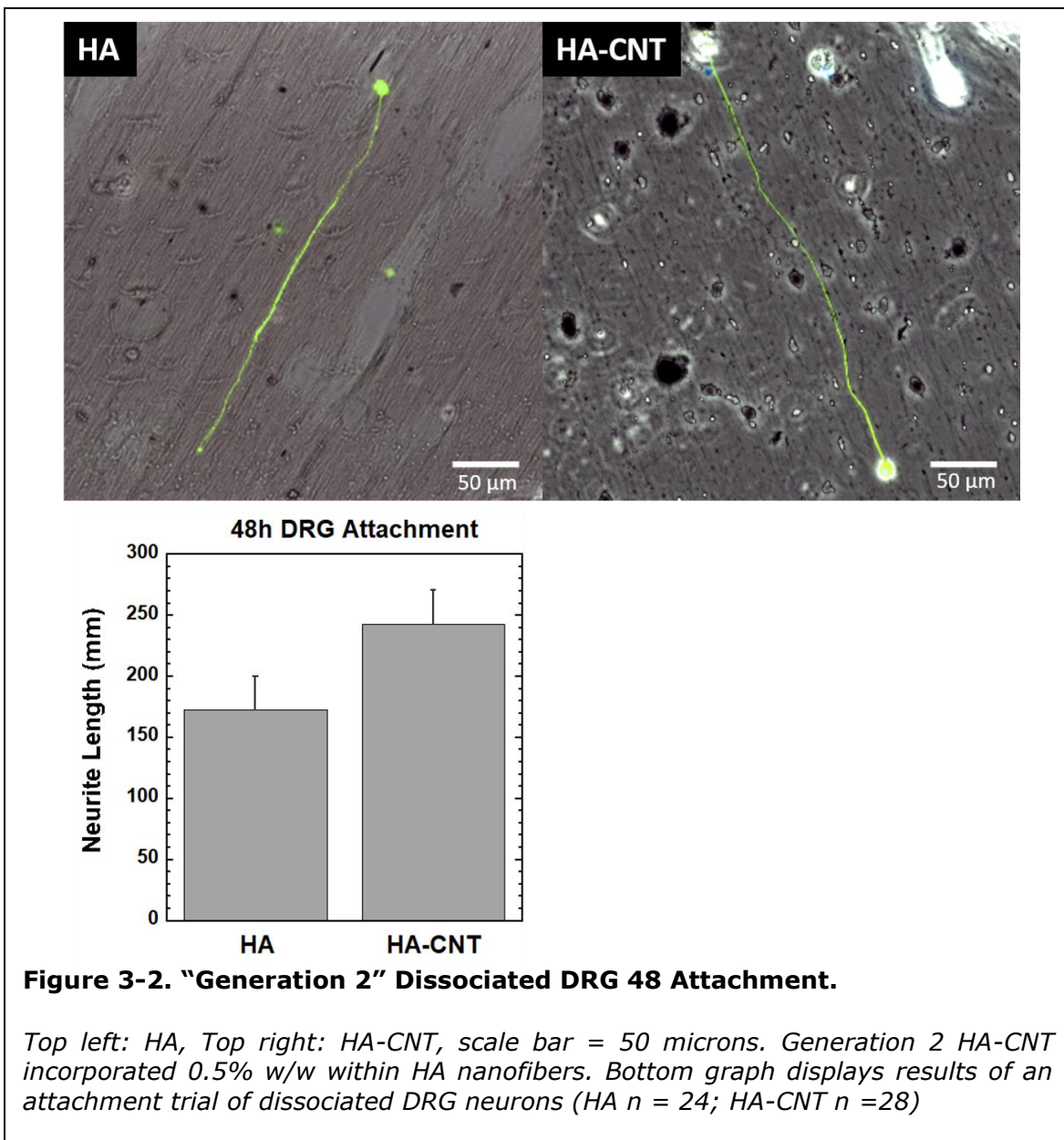
Preliminary attachment tests using whole DRGs from E9-E11 chicks revealed that 1% HA-CNT fibers had no observable negative effects on neurite outgrowth from the chick embryo DRGs. Rather, HA-CNT fibers appear to promote DRG attachment and encourage neurite outgrowth. Relative neurite outgrowth (measured as total neurite area/DRG body area) was  $4.31 \pm 1.09$  for the HA-CNT scaffolds and only  $3.18 \pm 0.33$  for control scaffolds (Figure 3-1). Student’s t-test revealed that relative neurite outgrowth was not statistically different, however,  $p=0.07$  indicates a strong trend towards improved growth on the composite nanofibers.



## "Generation 2" HA-CNT

### *in vitro* Neuron Attachment

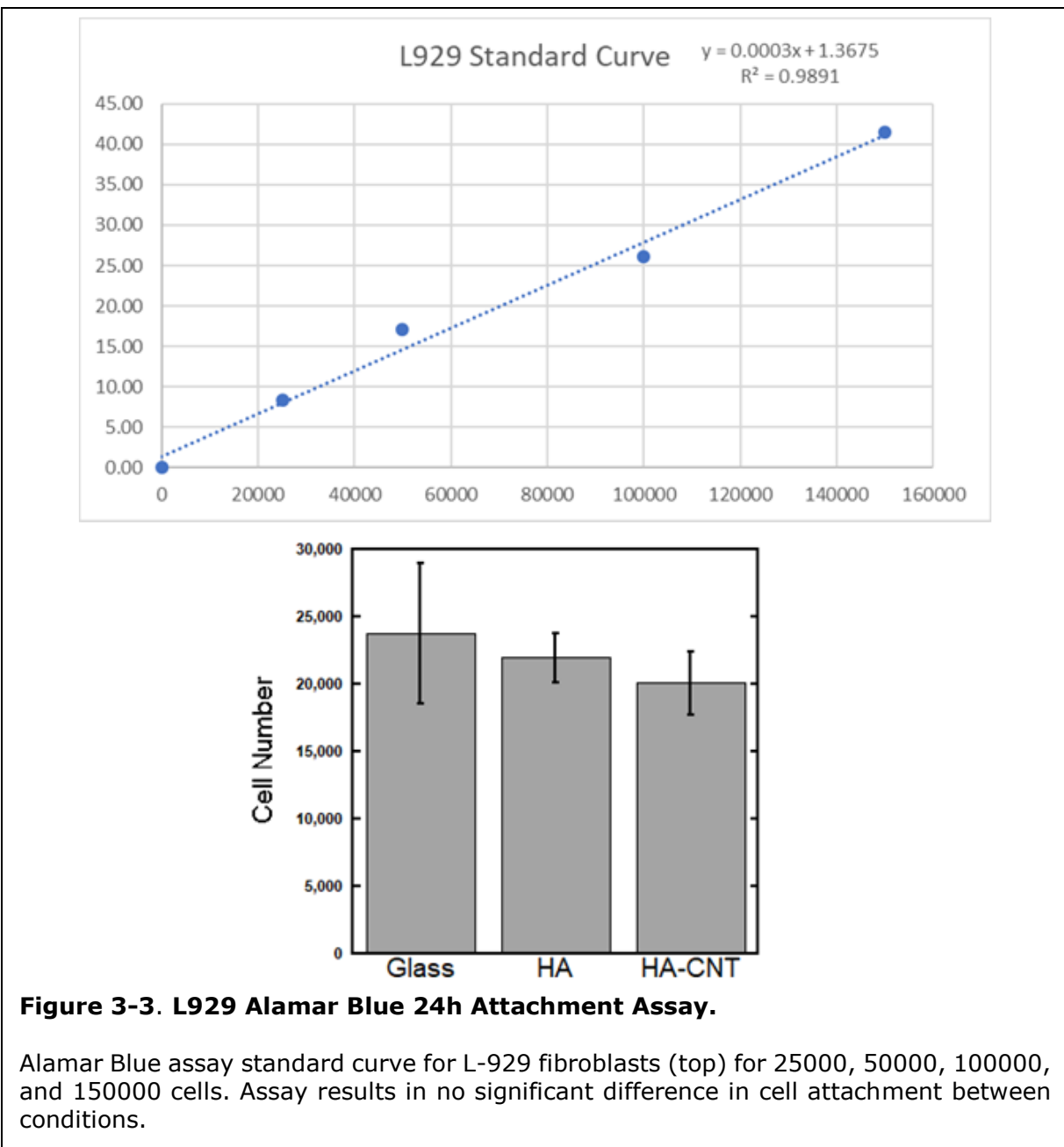
Dissociated E11 DRG neurons were cultured for 48h on aligned HA nanofibers electrospun either with or without CNTs. Generation 2 electrospinning solution for HA-CNT contained 0.5% w/w CNT/HA. Student's t-test revealed a significant increase in neurite length. Trial included n = 25 neurons for each condition.



### "Generation 3" HA-CNT

#### L-929 Fibroblast Attachment

The L-929 proliferation assay method produced reliable and reproducible results. Figure 3-3 (top) provides an example standard curve employed when comparing cell number 24h post-seeding to one another. There was no statistically significant difference in metabolic activity as assessed by Alamar Blue reduction between any substrate type.





*HA-CNT (0.01%, 0.02%, 0.3%) in vitro Neuron Attachment*

Figure 3-4 depicts the results from one trial of dissociated E10 chick lumbar DRG neurons seeded and cultured for 24h on HA and 0.01%, 0.02%, and 0.3% HA-CNT nanofibers (n = 3 culture samples of each nanofiber type). The number of neurons counted according to exclusion criteria for each scaffold type HA, 0.01% HA-CNT, 0.02% HA-CNT, and 0.3% HA-CNT were n = 29, n = 31, n = 43, and n = 23, respectively. Test for homogeneity resulted in unequal variances between the cell populations measured in the trial, thus eliminating the ability to perform a one-way ANOVA to test for effect of CNT concentration on the cell behavior outcome measure neurite length. Therefore, statistical analysis was conducted to compare each HA-CNT concentration type to the control HA nanofiber condition. An F-Test for variance between two sample samples was conducted for each comparison before choosing between a two-tail Student's t-Test assuming either Equal or Unequal Variance. HA and HA-CNT 0.3% exhibited no significant variance between one another, and no difference in neurite length using a Two-Sample Student's t-Test assuming Equal Variances. HA-CNT 0.01% and 0.02% conditions both did not pass the F-Test Two-Sample for Variances check prompting the associated Student's t-tests to be conducted assuming unequal variances. HA-CNT 0.02% did not result in an observed effect of CNT presence relative to HA on neurite length. HA-CNT 0.01% did result in an observed effect of CNT presence relative to HA on neurite length ( $p < 0.01$ ).

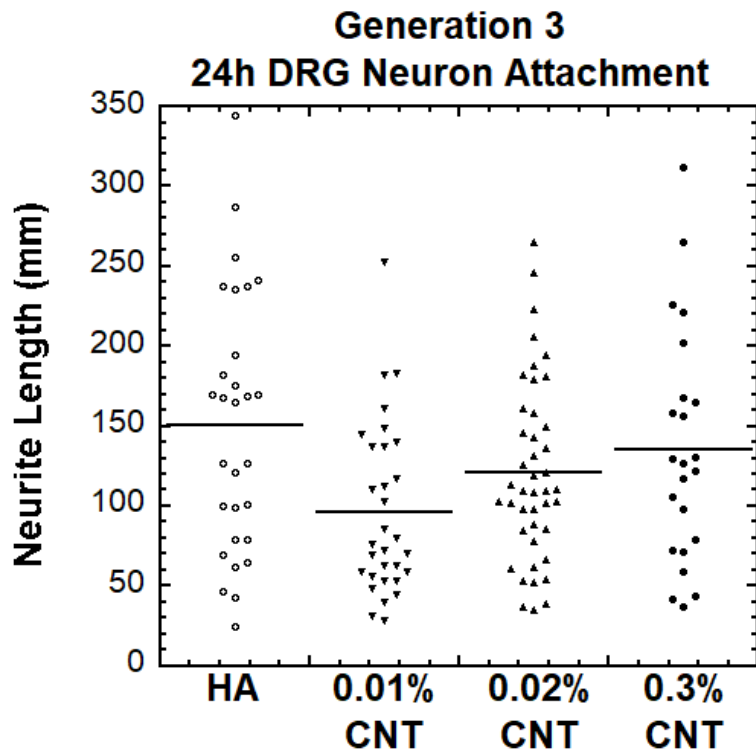
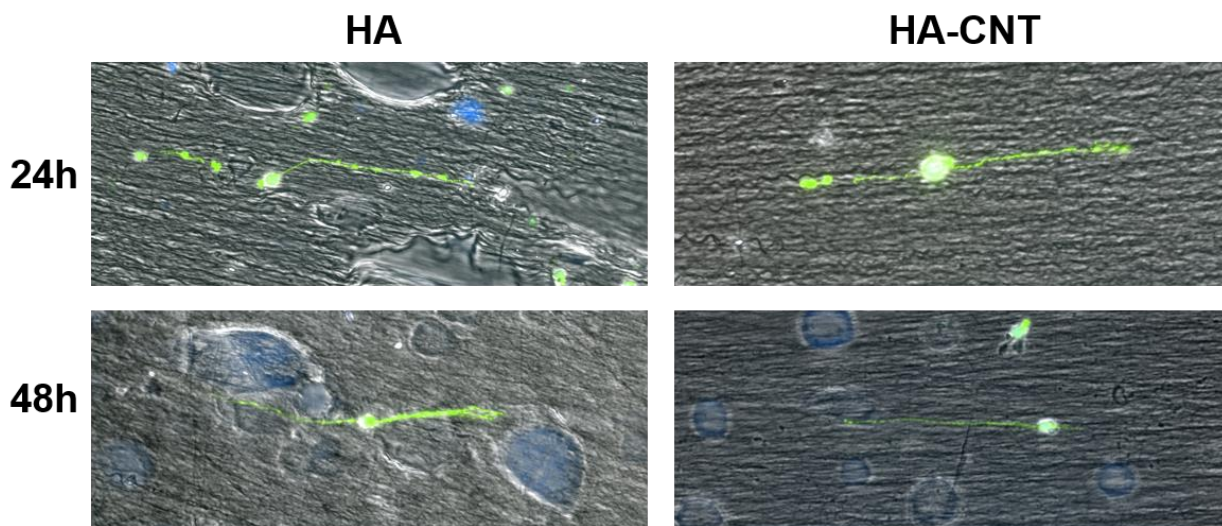


**Figure 3-4. "Generation 3" DRG Neuron 24h Attachment 0.01%, 0.02%, 0.3% HA-CNT Nanofibers.**

Dissociated DRGs from E10 chick embryos displayed varying neurite lengths dependent on percent CNT incorporated into HA nanofibers. Cumulatively considering the attachment data presented to this point prompted usage of lumbar DRGs explanted from E12-E13 chicks in future DRG dissociations.

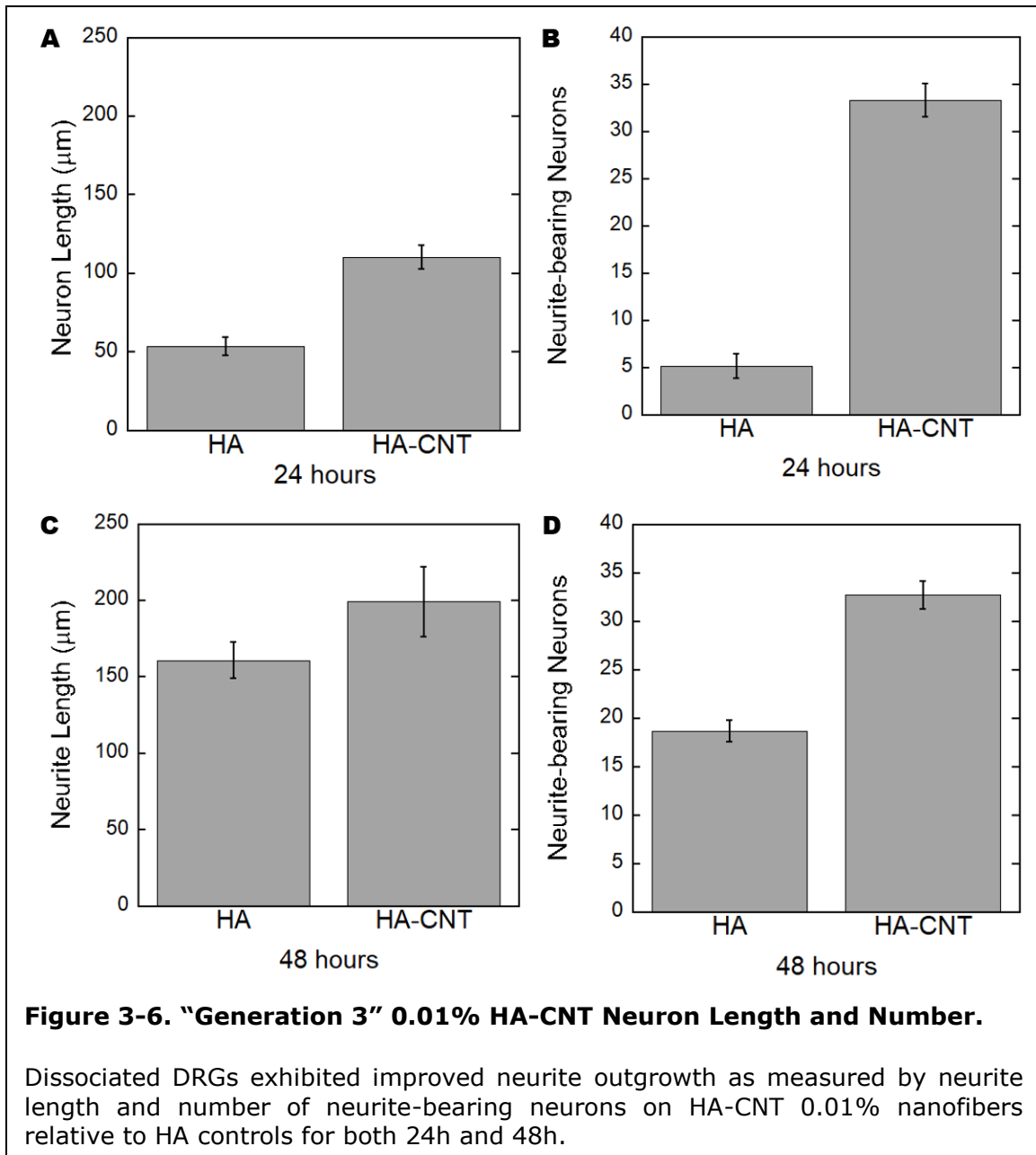
### *HA-CNT (0.01%) in vitro Neuron Attachment*

Figure 3-5 depicts epifluorescence images merged with bright field for E12-E13 DRG neuron dissociations cultured on HA and 0.01% HA-CNT nanofibers. Images represent neurons with neurite lengths which fall within the standard deviation. Neurons are labeled with FITC secondary antibody specific to primary anti-neurofilament antibody, DAPI labels the nuclei.



**Figure 3-5. "Generation 3" 0.01% HA-CNT Neuron Attachment.**

Mean neurite length and number of neurite-bearing neurons are reported in Figure 3-6 with error bars signifying standard error. Panels A and B show that significantly increased neurite length from a significantly higher number of number of neurite bearing neurons were measured on HA-CNT nanofibrous substrates at 24 hours. At 48 hours, neurite length was measured to be longer than the 24-hour population for both HA-CNT and HA conditions, as displayed in panel C. Panel D notably provides evidence that the number of neurite-bearing neurons on HA-CNT is maintained over 48 hours when compared to the independent 24-hour time point. Interestingly, the number of neurites measured from neurons cultured on HA increases increased between 48 hours.



## Discussion

### “Generation 1” HA-CNT *in vitro* Neuron Attachment

The outgrowth aspect ratio was not significantly different between the two conditions (HA-CNT: 1.56 +/- 0.11, HA control: 1.39 +/- 0.17) (Figure 3-1). This behavior was attributed to low fiber alignment and similar nanofiber diameter characteristics for HA and HA-CNT nanofibers. From these cell behavior results and SEM qualitative observation of surface roughness, we hypothesized that the HA-CNT fibers showed improved cell interactions over HA controls because of increased fiber surface roughness from the presence of the CNTs. Although not quantified in this thesis, our prediction proffered a theory that neuron behavior was a result of surface roughness which previously had been studied by other groups as a mechanism to improve neuronal cell attachment, longevity, and neurite outgrowth (Khan et al., 2005; Li et al., 2010).

### “Generation 2” HA-CNT *in vitro* Neuron Attachment

Dissociated DRGs exhibited greater neuron length on HA-CNT nanofibers electrospun with 0.5% w/w CNT to HA. Notably, the bright field images for the HA-CNT condition reveal large black agglomerates as visualized under 10X conditions. This prompted further optimization methods to reduce agglomeration and aggregation.

### “Generation 3” HA-CNT

#### *L-929 Fibroblast Attachment*

One-way ANOVA statistical analysis was performed to test for the effect of CNT incorporated into HA nanofibers by culturing L929 fibroblasts on glass, HA nanofibers, and HA-CNT nanofibers. The statistical analysis indicated L-929 proliferation was not altered significantly following assessment by Alamar Blue after a 24h culture period. There was no difference between any of the three groups.

#### *HA-CNT (0.01%, 0.02%, 0.3%) in vitro Neuron Attachment*

Electrospun HA and HA-CNT with 0.01, 0.02, and 0.3 wt. % (HA-CNT) scaffolds were evaluated for their abilities to maintain cell viability and promote neurite extension *in vitro*

over a 24h culture time. Dissociated DRGs from E10 chick embryos displayed varying neurite lengths dependent on percent CNT incorporated into HA nanofibers. The adaptation for dissociated spinal lumbar dorsal root ganglia technique (Song and Uhrich, 2007) employed within Chapter 3 was informed by the stage-dependent behavior observed by Ebendal in 1979 when culturing chick spinal DRGs on collagen gels cocultured with explanted heart (Ebendal, 1979). Ebendal reported peak neurite length from E8 whole DRG explants in the presence of NGF when co-cultured with heart explants followed by a short decline between E8-E10 and a plateau between E10-E12 followed by a sharp decline (Ebendal, 1979). Cumulatively considering the attachment data presented in Chapter 3 and electrochemical characterization of Chapter 2 prompted usage of lumbar DRGs explanted from E12-E13 chicks in DRG dissociations for the electrical stimulation studies presented in Chapter 4. These results and conclusions prompted us to conduct the 24h and 48h *in vitro* neuron attachment study using E12-E13 DRG neurons cultured on 0.01% HA-CNT.

#### *HA-CNT (0.01%) in vitro Neuron Attachment*

Electrospun HA and 0.01 wt.% HA-CNT were evaluated for their abilities to maintain cell viability and promote neurite extension *in vitro* over 24h and 48h culture periods. The dissociated DRG neurons displayed material attachment preference to HA nanofibers containing CNT. Neurite length is increased when neurons are cultured on HA-CNT substrates regardless of a culture time of 24h or 48h. Under bright field, we observed HA nanofiber topography to be less distinct between time points relative to HA-CNT nanofibers which appeared to maintain their nanofiber structure. Chapter 2 contact angle and FTIR studies data provided evidence to support our conclusion that -COOH moieties located on the surface of the CNTs influence the surface charge of the scaffold thus increasing hydrophilicity that promotes increased neuron attachment, as evidenced in Figure 2-10.

These *in vitro* outcome measurements are significant in the context of observations made by our research groups that neurons do not attach easily and consistently to uncoated polymer surfaces like PCL and methacrylated hyaluronic acid. Wrobel(Wrobel and

Sundararaghavan, 2014) explored the incorporation of adhesive guidance cues like fibronectin and laminin, while investigating the potential for combinatorial approaches to establish positive and negative cues as opposing gradients to guide neural regeneration. Hamzeh Omar (unpublished) conducted axial strain experiments exploring the effect of mechanical cues on neurite extension from DRG explants cultured on PCL nanofibers. Whitehead has reported neurite extension on uncoated methacrylated hyaluronic acid nanofibers compared to nanofibers embedded with microspheres for controlled delivery of neurotrophic factors (Whitehead et al., 2018). Cumulatively, our group has observed that chick dorsal root ganglia (explanted or dissociated) prefer aligned nanofiber substrates combined with an adhesive coating like laminin or fibronectin, mechanical stimulation, or an introduced chemical cue like NGF (*in vitro*, (Whitehead et al., 2018)) or BDNF (*in vivo*, (Whitehead, 2017)).

### **Biocompatibility of HA-CNT Nanofibers**

A robust trend in increased neurite outgrowth was measured on unstimulated HA-CNT nanofibers regardless of electrospinning formulation (denoted as Generation 1, 2, or 3) and CNT weight percentage (1% Generation 1, 0.5% Generation 2) or dispersion volume percentage (0.3%, 0.02% and 0.01% Generation 1). As discussed in Chapter 3.4.1 discussion of Generation 1 HA-CNT nanofibers, the early observations of robust neurite outgrowth on HA-CNT nanofibers relative to HA in juxtaposition to surface roughness observed in concomitant SEM images led us to consider surface roughness may play a role in neuronal attachment behavior.

The sequential formulation optimization and dispersion optimization methods outlined in Chapter 2 resulted in comprehensive material characterization enabled near-time simultaneous cell behavior interpretation. Observing and measuring material characteristics of the HA-CNT nanofibers while performing *in vitro* attachment trials throughout the optimization process enabled educated decision making on which material characteristics were most relevant to neuron behavior, which characteristics may need further optimization, and which may have nominal effects relative to HA nanofibers.

Chapter 2 provides qualitative visual evidence from Generation 3 atomic force microscopy imaging that HA-CNT nanofibers hydrated to equilibrium do not display a rough topography on the nanofiber surface. Considering the expansion of the Generation 3 0.01% HA-CNT nanofibers as discerned from the scale on the height image from the 3D panel (Chapter 2 Figure 2-9) relative to the diameters measured from SEM images taken under vacuum, it may be reasonable to infer that the hydrated hyaluronic acid polymer network overcomes the nominal 20 nm scale contribution of CNT agglomerates as measured in TEM and SEM images. These topographical observations led us to perform contact angle measurements to discern how surface chemistry of the nanofibers may contribute to hydrophilicity.

Chapter 2 contact angle data measuring the degree of water droplet spreading on HA and HA-CNT nanofibers provided material characterization evidence that surface chemistry may be influenced by the HA-CNT composite material constituents. In this thesis, the increased hydrophilicity is assigned to a relative increase in number of  $-COOH$  groups (qualitative FTIR data presented in Chapter 2) within the composite polymer network due to the addition of carboxylated carbon nanotubes. A slight hydrophobic surface property of methacrylated hyaluronic acid could be contributed to the formation of methylene groups during photo-crosslinking of the methacrylated hyaluronic acid polysaccharide chains. Sundararaghavan and Burdick (Sundararaghavan and Burdick, 2011) report "inter- and intra-fibrous crosslinks (to) occur during the polymerization process" to enable stabilized nanofibers and a cohesive nanofibrous mat. Further, the study reported an indirect fluorescence measurement technique using methacrylated rhodamine (MeRho) to correlate rhodamine ( $1500-1700\text{ cm}^{-1}$ ) to methylene groups ( $2800-3000\text{ cm}^{-1}$ ) present in methacrylated hyaluronic acid nanofibers containing known concentrations of MeRho. using a Attenuated Total Reflectance Fourier Transform Infrared Spectroscopy (ATR-FTIR) technique. In comparison to the gradient techniques (Sundararaghavan and Burdick, 2011; Wrobel 2017) previously studied by the Sundararaghavan group, embedding an ultra-low concentration of



carboxylated carbon nanotubes within methacrylated hyaluronic acid nanofibers offers an additional mechanism to improve cell attachment for directed cell behavior.

Aligned HA-CNT nanofibers from the Generation 3 subset fabricated with an 0.01% (w/v) CNT dispersion were concluded to be the most attractive nanofibers to use in an electrical stimulation application for neural regeneration in peripheral nerve injuries. This conclusion is drawn from the cumulative data regarding material characterization (Chapter 2), namely electrochemical properties optimized by improved CNT dispersion, and the resulting *in vitro* cell behavior documented within Chapter 3 of this thesis. L-929 fibroblast proliferation was not aberrantly altered when cultured on 0.01% HA-CNT nanofibers versus HA or glass. Neurite length and number of neurite-bearing neurons were significantly improved when cultured on HA-CNT substrates at both 24h and 48.

#### *Study Limitations*

While evidence in this thesis documents the biocompatibility of HA-CNT nanofibrous substrates with no discernable or measured toxicity potential, it is important to note that these results were evaluated relative to HA nanofibrous substrates and not to positive and negative controls specifically designed with expected results of positive and negative cytotoxic responses. The use of such positive and negative controls would be most appropriate when HA-CNT nanofibrous scaffolds are fabricated under GMP standards and evaluated under GLP practices for consideration in advancement to pre-clinical and clinical trials as part of regulatory documentation to include in the Design History File for an HA-CNT based nerve guide conduit.

#### **Conclusions**

The HA-CNT nanofiber constructs were concluded to be cytocompatible following the methods relevant to ASTM standard for testing material contact with biological tissues. L-929 proliferation was not altered indicating compatibility. Additionally, neurite outgrowth resulted in increased neuron lengths on unstimulated HA-CNT nanofibers. This behavior is attributed to increased hydrophilicity measured by contact angle, which is assigned to the increased

number of  $-COOH$  groups within the composite polymer network due to the addition of carboxylated carbon nanotubes. A slight hydrophobic surface property of methacrylated hyaluronic acid could be contributed to the formation of methylene groups during photocrosslinking of the methacrylated hyaluronic acid polysaccharide chains. In comparison, embedding an ultra-low concentration of carboxylated carbon nanotubes within methacrylated hyaluronic acid nanofibers offer a mechanism to improve cell attachment. Now that a reproducible biomaterial can be fabricated with defined topography, mechanics, and electrochemistry, the next Chapter will validate the scaffold for electrical stimulation (ES) for neural tissue engineering applications using a custom ES stimulation system.

## **Chapter 4 : Electrical Stimuli Delivered Through HA-CNT Nanofibers Enhances Neuron Growth**

### **Introduction**

In Chapter 3, our primary research question was whether HA-CNT nanofibers were cytocompatible as assessed by attachment experiments using L-929 fibroblasts and dissociated dorsal root ganglia (DRG). Our driving motivation in Chapter 4 is to determine whether an electrical stimulus can be passed through Generation 3 HA-CNT nanofibrous scaffolds to enhance neuron length and viability. Voltage-gated calcium channels, specifically L-type VGCCs and the pathways involved with the predicted molecular mechanism involving BDNF expression and secretion have been established in avian species within the chicken family (Barde, 1989; Burt, 2005; McCaig et al., 2005). We predicted that HA-CNT nanofibers would provide a suitable permissive environment to recapitulating the extracellular matrix of healthy neural tissue.

A comprehensive 2005 review from McCaig, Rajniecek, Song, and Zhao illustrates the nearly 30-year evolution of studies demonstrating the effect of electrical stimulation on embryogenesis, nervous system wound repair, and neuritogenesis and growth cone guidance (McCaig et al., 2005). The Borgens Neuroscience 1999 article translated effects of electrical gradients during embryonic development to a tissue-engineered approach by applying electrical stimulation (ES) within polymeric guidance channels (Borgens, 1999). Graves et al. (2011) offered quantified experimental evidence that 200  $\mu\text{A}$  AC waveforms resulted in significantly longer neurite outgrowth and neuronal guidance in an *in vitro Xenopus laevis* model. Phase 1 human clinical trials implanted oscillating field stimulators to enhance regeneration in spinal cord injuries using a 200  $\mu\text{A}$  stimulus (Shapiro, 2014; Shapiro et al., 2005).

The conduction properties defined in chapter 2 provided a baseline from which to calculate an equivalent voltage amplitude that could be delivered through our HA-CNT nanofibers. By achieving the delivery of a biphasic 200  $\mu\text{A}$  electrical stimulus target as

described in the above literature, I hypothesized that the resulting dissociated DRG neuronal response would result in extended neurite outgrowth and concomitant neuronal viability that may result from successfully VGCC activated BDNF production (Wenjin et al., 2011). The expression and release of the neurotrophin BDNF is calcium dependent through calcium responsive elements affecting the *cis*-element in the BDNF promoter (Zheng et al., 2011) and has been experimentally linked to L-type VGCC activation in neurons (Wenjin et al., 2011). In Chapter 4, we will present the validation of the custom electrical stimulation system using an L-929 model to test toxicity and culminate with the validation that the HA-CNT nanofibers engineered in Chapter 2 and tested for cytotoxicity in Chapter 3 are capable of delivering a controlled electrical stimulus to predict a neuronal response of increased neurite outgrowth and number of neurite-bearing neurons. The outcome measures are endpoint measurement of neurite length and number of neurite-bearing neurons cultured on HA-CNT nanofibers following electrical stimulation. Finally, we will present a method and preliminary results for a calcium imaging assay to test activation of voltage-gated calcium channels in neurons cultured on 1% HA-CNT nanofibers following electrical stimulation.

In clinical neuroanatomy, the peripheral nervous system tissue structure known as the dorsal root ganglia is defined to contain "cell bodies of primary sensory neurons that innervate the skin and deep tissues of the back of the head, neck, limbs, and trunk" (Martin and McGraw-Hill Professional eBook Library - Medical: Primary, 2012). The Zhang PNAS 2007 study implicates L-type VGCCs in cell-cell signaling between neurons and satellite cells through soma driven ATP release following electrical stimulation of DRG explants as measured by electrophysiology and calcium imaging (Zhang et al., 2007a). Confocal microscopy imaging technique at 60x magnification provided the resolution at the cell-cell interface necessary to capture sequential, time-resolved evidence of glial-neuron signaling occurring in the tissue explant as the result of electrical stimulation. Moreover, the group collected evidence that satellite cell release of TNF $\alpha$  is receptor-mediated process in ganglia (Zhang et al., 2007a). When considering this glial function of satellite cells with other evidence in the literature that

show the pro-inflammatory TNF $\alpha$  cytokine has the potential to Chapter 3 attachment results demonstrated that measuring cell response to culture on the HA-CNT nanofibers gave more direct quantification of a cell-matrix interaction and eliminating the confounding variables of a cell culture model that was based in tissue level structure that has both cell-cell and cell-matrix components.

The main challenge to initiating a cellular response to electrical stimulation through a conductive biomaterial is converting electron conductivity from metallic electrodes to ionic conductivity in the electrolyte (Meng S, 2011). While traditional experimental methods use salt bridges, vacuum grease, and cover slips to assemble electrical stimulation chambers (McCaig et al., 2005), testing hydrogel nanofibers using similar components was not feasible beyond preliminary proof of concept studies for two main reasons. First, we decided to use a capacitively coupled (CC) design as it was most appropriate for the delivery of an AC signal which eliminated the salt bridge set-up which is for *in vitro* DC application. Second, the vacuum grease and cover slip strategy resulted in a more than 20% loss of samples. This sample loss value was comparable to similar percent loss experienced and confirmed by generous correspondence with Professors John H. Hardy and Christine E. Schmidt (unpublished). Building on these foundations along with designs (Durgam et al., 2010; Xia et al., 2007) published and validated for ES studies with sample replicates, we designed a reproducible and stable *in vitro* electrical stimulation chamber from common and readily available materials and equipment that allow for a stable electrical connection that is connected to the conductive nanofibers while separated from the culture media. We achieved an improvement in sample recovery from approximately 80% to 94.6%. Sample recovery was calculated by dividing the number of ES chambers that produced quantifiable data by the number of ES chambers fabricated.

The next consideration for ES experimental set-up is testing efficacy of the chosen electrical stimulus. We chose electrical stimulus parameters to be 20 Hz square wave for 1 hour, consistent with studies reported using these parameters to enhance regeneration and

reinnervation (Al-Majed et al., 2000a; Al-Majed et al., 2000b; Al-Majed et al., 2004; Brushart et al., 2005; Geremia et al., 2007). Our prediction is that electrical stimulation activates Voltage Gated Calcium channels in the cell membrane, permitting calcium influx. Calcium, a potent second messenger, mediates cellular pathways controlling cytoskeletal organization (calcium/calmodulin signaling pathway (Aigner, 1995; Onuma and Hui, 1988)) as well as BDNF production in neurons (Wenjin et al., 2011; Zheng et al., 2011) and release from Schwann cells (Luo et al., 2014). Media formulation is a crucial experimental design factor when testing cell behavior. Kotwal and Schmidt (2001) tested how immediate and delayed electrical stimulation altered protein adsorption to a biomaterial surface. The serum protein fibronectin significantly adsorbed to the surface of the conducting polymer polypyrrole substrate immediately after stimulation resulting in enhanced neurite outgrowth; whereas, delayed stimulation after cell seeding resulted in no difference in fibronectin adsorption or neurite length when compared to a 4 h room temperature adsorption timepoint (Kotwal and Schmidt, 2001). We eliminated these known confounding factors by implementing a standardized procedure for electrical stimulation application at least 12 h under normal culture conditions.

In Specific Aim 3, we demonstrate that an electrical stimulus can be delivered through HA-CNT nanofibers to increase and accelerate neuron growth as measured by neurite extension and number of neurite-bearing neurons.

We hypothesize that a stable electrical system will enable reproducible and repeatable experimental conditions to observe *in vitro* cell response to electrical stimuli delivered through a conductive nanofibrous biomaterial.

We hypothesize electrical stimulation delivered through the HA-CNT nanofibrous scaffold will result in significantly greater neurite length in chick dissociated dorsal root ganglia neurons.

## **Experimental Methods**

### **Custom Electrical Stimulation Chambers**

Nanofibrous scaffolds were electrospun onto 12x12 mm standard Number 2 glass cover slips using permanent double-sided tape (3M) adhered to standard Painter's tape (3M) to withstand the forces of the rotating mandrel. Custom ES chambers were assembled as depicted in Figure 4-1. Custom glass bottom culture plates were created by drilling holes through the wells of standard 12-well or 35 mm culture dishes using a Dremel mounted on a drill press kit equipped with a diamond blade drill bit (6mm diameter). The nanofibrous samples on glass first underwent a procedure to prepare the surfaces for bonding with the custom culture dishes. A 6mm x 12mm (height x length) rectangular strip of aligned nanofibers were retained within the center of the cover glass, while the outer edges above and below were scraped away with a razor blade. Anecdotally, from a process optimization perspective, it was observed that scraping was easier to achieve prior to UV cross-linking of the HA substrates. Regardless, samples must be cross-linked prior to advancing to the next step. Fine tipped cotton applicators soaked in ethanol (200 proof, Sigma Aldrich) and blotted on a delicate task wipe to remove excess were then utilized to prepare the surface of the glass coverslips *and* the underside of the custom cut plastic culture dishes. Prior to using the drill press scheme to cut a 6-mm diameter hole in each well. The underside of the dishes was gently but firmly scored with a sanding block and debris was wiped away with a delicate task wipe and 200 proof ethanol. These surface preparation procedures were optimized based on documentation provided by 3M for effective environmental sealing using Very High Bond (VHB) adhesive. Immediately following the surface treatments of the culture dish, VHB tape was applied to the bottom, then holes were drilled. Separately, two strips of copper tape (one-side adhesive) was applied over the top of the rectangular fibrous mat (adhesive side against glass) in an orientation which would flank the well in parallel. This orientation treats the nanofibrous scaffold as a circuit element that is connected to one copper electrode which provides the voltage input from the function generator and the opposite side copper electrode

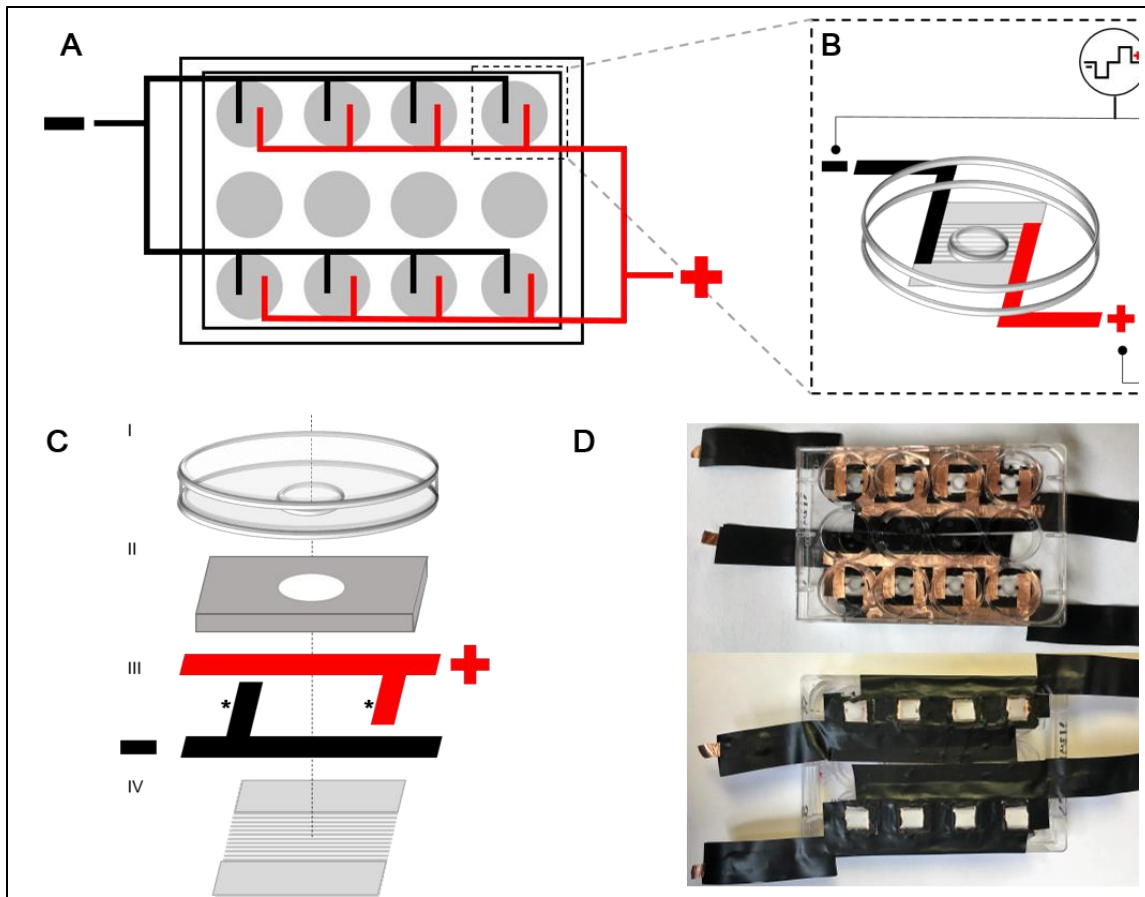


**Figure 4-1. Custom Electrical Stimulation Culture Dish.**

(A) Illustration of custom electrical stimulation (ES) culture plate designed to promote interlab adaptability for early-stage electroactive biomaterials testing.

(B) Each custom well experienced an AC Waveform from Function Generator to simulate a pulsatile electrical stimulus: 20 Hz biphasic square wave,  $\pm 25$  ms pulse width,  $\pm 50\%$  duty cycle. ES stimuli from every experiment stored through custom DAQ system (Raspberry Pi B/Ubuntu Mate/python interfaced with digital oscilloscope via USB).

(C) Illustration of each custom well (I) within commercially available 12-well cell culture dish assembled by drilling 6mm-dia. hole through bottom of well and (II) high bond acrylic foam adhesive. (III) Copper tape (\*) is overlaid nanofibers cross-linked to glass coverslip (IV). The copper tape in the III-IV assembly is connected to longer copper tape rails (-/+). Following curing at RT for 24h, the conformable foam adhesive (II) provides a seamless hydrophobic barrier between assemblies I-II and III-IV enabling the nanofibers to be hydrated while separating electrodes from the culture media.

(D) Photographs of a fully assembled, cured culture plate following insulation of copper tape. Thin layer of liquid vinyl around each glass coverslip and vinyl electrical tape along the length of the copper rails insulates the electrodes from the environment providing stable electrical stimulation conditions. This custom assembly fits a standard fluorescence microscope allowing live or endpoint imaging, achieving a 94.6% sample recovery rate as calculated by the number of nanofiber sample wells from which immunofluorescence data was collected relative to the total number of nanofiber sample wells assembled.



connected to a common ground. The scaffold area exposed to electrolyte media was limited by the unique properties of 3M VHB. Prior to curing, VHB exhibits viscous flow at the surface enabling it to create a thin, tight seal between bonding surfaces. These properties are why the surface treatments were necessary, particularly when bonding glass, metal, and plastic to effectively initiate a hydrophobic seal at the surface of the HA. These steps resulted in no observable copper electrode corrosion even after sitting in a humid environment for 2-3 years (unpublished); these observations are in stark contrast to methods that used vacuum grease to separate media from copper electrodes during preliminary studies. In those cases, corrosion evident by the classic green color of copper oxide could be observed within 12 hours.

Following assembly of the custom stimulation chambers, the same 100 W long wave UV light used to cross-link the HA scaffolds was employed for 20 minutes to sterilize the dishes in preparation for cell culture. All electrical stimulation waveforms described in this chapter were delivered by an analog function generator (GW INSTEK GFG-8020H) connected to a breadboard (Jameco). Shorter copper electrodes from each custom well were connected to a longer copper strip (Figure 4-1, panels b and c); all exposed copper electrodes were shielded from the environment by a combination of liquid electrical tape and standard electrical tape, except for a small square at the end which enabled connection by alligator clips to the Jameco breadboard. A Raspberry Pi and custom python script implementing the PYTHONUSBTMC driver (2013, Alex Forencich) was employed for digital data acquisition from two channels of a digital oscilloscope (RIGOL DS1102E) that were connected to the breadboard, Channel 1 monitored the function generator input, and Channel 2 was wired to observe the "output" copper bus from the custom ES culture dish that was connected to a common ground.

Reliable and stable electrical connections are the foundation for effective electrical engineering methods. Electrical connections employed in this study were: (1) culture plate copper rails connected by alligator clips to wire jumpers on breadboard and (2) power source (function generator) cathode and anode connected to breadboard by alligator clips to wire

jumpers secured in binding posts. This versatile set-up was designed with an “electroactive biomaterial plug-and-play” strategy for integration with diverse culture environments and conditions, including a standard incubator and a fluorescence microscope outfitted with an environmental chamber. The 6-mm diameter “custom well” resulted in dimensions comparable in scale for 96-well plate assays, while also enabling interfacing with readily-available components common to electronics laboratories. eliminating the need for the design, validation, and costs associated with other approaches.

### **Electrical Stimulation *in vitro* Assays**

#### *L929 Cytotoxicity Assays with Electrical Stimulation*

To assess potential cytotoxic effects of electrical stimulation parameters and culture conditions, ES was delivered through HA and HA-CNT nanofiber scaffolds ( $n = 3$  scaffolds each HA, HA-CNT) to L929 fibroblasts cultured in a custom 12-well plate format like the illustration depicted in Figure 4-1 and the real example in the bottom center of Figure 4-1. The Alamar Blue proliferation assay described in Chapter 3 was adapted and scaled to appropriate dimensions. Empirical testing was performed to determine media and Alamar Blue reagent volumes and cell density that were appropriate for a 6mm custom culture well (akin to a 96-well plate assay). All glass control conditions were unstimulated but otherwise mirrored the nanofiber culture conditions in this experimental method by utilizing the middle row of wells in the 12-plate format.

L929 fibroblasts seeded and cultured as described in Chapter 3 except at a lower cell number to accommodate the reduction in culture surface area. The volume of each culture well is 100  $\mu\text{L}$ . Cells were seeded by dropping a 75  $\mu\text{L}$  aliquot of a single cell suspension (30000 cells/ml) to seed approximately 2250 cells in each custom well. The cell suspension aliquot was gently added to 25  $\mu\text{L}$  of media. Cell density and the custom well back-filling volume was determined empirically. The data reported here are the results following establishing these parameters. The 25  $\mu\text{L}$  of media backfilling strategy was determined to promote homogeneous attachment across the scaffold surface by preventing fluid wicking

towards outer edges of the confined culture area. Four hours after cell seeding to allow for attachment, 300  $\mu$ l of modified DMEM supplemented with Alamar Blue (ThermoFisher, abbreviated as AB) reagent was used to gently flood the custom well to a final AB concentration to the supplier suggested final concentration of 10% AB. Twenty-four hours following fibroblast seeding, a 300 mV biphasic, 1 Hz(Cho et al., 2002) square wave electrical stimulus was applied for 5 minutes. L929 were cultured for 72h total with aliquots of culture media containing 10% AB were transferred to a 384 well plate for optical measurements using a UV/VIS spectrophotometer (Fisher Scientific, GO) according to supplier protocols and mirroring measurement methods established in Chapter 3. Each experiment included blanks, including the aliquots from the AB-containing stock media as well as aliquots obtained from AB-containing stock media applied to the first well in the 4-well scaffold type sample series. The latter set of blanks served as a cell-free scaffold blank for background subtraction from the 3 cell-containing scaffold samples. The AB-containing stock media was freshly prepared for each experiment and stored in incubator during the duration of the experiment. Aliquots were collected and transferred for measurement 24h post-seeding immediately preceding electrical stimulation, and then at 24h and 48h post-stimulation. The AB assay and experimental volume allowed for the samples to be cultured in the same media throughout the duration of the experiment, with aliquots collected and measured at the timepoints described above.

Two 12-well plates were included in each experiment ( $N = 3$ ). One set of L929 samples cultured within the middle row on glass ( $n=3$ ) were prepared as outlined above including the first well serving as a blank. The set of 4 glass L929 culture samples on the other 12-well plate served as the standard curve samples, with L929 seeded at a density of 0, 2000, 4000, and 8000 cells/well. A typical standard curve generated employing this technique with the custom electrical stimulation chambers can be seen in (Figure 3-3A). Statistical analysis of the 24h attachment, pre-stimulation conditions were performed using a One-Way ANOVA,  $\alpha = 0.05$ . Statistical analyses for the electrical stimulation data 24h and 48h post stimulation

were employed using F-test Two-sample tests for variance between unstimulated and stimulated samples for each nanofiber type followed by a two-tail t-Test with  $\alpha = 0.05$  (Microsoft Excel Data Analysis Add-on).

#### *Electrical Stimulation Assays with Dissociated Dorsal Root Ganglia*

Lumbar dorsal root ganglia were dissected from E11-E12 chick embryos, dissociated, and seeded on nanofibrous substrates (2250 cells/custom well) in serum-free media composed of 1:1 v/v DMEM/Hams F-12 supplemented with 50 ng/ml NGF. The same back-fill technique described earlier was employed here. Cells were cultured on HA and HA-CNT substrates for 24h before electrical stimulation groups were connected to the custom ES circuit described earlier. Briefly, alligator clips connected the custom ES culture plate like a circuit element being spliced into a test circuit mounted on a breadboard. The power source connected to the circuit board was a standard analog function generator (GW INSTEK, GFG-8020H). The same electrical stimulation regime was delivered to the neurons cultured on HA and HA-CNT samples ( $n = 4$  each nanofiber type), powered by the culture plate electrode connections through the bread board. The neuron electrical stimulation assays were performed based on a factorial design outlined in Table A1 in Appendix A. Briefly, electrical stimulus parameters were applied 24h after seeding constituting either 30- or 60-minute applications of either 150, 200, or 250 mV/mm bi-phasic square AC waveforms. Unstimulated neuron cultures served as controls and were cultured using the same configuration described above, with the exception of connecting the custom culture dish electrodes to the breadboard.

Neurons were fixed 48h after ES, for a total culture time of 72h. Neurons labeled with anti-neurofilament and DAPI were imaged and quantified to analyze neurite length and number of neurite-bearing neurons. Inclusion criteria for analysis required a neuron consisting of a single soma with neurites whose length were at least twice the width of the soma and not touching adjacent neurons. Inclusion criteria were cross-checked between Bright Field, FITC, and DAPI channels. Each experiment included one unstimulated and one stimulated culture plate of each electrical stimulus regime described in Table A1, with a total of  $N \geq 3$

experimental cultures derived from independent cell suspensions. Results are reported as raw neurite lengths as measured from data collected from every neuron in each custom well that met inclusion criteria. As cited earlier, 94.6% of samples seeded with neurons were intact and quantifiable by the end immunofluorescent labeling and imaging of each experiment. The neurons counted for each condition are listed in Appendix A - Table A1.

All data is reported as mean +/- standard error. Statistical tests were performed using SPSS for 3-way ANOVA (nanofiber type, voltage amplitude, ES stimulus duration) and Tukey post-hoc analyses ( $\alpha = 0.05$ ). Microsoft Excel was used to calculate descriptive statistics. Descriptive statistics reported in Appendix A – Table A1 were part of the SPSS 3-way ANOVA Output Report. For the dependent variables of Neurite Length and Number of Neurite-bearing Neurons, the Levene's Test of Equality of Error Variances resulted in a  $p = 0.000$ . Consequently, 3-Way ANOVA results for Between-Subjects Effects were only considered for significance for main effects which each were confirmed to have an Observed Power greater than 0.8; the 3-Way interaction was not considered with an Observed Power of 0.082 (Table A3, Appendix A).

Since there were *no data points excluded* following the data point being collected provided inclusion criteria were maintained, we employed a secondary set of statistical tests to compare two means for groups part of factorial design interactions that fell below an Observed Power of 0.80. As evident in the Descriptive Statistics reported in Table A2 listed in the Appendix A, there was a disproportionately lower number of neurons on HA nanofibrous substrates that met the strict single neuron inclusion criteria. The Microsoft Excel Data Analysis Add-in was employed for computing an F-test for variance when comparing two means when considering a result of a Tukey post-hoc from the SPSS analysis, as a second means of evaluation for significance in an effort to avoid Type I error. In other words, we approached Tukey post-hoc analyses with a degree of skepticism since the assumption of homogeneity was clearly violated and employed Student's *t test* for unequal variances. In these cases, an Excel F-Test Two-Sample for Variances yielded a  $p$ -value  $< 0.05$ , and a

Student's *t* test assuming unequal variances was applied. Statistical significance for all tests discussed were accepted at  $p < 0.05$  (denoted by \*) and  $p < 0.01$  (denoted by \*\*).

The mean number of neurite-bearing neurons for each condition in Appendix A Table A1 was calculated by dividing the total number of neurons in a conclusion that met inclusion criteria by the total number of wells in the experiment. This distinction is important because there were some wells that had zero neurons meeting inclusion criteria and were included as a  $n = 0$  when calculating the mean value reported for neurite-bearing neurons. Descriptive statistics and Two-Way ANOVA statistical analysis were performed in SPSS, Outputs for which can be viewed in the Appendix A Tables A4 – A7. The dependent variable was “mean number of neurite-bearing neurons” and the fixed factors were ES Amplitude and Time of ES application. Due to the variance in results in mean number of neurite-bearing neurons for each experimental group, data was analyzed using the Two-Way ANOVA statistical method described with Tukey *post-hoc*. Statistical significance for all tests discussed were accepted at  $p < 0.05$  (denoted by \*) and  $p < 0.01$  (denoted by \*\*).

## **Mechanistic Studies**

### *Rationale*

Several studies have reported accelerated motoneuron axonal regeneration in response to an AC square wave signal that was associated with an upregulation in BDNF and the receptor *trkB* (Al-Majed et al., 2000a; Al-Majed et al., 2004). Multiple promoters can be activated to induce BDNF transcription by pathways involving *trkB* receptors as well as through calcium influx through voltage-gated calcium channels and NMDA receptors.  $Ca^{2+}$ -dependent signaling is propagated to calcium responsive elements regulated by calcium stimulated protein kinases (Zheng et al., 2011). After being released from the post-synaptic membrane, BDNF can act in an autocrine fashion on local *trkB* receptors triggering the MAPK signaling cascade that increases actin polymerization (Brushart et al., 2002; Difato et al., 2011; Hronik-Tupaj et al., 2013). Calcium influx has also been associated with f-actin

polymerization during growth cone formation (Kamber et al., 2009). GAP-43 stabilizes f-actin polymerization and microtubule formation in the growth cone (Aigner, 1995).

Wenjin et al. (2011) demonstrated that BDNF expression following electrical stimulation is dependent on calcium influx through voltage-gated calcium channels (VGCC) which activates the extracellular signal regulated kinase (Erk) pathways. Electrical stimulation of spinal cord neuron cultures treated with the L-type VGCC inhibitor nifedipine resulted in a reduction in the upregulation of BDNF expression seen with the stimulated controls (Wenjin et al., 2011). Nifedipine is in the dihydropyridine class of antagonistic molecules that block L-type VGCC activity (Gurkoff et al., 2013). We sought to develop a method to assay for changes in intracellular calcium levels in response to electrical stimulation. The rationale for using electrical stimulation in combination with conductive nanofibers for neural regeneration is that voltage-gated calcium channels are responsible for increased neurite outgrowth and increased neuron viability. By using a calcium imaging assay, we hypothesize that there will be no change in intracellular calcium concentration in unstimulated neurons and will increase in electrically stimulated neurons. Further, neurons treated with the L-Type VGCC inhibitor nifedipine will exhibit no increase in intracellular calcium concentrations.

#### *Mechanistic Experimental Method*

Experimental cultures were either unstimulated or stimulated. One set of cultures were pre-treated with 10  $\mu$ M nifedipine for 30 minutes. As a selective inhibitor for L-type VGCCs, the nifedipine group served as a test of the hypothesis that L-Type VGCCs are involved in activating calcium sensitive signaling pathways responsible for increased neurite outgrowth and neuron viability.

DRG neurons were cultured on 0.01% HA-CNT nanofibers in 35 mm custom electrical stimulation dishes for 24h using culture methods previously described. Neurons were incubated at room temperature for 30 minutes protected from light in an HBSS<sup>+/+</sup> solution containing 2.5  $\mu$ M Fluo-4 AM (ThermoFisher). Fluo-4 AM is a calcium indicator that fluoresces under 488 nm excitation upon binding with calcium. HBSS solutions used during the

experiment either contained calcium and magnesium (HBSS<sup>+/+</sup>) or contained no divalent cations (HBSS<sup>-/-</sup>) (Gibco).

After Fluo-4 AM loading, the solution was exchanged with HBSS<sup>+/+</sup> and protected from light until imaging. The culture plate was then mounted on the microscope and the lid was replaced with a custom perfusion lid attached to microfluidic tubing connected to two Leur lock syringes to allow for manual solution exchange. Solutions were exchanged by slowly and steadily drawing on one syringe to induce solution to drain from the culture chamber while slowly advancing the exchange solution through the second syringe. Solution exchange occurred such that the volume never depleted the custom well. A region of interest (ROI) was chosen and focused using 5 ms exposures to BrightField. Once an ROI was selected, approximately three 300 ms FITC exposures were captured to ensure sufficient focus so that cell boundaries were apparent during analysis.

Once the ROI was selected, an automated 10-minute image acquisition program was initiated. Brightfield and FITC filtered images were captured every 10 seconds using a PL FL 20X objective with a Nikon Ti-E inverted microscope illuminated with a Xenon arc lamp. The first 3 minutes of images serve as a fluorescence baseline for each experiment. At the 2-minute mark, 5 ml of HBSS<sup>+/+</sup> was exchanged. At the 5-minute mark, electrical stimulation was applied for 5 minutes using a 20 Hz, 250 mV/mm biphasic square wave from a function generator. Afterwards, 4  $\mu$ M Ethidium homodimer-1 solution was exchanged through the chamber to distinguish live and dead cells (ThermoFisher Cytotoxicity Kit). A composite still image was then acquired using BrightField, FITC, and Texas Red. Cells staining positive for Ethidium homodimer-1 were not included in subsequent analysis.

Each cell of interest was outlined using the Nikon Elements software Bezier tool to obtain the mean FITC intensity value,  $F$ . The first 3 minutes of image acquisition was averaged and served as the baseline FITC fluorescence value,  $F_0$ , representing the intracellular calcium concentration. Experimental values are reported as a ratio  $F/F_0$ , where  $F$  is the mean intensity at each time point.



## Experimental Results

### L929 Cytotoxicity Assays with Electrical Stimulation

No evidence of cytotoxicity in L929 fibroblasts was observed either morphologically (Figure 4-2) or when considering Alamar Blue assay results (Figure 4-3). There was no statistical difference detected between any groups as assessed by the percent reduction of Alamar Blue reagent which correlates to metabolic activity. After 24h, prior to electrical stimulation, there was no evidence of altered cell proliferation between L929 cultured on HA and HA-CNT nanofibers compared to L929 cultured on glass (Figure 4-3 Panel B). As expected

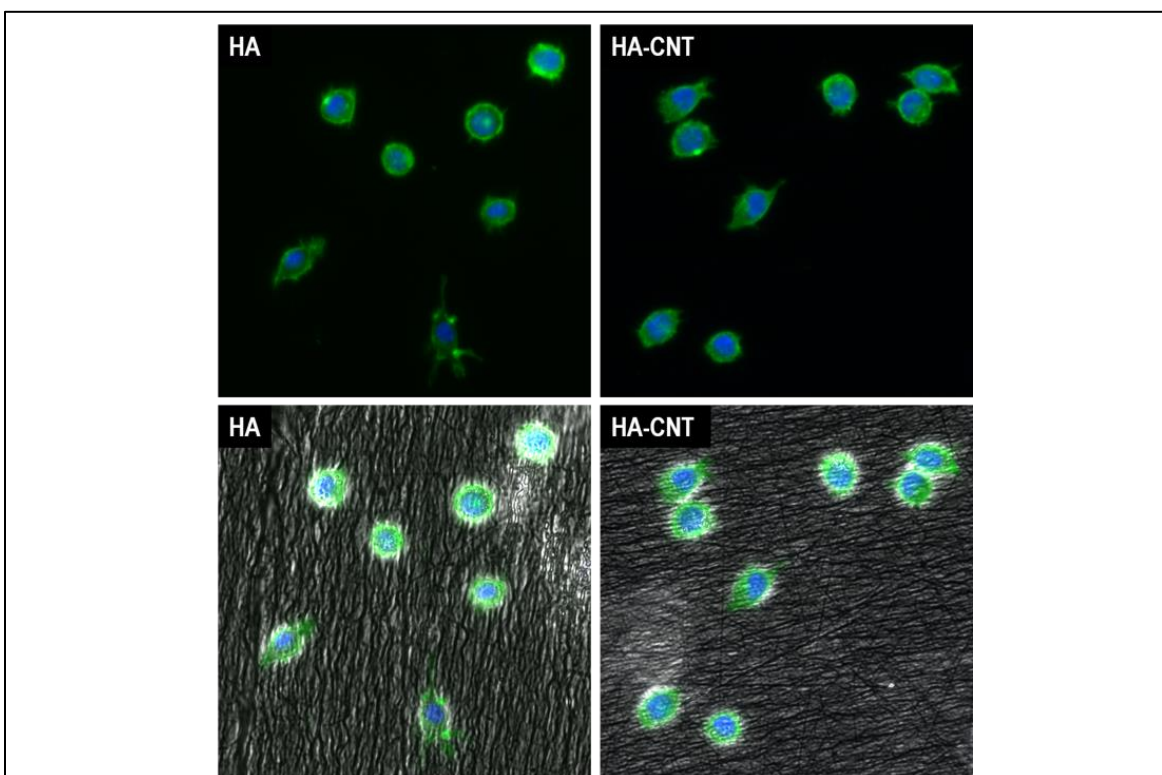
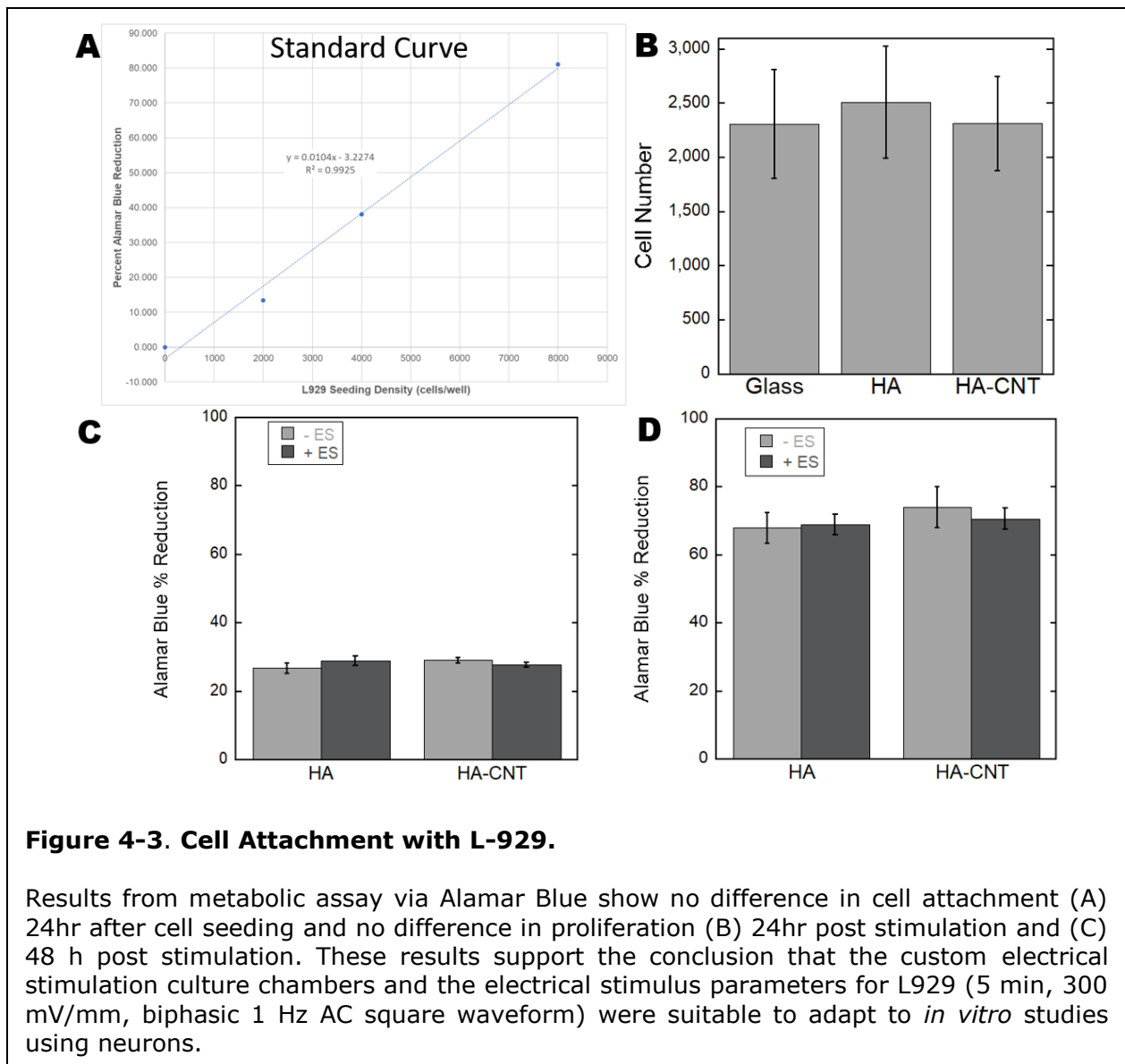


**Figure 4-2. Cytotoxicity Testing with L-929.**

Cytotoxicity testing of custom electrical stimulation system for *in vitro* experiments using L-929 fibroblasts cultured on HA and HA-CNT nanofibers. L-929 fixed and labeled with FITC-phalloidin (green) and DAPI (blue) to visualize cell morphology and nuclei following 72h in culture (first row). Bright field images (2<sup>nd</sup> row) merged with epifluorescence images allow for visualization of cells on nanofibers. Results from metabolic assay via Alamar Blue show no difference in cell attachment (A) 24hr after cell seeding and no difference in proliferation (B) 24hr post stimulation and (C) 48 h post stimulation. These results support the conclusion that the custom electrical stimulation culture chambers and the electrical stimulus parameters for L929 (5 min, 300 mV/mm, biphasic 1 Hz AC square waveform) were suitable to adapt to *in vitro* studies using neurons.

in the absence of cytotoxic effects of culture conditions on nanofibers and materials used in custom ES chamber fabrication, there was no change in L929 proliferation as measured by percent Alamar Blue reduction. These results were standard across the board, regardless of fiber type and whether the samples received electrical stimulation or not. Moreover, the proliferation rate was not altered as evidenced by percent increases in Alamar Blue reductions from 24h to 48h post-treatment, with no differences between any groups.



### **Electrical Stimulation Assays with Dissociated Dorsal Root Ganglia**

Neuron cultures were either unstimulated or stimulated for 30 or 60 minutes using a charge balanced, biphasic square wave with amplitude of 150 mV/mm, 200 mV/mm, or 250 mV/mm. Examples of fluorescence images can be seen in Figure 4-4 as a result of merging Bright Field, FITC, and DAPI channels. The neurofilament labeled with FITC clearly delineates axons aligned with the nanofibers viewable in the Bright Field channel. The DAPI-labeled nuclei are more easily distinguished in the individual panels displayed in Figure 4-4.

The bar charts displayed in parts **b** and **c** of Figure 4-4 depict the neurite length and number of neurite bearing neurons analyzed from the 14 experimental groups from Appendix A Table A1. Three-way ANOVA revealed significant main effects for nanofiber type, time, and amplitude ( $p < 0.01$ ) (Table A3, Appendix A). After 72h in culture, neurons on unstimulated HA-CNT nanofibers were longer than those cultured on HA which follows the behavior seen after 48h reported in the attachment studies in Chapter 3. There appears to be a threshold for obtaining longer neurite outgrowth with a voltage amplitude of at least 200 mV/mm for both the HA and HA-CNT nanofibers, with neurites on the 200 mV/mm 30-minute condition being significantly longer than 150 mV/mm and the unstimulated conditions. For neurons grown on the HA substrates, the 200 mV/mm 30-minute condition resulted in significantly longer neurites when compared to the unstimulated and 150 mV/mm conditions but not the 250 mV/mm 30 min condition.

On the other hand, neurons stimulated on HA-CNT nanofibers for 30 min at both 200 and 250 mV/mm were significantly longer than those on the unstimulated control. While there was a significant difference between HA and HA-CNT for the 30-minute 150 mV/mm for HA-CNT condition, there was no difference at the higher amplitude 30-minute conditions when comparing fiber type. However, when stimulation time was doubled to 60 minutes, a definitive improvement in neurite growth on HA-CNT nanofibers was achieved at all voltage amplitudes when compared to both unstimulated fiber type and the HA nanofibers at the same ES

conditions. The 250 mV/mm 60-minute HA-CNT group resulted in statistically longer neurons than all other groups.

The average number of neurons bearing neurites per well on HA-CNT nanofibers following the 60-minute electrical stimulation regimes at all amplitudes far outnumbered the unstimulated and 30-minute conditions of both fiber types. While there was no statistical significance between the 150, 200, 250 mV/mm amplitude conditions at 60 minutes for the HA-CNT nanofibers, each of these conditions were statistically different than all other groups. FIGURE 4-4 panel c and the statistical reports in Appendix A (Tables A4 – A7) should be considered together when drawing conclusions regarding the effects of electrical stimuli on neuron number, as this output measure is dependent on the quantification of number of neurite-bearing neurons and considered each well within these experiments. In other words, there were some wells in which no individual neurons which met the inclusion criteria could be counted. When reporting the mean number of neurite-bearing neurons for each condition in Appendix Table A1, wells that had zero neurons meeting inclusion criteria were included as a  $n = 0$  when calculating the mean value reported for neurite-bearing neurons. For example, for the HA 200 mV/mm 30-minute condition, there were a total of 11 wells from 3 separate experiments but only 7 of those wells contained neurons that met the inclusion criteria. The reported length values discussed earlier do not take into account this parameter, but this phenomenon was observed and reportable in a reproducible and consistent manner following this method.

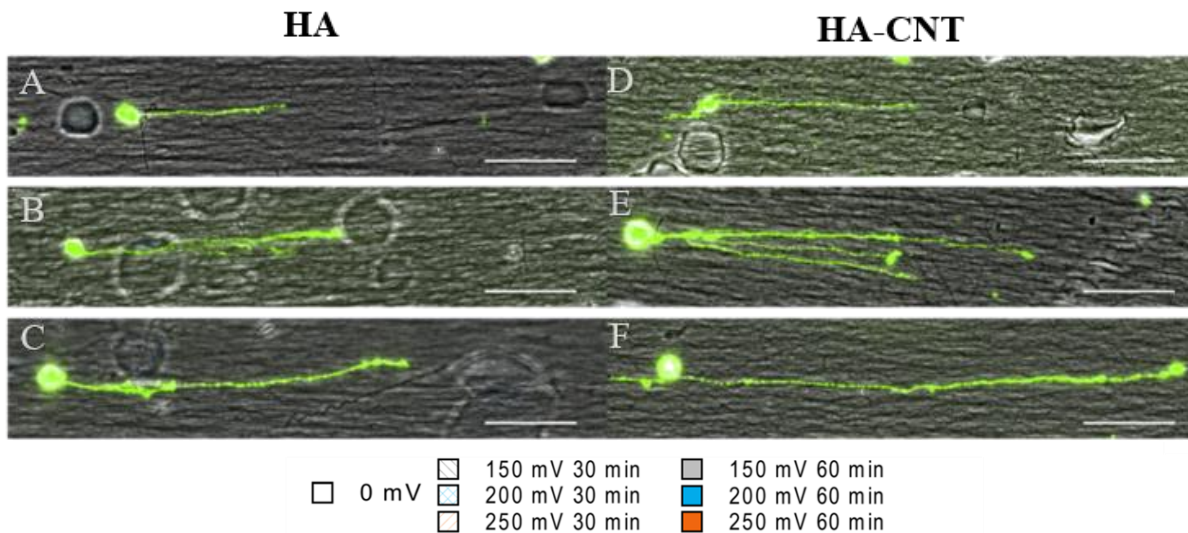


**Figure 4-4. Electrical Stimulation of Neurons Cultured on HA and 0.01% HA-CNT nanofibers.**

Merged fluorescence micrographs (scale bar 50  $\mu\text{m}$ ) of dissociated dorsal root ganglia neurons fixed after 72h of culture in serum-free media supplemented with 50ng/ml NGF. 24h after attachment, neurons were electrically stimulated with a 200 mV/mm biphasic 20 Hz AC square waveform for either 30 minutes (B, E) or 60 minutes (C, F). Compared to unstimulated neurons on HA and HA-CNT (A, D), stimulated neurons cultured on nanofibers exhibited significantly longer neurites. Moreover, neurites measured from neurons cultured in each HA-CNT condition were longer than their HA counterparts, both unstimulated and stimulated. The number of neurite-bearing neurons significantly increased with electrical stimulation at 60-minute 200 mV/mm compared to unstimulated for all groups. Again, there were significant increases relative to unstimulated HA-CNT and unstimulated HA when considering neuron number. The inclusion criteria for quantification of neurite length and neuron number were single soma neurons with a neurite at least twice the width of the soma and not touching any other neuron or its processes. Notably, the number of neurons that fit these criteria were decreased in the 30-minute conditions for both HA and HA-CNT relative to the unstimulated and 60-minute conditions.

### Calcium Imaging and Electrical Stimulation Assay Results

Figure 4-5 displays results obtained from a preliminary study in which neurons loaded

with a calcium sensitive indicator were either left unstimulated or were electrically stimulated with a 20 Hz, 250 mV biphasic square wave. One of the electrical stimulation experimental conditions included pre-treatment with the L-Type VGCC inhibitor nifedipine. In the unstimulated condition, there was a negligible increase in intracellular calcium concentration (<1%). There was approximately 10% increase in intracellular calcium in the electrically stimulated condition and a 17% decrease in the nifedipine condition. These percent changes are based on the  $F/F_0$  values at the onset of electrical stimulation divided by the final  $F/F_0$  value at the end of the experiment. No statistical analysis was performed due to low number of trials per treatment (N = 1 trial, n = 2 neurons Unstimulated; N = 1, n = 5 neurons, Nifedipine; N = 2, n = 6 neurons Stimulated).

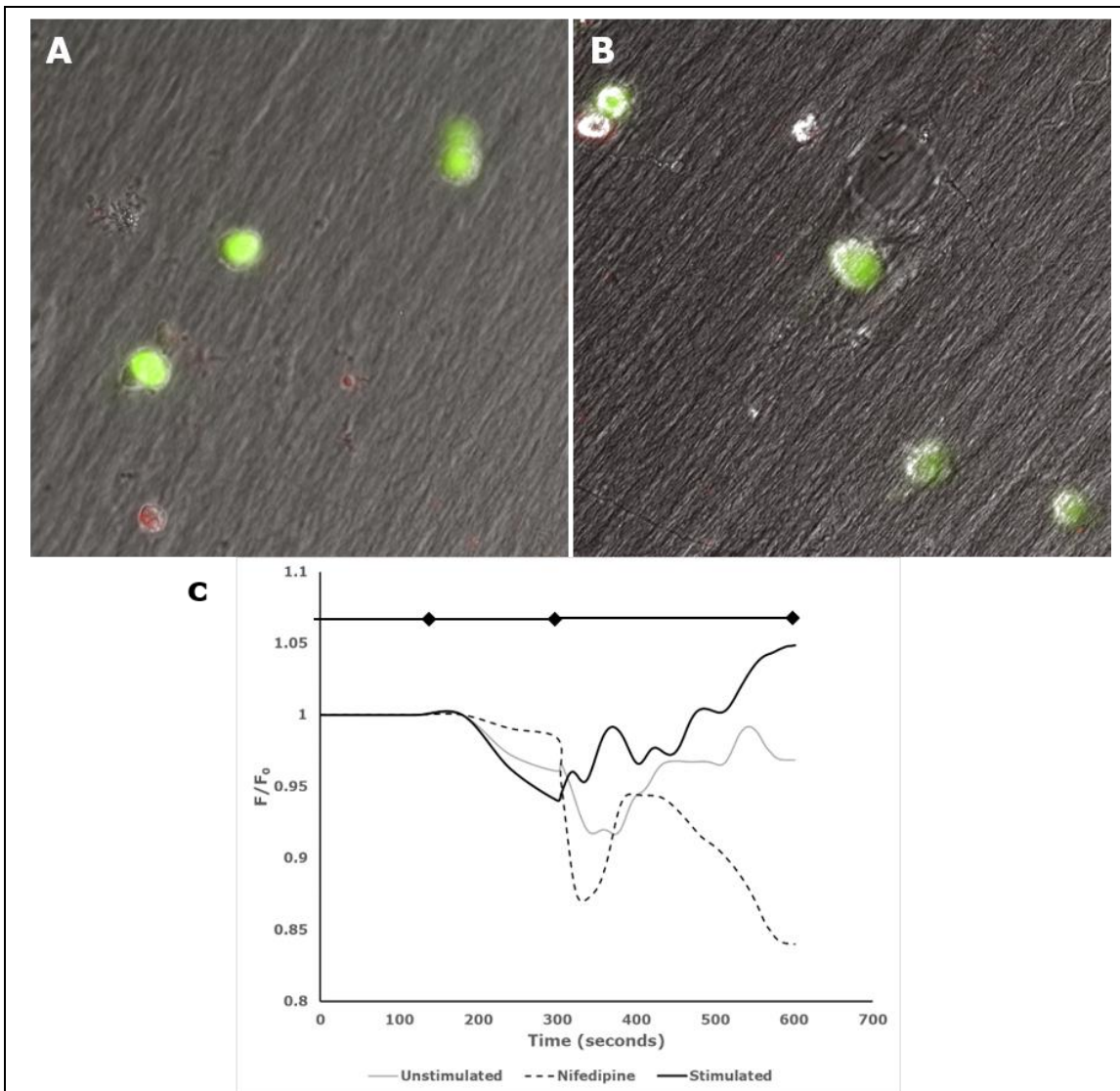


**Figure 4-5. Relative Intracellular Calcium Changes in Neurons Upon Electrical Stimulation.**

DRG neurons loaded with FITC-conjugated calcium indicator to probe calcium responsiveness to (A) electrical stimulation and (B) electrical stimulation after pre-treatment with nifedipine. (C) Neurons loaded with a fluorescent calcium indicator were unstimulated, stimulated or were treated with the L-Type VGCC inhibitor nifedipine and then stimulated. Each diamond on the line at the top of the graph denotes an experimental event dividing the experiment into sections. The  $F/F_0$  values within the first section were averaged to serve as a baseline. Consecutive flushes of HBSS<sup>-/-</sup> followed by an HBSS<sup>+/+</sup> exchange occurred during the second section. At time = 300 seconds, the electrical stimulus was applied for the duration of the third segment. Comparing the endpoint relative fluorescence ( $F/F_0$ ) to those values at the onset of electrical stimulation, intracellular calcium concentration increased for the electrical stimulation condition, decreased for the nifedipine condition, and approximately no net change in the unstimulated condition.

## Discussion

The electrical stimulation assays testing L929 proliferation when cultured in the custom electrical stimulation chambers on glass and HA and HA-CNT substrates illustrate several key findings. First, L929 proliferation was not altered regardless of substrate type within 24h of initial cell seeding. Second, L929 proliferation was not impacted when comparing metabolic activity between cells cultured on HA and HA-CNT nanofibrous substrates with or without electrical stimulation using a 300 mV/mm biphasic square AC waveform. Considering these two outcomes, we concluded that our custom electrical stimulation system: (1) provided a biocompatible electrical stimulation environment for (2) observing cell behavior on electroactive biomaterial substrates in a (3) with reproducible, predictable outcomes. By establishing these 3 key factors, we concluded our electrical stimulation system was well-suited for experimental observations in cell types known to be sensitive to culture conditions and microenvironments.

We report the quantification of neuron behavior as measured by neurite length and number of neurite-bearing neurons following electrical stimulation through HA and HA-CNT nanofibrous systems using a dissociated DRG *in vitro* model. We demonstrate that HA-CNT nanofibrous substrates increase the effectiveness of sustained neuron growth as evidenced by neurite length and neuron number through 72h with only 1 hour of an applied 20 Hz biphasic AC waveform 24h following initial seeding. While it should be noted that there are three potential cell phenotypes present in a dissociated DRG cell suspension, Schwann cells, neurons, and satellite cells, our results are nonetheless profound. Future advancement in the field would ideally quantify cell behavior of all phenotypes present in a co-culture.

Other groups have reported the use of carbon nanotubes as part of bioactive material composites to elicit cellular repair mechanisms (Huang et al., 2012). Our results corroborate evidence previously reported by (Koppes et al.) that electrical stimulation significantly enhances DRG neurite growth regardless of the integration of SWCNT to 3D collagen I-matrigel hydrogels. Moreover, they observed increased neurite length both with and without



electrical stimulation in SWCNT composite hydrogels, reporting their results were not attributable to bulk mechanical properties based on rheological data.

The main contribution of this thesis to the neural engineering field is the comprehensive quantitative material characterization that underscores the additive roles of biochemical and electrochemical material properties in activating cell behavior in response to electrical stimulation. The topography and composition, bulk and nanoscale mechanical data, and contact angle data provide evidence that topography, mechanics, and surface chemistry support neurite outgrowth in both HA and HA-CNT culture conditions. AFM topographical images of hydrated nanofibers confirmed the nanoscale fiber topography is conserved when COOH-MWCNTs are incorporated within the nanofiber core. Comparatively, the HA nanofibers displayed significant swelling behavior apparent both in traditional brightfield microscopy and in height AFM images. The addition of the electrical cue during culture significantly increased neurite number and length. By providing extensive quantitative nanomechanics and electrochemical data in conjunction with neuron behavior in response to electrical stimuli, we demonstrate the unique contribution of this work proposing the combination of extracellular matrix mimicry combined with electrical stimulation for neural regeneration applications. Several studies have reported the important roles hyaluronic acid and mature extracellular matrix play in regulating synaptic activity by affecting the diffusion of signaling molecules and function of membrane receptors, such as L-type VGCCs (Frischknecht et al., 2009; Kochlamazashvili et al., 2010b).

Experimental perturbations investigated the role of L-type Voltage-Gated Calcium Channels (VGCCs) in modulating calcium influx using an electrical stimulus that previously resulted in significantly increased neurite outgrowth and neuron viability. Preliminary data indicated a potential role of L-type VGCCs in neuron response when electrically stimulated in culture on HA-CNT nanofibers. We present here a method for future exploration of the molecular mechanisms underlying the effects of electrical stimulation on the regenerative behavior in dorsal root ganglia neurons.

Method development was challenging given the multiple factors contributing to experimental success. Examples of experimental factors contributing to successful trials include cell density, Fluo-4 AM loading concentration and time, imaging conditions and acquisition including illumination intensity. It is possible to use an excitation intensity that is too high; we observed membrane blebbing in earlier trials indicative of the activation of apoptotic cascades. It was determined the observed apoptosis was due to phototoxicity. By reducing the power of the illumination source, increasing the time between frame acquisition, and incorporating an endpoint viability stain, we were able to confirm that apoptotic responses to experimental conditions were eliminated. Using a perfusion set-up enabled a stable region of interest to be imaged enabling data collection throughout the time course of the experiment, from initial baseline cytoplasmic fluorescence through the live/dead stain at the end of each experimental trial.

There are two major limitations in the experimental method and preliminary data shown reported here. First, perfusion was performed manually versus by a peristaltic or syringe pump which results in inconsistent temporal resolution between experimental groups. Second, there is a limited sample size. The preliminary data reported here includes one trial and low sample number for each of the nifedipine ( $n = 5$  cells) and unstimulated ( $n = 2$  cells) groups. The reported stimulated data set is an average of 2 trials with  $n = 3$  cells each.

Future work should explore the relationships between electrical stimulation of neurons cultured on conductive nanofibers and molecular mechanisms that are dependent on voltage-gated calcium channels. Calcium signaling and calcium-sensitive protein transcription such as BDNF and its receptor *trkB* which have been demonstrated to have downstream effect on increased f-actin polymerization during growth cone formation (Al-Majed et al., 2000a; Kamber et al., 2009; Wenjin et al., 2011).

A major contribution of the work presented in this chapter is the elucidation of electrical stimulation (ES) parameters and their effects on neuron growth, particularly the parameters of time duration of application and voltage magnitude. In the electrical stimulation for neural

tissue engineering and regeneration literature, time durations for ES range from one application for 1 hour duration to four consecutive days of ES for 6-8 h durations each time (Steel and Sundararaghavan, 2016). For realistic clinical therapeutic applications, Al Majeed et al demonstrated the feasibility *in vivo* of a 1-hour stimulation. Our results here provide the first to our knowledge demonstration *in vitro* of side by side comparison of single application of AC waveform regimes delivered through conductive nanofibrous biomaterial substrate on neuron outgrowth and viability. Not only did we verify previous reports in the literature of short durations of electrical exposure with lasting results (72h post stimulation), we also have identified a threshold signal intensity (200 mV) for despite substrate type. If considering the 20 Hz impedance values for HA-CNT versus HA (approximately 9800 Ohms and 16500 Ohms respectively), it could be logical to infer that a lower impedance material would exhibit a time dependent dose response effect compared to a higher impedance material under the same stimuli given that impedance describes resistance to the flow of current. If downstream BDNF expression is dependent on ionic influx and ion flow across the membrane can be described as ion current, it may be a reasonable to identify the calcium-dependent BDNF expression and release as a target molecular mechanism in our system.

Previous work has shown whole DRGs to exhibit significantly more neurite outgrowth following electrical stimulation when compared to unstimulated controls.(Xie et al., 2009b) Recent work by the Thompson group has revealed that Schwann cells increase secretion of NGF following electrical stimulation.(Koppes et al., 2014a) It is possible that the enhanced neurite outgrowth observed in the Xie study was due to increased secretion of NGF by Schwann cells. A limitation of our study is that other cell types present as a result of the use of a dissociated tissue explant that were affected by the applied ES prevents us from assigning neuron behavior purely as a results of neuron response to ES. However, we can recognize that if Schwann cells were affected by ES, there is supporting evidence in the literature that there is T-Type VGCC mediation of NGF production and release in Schwann cells (Luo et al., 2014) and that ES has a significant growth-promoting effect on neurons (Koppes et al.,

2014a; Koppes et al., 2011). T-type VGCC is related to a Schwann cell proliferation and a pro-myelinating SC phenotype, with far reaching implications for treatments beyond traumatic nerve injury to de-myelinating neurodegenerative diseases (Luo et al., 2014). Moreover, Schwann cells have also been implicated in NGF production and release in response to ES (Koppes et al., 2014a; Thompson et al., 2014). There is potential that electrical stimulation activates intracellular molecular cascades for any cell type present in the dissociated DRG culture that contains membrane voltage gated channels. Future studies are required to identify which voltage sensitive channels act synergistically to activate regenerative behavior when neuron and support cells cultured on conductive materials are electrically stimulated.

### **Conclusion**

With the comprehensive consideration of the material characterization presented in Ch 2, the data supporting the appropriate *in vitro* model in Ch 2 and Ch3 culminating in a clear cell response to electrical stimuli delivered through electroactive nanofibrous HA scaffolds, further enhanced by the presence of ultra-low concentration of dispersed and confined COOH-MWCNTs within the nanofiber geometry, we conclude that it is reasonable to advance investigations to molecular biological techniques to quantify major players in the L-type VGCC - BDNF pathway. RT-PCR, microarray, and more specific techniques like single cell analysis could elucidate the cellular phenotypes and sub-phenotypes responsible for this observed behavior. This body of work has great potential in providing a foundation to merge biomaterial scientists with efforts like those of the Human Cell Atlas consortium to usher in a deeper understanding of unresolved mechanisms of cell behavior responses to biomaterials.

## **Chapter 5 : Successful Biomaterials Engineering Requires Failure**

Portions of this chapter are contained in the publication:

Steel E.M., Sundararaghavan H.G. (2016) Electrically Conductive Materials for Nerve Regeneration. In: Zhang L., Kaplan D. (eds) Neural Engineering. Springer, Cham.

### **Design Iteration for Biomaterial Development**

To Engineer Is Human: The Role of Failure in Successful Design by Henry Petroski provides a window into the engineering ethos and oft underappreciated humanistic factors that are the foundations of the greatest advancements in human civilization. Engineering solutions for society's greatest problems require an understanding of as applied to a specific system. To design a solution for a problem, the circumstances and parameters of the problem must be defined. For complex problems, all the parameters of the system under investigation are not known quantitatively. In these cases, to converge upon a solution, quantitative measurements must be acquired to reduce the number of unknowns and in cases for which it is impossible or impractical to replace an unknown with a value derived from quantified data, it is necessary for the practitioner to substitute the unknown with an assumption. The assumption should be derived from what is generically referred to as "an educated guess" which should be backed by a clear rationale *and* an understanding that presented new evidence, that "educated guess" can be replaced with a refined value. Thus, Professor Petroski's main argument provides an apt perspective for the process to fabricate, test, and validate the HA-CNT nanofibers for electrically stimulating regeneration in Neural Tissue Engineering (NTE) applications: "... the concept of failure... is central to understand(ing) what engineering is and what engineers do." Further, "to understand how failures can happen" contributes more to technological advances than do successes (Petroski, 1992). The body of work reported here is the result of design iterations seeking to match our material properties (topography(Xie et al., 2009a), modulus(Borschel et al., 2003), impedance(Donnelly, 1994; Sharp et al., 2017)) and cell responses (Xie et al., 2009a) to the predicted "educated guesses"

obtained from the associated literature (Borschel et al., 2003; Harris et al., 2013; McCaig et al., 2005).

Chapter 1 and the introductions of each of the subsequent chapters provide a sampling of the expansive body of literature substantiating the effects of electrical stimulation on nervous system development, repair, and neuronal guidance and the application of that knowledge to investigating a variety of biomaterials to facilitate tissue regeneration with combinatorial cues. Chapter 2 provided comprehensive material characterization evidence of the successful fabrication of hyaluronic-acid carbon nanotube nanofibers through an environmentally-controlled electrospinning technique using an optimized formulation. Design targets of topographical, mechanical, and conductive properties relevant to peripheral nerve (PN) regeneration were achieved. SEM and TEM were used to validate the electrospun nanofibers were incorporated with CNTs within the nanofibers with reduced number of agglomerations with a well-dispersed CNTs at ultra-low concentrations as opposed to higher concentrations. Smooth, aligned nanofibers encapsulating an ultra-low concentration of COOH-MWCNTs were successfully electrospun within methacrylated hyaluronic acid nanofibers to achieve a material with modulus below the 1 MPa and 10,000  $\Omega$  targets for PN. To our knowledge, this is the first demonstration of COOH-MWCNTs incorporated into hyaluronic acid nanofibers electrospun from an aqueous medium. Moreover, this study is the first to chronicle the local moduli of fully submersed biopolymer CNT composite nanofibers in PBS by performing Atomic Force Microscopy in Fluid using the Quantitative Nanomechanical Mapping Mode. Electrochemical characterization surveyed the impedance and capacitance properties of HA-CNT nanofibers demonstrating the ability of carbon nanotubes to conduct electrons and ions in PBS. Further, when compared to impedance values of native tissue, HA-CNT nanofibers more closely resemble peripheral nerve. The nanostructured nature of these composite hydrogel nanofibers offers the first hydrogel-based peripheral nerve interface that, at 50  $\mu\text{m}$  thickness, mimics native tissue matrix mechanics and topography, possesses the electrochemical behavior to deliver a stable and effective electrical stimulus, *and* has the

potential to be degradable. The next nearest peripheral nerve interface has been fabricated by the Otto, Judy, and Schmidt at University of Florida; the TEENI device is revolutionary in its function but unfortunately elicits a foreign body response due to its topological and mechanical mismatch with surrounding tissue (Spearman et al., 2017).

Chapter 3 validates the HA-CNT nanofibrous material as non-cytotoxic and permissive to neuron growth. Chapter 4 provides statistically significant evidence from electrical stimulation assays using dissociated dorsal root ganglia neurons that an Alternating Current electrical stimulus can be delivered through the HA-CNT nanofibers to elicit increased neurite outgrowth and viability. Further, when our *in vitro* functional end-point outcome measures are juxtaposed to the electrochemical characterization data, there is a clear, predictable pattern that emerges validating our biomaterial design using the 200  $\mu$ A electrical stimulus to increase neurite outgrowth and number of responding neurons as framed in the historical context of successful *in vitro* and human clinical trials of safe and efficacious oscillating field stimulators (Graves et al., 2011; Hamid and Hayek, 2008; Shapiro, 2014; Shapiro et al., 2005).

### **Study Strengths: in vitro neuron model**

We used a primary neuron cell model of dorsal root ganglia (DRG) neurons dissociated from DRG explants from the lumbar spinal regions of chick embryos embryonic stages day 11-13 (Song and Uhrich, 2007). Other Neural Tissue Engineering (NTE) researchers use primary neuronal cell models like those DRG dissected from chick embryos or neonatal rats, including suspensions that have been cryogenically stored (Seggio et al., 2008). Studies using other cell sources are well documented in the literature and reviewed in *Biomaterials* by Gu *et al.* including the PC-12 line, neural stem cells, and neural progenitor cells derived from induced pluripotent stem (iPS) and human embryonic stem cells, and support cells derived from marrow stromal cells (Gu et al., 2014). Chick dorsal root ganglia have a number of advantages when conducting early stage biomaterial testing. The chick embryo is a well-established model organism for embryonic development of the nervous system, embryonic

development is critically dependent on the bioelectric behavior and pathways being investigated in Chapter 4 (Burt, 2005). It is of utmost concern for researchers to consider an *in vitro* model appropriate for the systems and pathways being affected by the biomaterial being tested. The chick embryo was deemed an appropriate animal model from which to derive our primary cell samples based on the evolutionary conservation of the nervous system physiological pathways under investigation (Barde, 1989; McCaig et al., 2005; Tyler, 2017). Phylogenetic mapping of intracellular signaling pathways downstream from the calcium 2<sup>nd</sup> messenger influx through VGCCs would be necessary in order to determine an appropriate model (Burt, 2005; Tyler, 2017). It should be noted that findings discussed in this body of work should be considered in the context of the *in vitro* model employed. To effectively translate electroceutical and electroactive tissue engineering based treatments into humans, relevant *in vivo* models should be employed, particularly when evaluating a combinatorial approach for potential in treatment of human critical gap defects (Bellamkonda, 2006; Kaplan et al., 2015).

### **Future Directions**

Repeating the calcium imaging experiments for the method developed in Chapter 4 would elucidate the molecular pathways involved to increase regeneration following electrical stimulation of neurons cultured on conductive nanofibers. The first step in this would be to perform high resolution, functional calcium imaging on neuron and glial voltage-gated calcium channel (VGCCs) activity (Luo et al., 2014; Shin et al., 2017; Wang, 2009; Wenjin et al., 2011). Neurons are known to express L-type VGCCs, Schwann cells T-type VGCCs, and cell-cell interactions like those described by Zhang with satellite cells releasing ATP make tissue level physiology feedback responses to electrical stimulation especially complex (Zhang et al., 2007a).

Developmental models can be advantageous to use when defining fundamental cell processes using basic science techniques, even if there is call for concern that chick and rodent models do not “directly translate” to human regenerative processes. By implementing the



technique outlined in this thesis, the next step is to quantify BDNF and other neurotrophic expression dynamics. Just as Borgens and colleagues used lower order animal models to elucidate basic mechanisms, and other groups like McCaig and et. al. (McCaig et al., 2002; McCaig et al., 2005) spring boarded to define mechanisms for neuronal targeting behavior, biomedical engineers should consider the strategy to refine molecular mechanisms in a simplified model. This strategy may then prove fruitful in long-term device development to adapt solid, fundamental cell and developmental biology to medical device development when underlying mechanisms are evolutionarily conserved. With the advent and exponential capacity of the scientific community to move from a basic model that has thorough genomic, proteomic, and cytomic characterization due to the capability of single cell analysis, evolutionary biologists like Dean Scott Lanyon at the University of Minnesota propose greater success can be achieved in relevant pre-clinical trials by performing phylogenetic mapping of developmental models against large animal models.

This body of work fills a gap identified by the 2014 Thompson review of electrical stimuli in the central nervous system that there are few comprehensive studies that investigate electrical stimulation in combination with other cues like topography, chemical, and mechanics (Thompson et al., 2014). Our future goals, that future work must systematically characterize the molecular mechanisms underlying regenerative cell behavior following electrical stimulation. Understanding the conductive material-protein -cell interactions informs material selection during scaffold design. Integration of these knowledge bases is crucial in developing clinically translational neural tissue engineering treatments.

Challenges experienced by biomaterials researchers are ever-increasing as we have more information at our finger tips than ever, but less bandwidth and capacity to review, integrate, and distill which studies are grounded in foundational concepts. Particularly challenging, is reviewing the literature and selecting material design criteria without a specific goal in mind. We found it particularly useful in the thesis reported here to choose a specific application within the nervous system, and further a specific application in the peripheral

nerve system. We believe our HA-CNT composite material has the potential to be developed for future applications across multiple indications of various nervous disorder and dysfunction as well as other systems. By simplifying our first use case, we created a simplified *in vitro* model using our nanofibrous scaffold. Most importantly, we modeled a dynamic system rather than a static system given the wealth of information available. Moving forward, future research could employ computer generated neural network seeded with values from literature reports could be used by biomaterials researchers to model their proposed material design akin to finite element modeling and analysis. Atomic Force Microscopy extracellular matrix topographical mapping of Type I collagen has served as a foundation(Wallace et al., 2010) for finite element modeling and analysis to predict cortical bone fracture.(Wang and Ural, 2018) This type of advancement could accelerate product development and decrease the resources necessary such as budgetary expenditures and time to market, thus ultimately impacting our intended customers. While training as a graduate level biomedical engineer, I was fascinated to learn that my target customers were not patients but the clinicians, insurance companies, regulatory entities, and other key decision-makers.

Reports in the literature of material characterization as a resistance value, an impedance value, and as dielectric constants make electroactive material design challenging for researchers to discern which differences are the most crucial for a given application. An understanding of the underling electrical engineering and mathematics to model the cell membrane could be instructive when designing a biomaterial for a specific application. If one is designing a material to target a single cell, or a tissue, could affect the selection of initial design parameters. Cellular, systems, and organismal level feedback mechanisms can be modeled using engineering techniques like mathematical modeling is applied to neurons, circuits, and systems.(Gutkin et al., 2003)

### **Electrical Stimulation: Incomplete Mechanistic Evidence**

A handful of studies have provided evidence identifying molecular targets affected by electrical stimulation. The 2012 Guo study observed an increase in the expression of the

extracellular matrix proteins collagen I, elastin, and fibronectin I by NIH 3T3 fibroblasts piezoelectrically excited through polyurethane (PU)/PVDF scaffolds affixed to a flexible-bottomed culture plate (Flexcell) by applying an 8% deformation at 0.5 Hz (Guo et al., 2012). The protein expression from cells cultured on nonpiezoelectric-excited PU/PVDF scaffolds and PU scaffolds under the same deformation conditions were not significantly different from one another (Guo et al., 2012). When PC12 neuronal-like cells were cultured on a CNT-coated PLCL fibrous scaffold, Jin et al. discovered increased expression of focal adhesion kinase (FAK), which plays a role in integrin-mediated binding (Jin et al., 2011b). Although this result suggests that FAK activation due to integrin receptors binding to CNTs may be involved in the pathway responsible for increased neurite outgrowth, further investigation is needed to determine if this observation is repeatable and quantifiable under electrical stimulation conditions. Using adult rat DRG neurons and PC12 cells, Eva *et. al.* demonstrated that the proteins ARF6 and Rab11 are required for optimal integrin-dependent axon regeneration following injury, due to their roles in trafficking of the integrin subunits,  $\alpha 9$  and  $\beta 1$  (Eva et al., 2012). These integrins may serve as viable targets to elucidate their involvement in FAK activation in future studies.

Other studies investigating receptor-mediated mechanisms indicate voltage-gated calcium channels to play a role in enhanced neurite outgrowth. Several studies have reported accelerated motoneuron axonal regeneration in response to an AC square wave signal that was associated with an upregulation of BDNF and the receptor trkB (Al-Majed et al., 2000a; Al-Majed et al., 2004). Multiple promoters can be activated to induce BDNF transcription by pathways involving trkB receptors as well as through calcium influx through voltage-gated calcium channels and NMDA receptors.  $\text{Ca}^{2+}$ -dependent signaling is propagated to calcium responsive elements regulated by calcium stimulated protein kinases (Zheng et al., 2011). After being released from the post-synaptic membrane, BDNF can act in an autocrine fashion on local trkB receptors triggering the MAPK signaling cascade that downstream increases actin polymerization (Brushart et al., 2002; Difato et al., 2011; Hronik-Tupaj et al., 2013). Calcium

influx has also been associated with f-actin polymerization during growth cone formation (Kamber et al., 2009). GAP-43 stabilizes f-actin polymerization and microtubule formation in the growth cone (Aigner, 1995). Interestingly, the electrical stimulation studies that found increased expression of BDNF and its receptor trk-B associated with accelerated motoneuron growth, also found an increase in GAP-43 expression and the cytoskeletal proteins tubulin and actin (Al-Majed et al., 2004; Hronik-Tupaj et al., 2013).

Wenjin et al. (2011) demonstrated that BDNF expression following electrical stimulation is dependent on calcium influx through voltage-gated calcium channels (VGCC) which activates the extracellular signal regulated kinase (Erk) pathways. Electrical stimulation of spinal cord neuron cultures treated with the L-type VGCC inhibitor nifedipine resulted in a reduction in the upregulation of BDNF expression seen with the stimulated controls. (Wenjin et al., 2011) Nifedipine is in the dihydropyridine class of antagonistic molecules that block L-type VGCC activity. (Gurkoff et al., 2013) The Erk phosphorylation inhibitor PD98059 eliminated the upregulation of BDNF seen in stimulated controls and reduced expression beyond the basal levels measured in the unstimulated controls. PD98058 specifically blocks the phosphorylation of Erk which then prevents the phosphorylation of the transcription factor CREB required in BDNF transcription. (Wenjin et al., 2011)

Calcium channels and two-pore domain potassium (2-PK) channels can be influenced by electrical stimulation serving to activate neurite outgrowth through cytoskeletal protein synthesis (Huang et al., 2012; Mathie et al., 2003). Electric field stimulation may regulate protein kinase A and C phosphorylation, which mediate the activation of the 2-PK channel (Mathie et al., 2003). Two groups have demonstrated that electrical stimulation of Schwann cells activates T-type voltage-gated calcium channels leading to increased intracellular calcium production resulting in calcium-dependent exocytosis of NGF (Huang et al., 2010; Koppes et al., 2014a). Similarly, through the use of calcium imaging, VGCCs have been identified as the transducers of electrical cues in neural stem cells differentiated into

neurons(Park et al., 2011) and embryonic rat hippocampal neurons(Wang et al., 2006) when stimulated through graphene and CNT substrates.

Towards defining electrical cue signal parameters, Shi *et. al.* applied both voltage-defined signals (100 mV/mm) and current defined signals (2.5, 25, and 250  $\mu$ A/mm) to human cutaneous fibroblasts cultured on gold-coated Petri dishes (Shi et al., 2008). They found no significant effect of the surface current density on cell adhesion or viability; whereas, the constant 100 mV/mm electrical field significantly increased adhesion and viability. These results taken in accordance with the previous discussion on VGCCs suggest that voltage rather than current modulates the effects of electrical stimulation on cell behavior. One theory suggests that enhanced neurite outgrowth may be due to ionic current in the culture medium or interstitial fluid due to the applied electric field (Patel and Poo, 1982; Schmidt et al., 1997).

There is debate concerning the method of electrical stimulation, as to whether the electrodes that are delivering the electrical signal to the conductive material must be separated from the media surrounding the cells during culture (Pires et al., 2015). Schmidt argues that if the stimulus is under the point at which electrolysis of water occurs (1.2 V), then the electrodes can in contact with the cell media..(Schmidt et al., 1997) Results from both Patel and Schmidt provide evidence that field-induced ion transport through the media played no role in the effects elicited by electrical stimulation. The former discovered more growth-controlling membrane glycoproteins in growth cones near the cathode, suggesting an electrophoretic redistribution of charged membrane components (Patel and Poo, 1982). When cells are cultured on plastic with an exogenously applied current, Schmidt and colleagues found results similar to the non-stimulated control (Schmidt et al., 1997).

Other studies attribute enhanced cell behavior to be due to the attraction and adsorption of serum proteins to the surface of the stimulated substrate. Kotwal and Schmidt observed enhanced neurite outgrowth in PC12 cells following surface adsorption of fibronectin to PPy films.(Kotwal and Schmidt, 2001) Interestingly, neurite outgrowth was not increased if stimulation was delayed for 2 hours. The group offered altered protein conformation

following stimulation to explain enhanced neurite outgrowth. Recently, Schmidt and colleagues have systematically investigated the effects of protein adsorption and electric field strength on Schwann cell behavior. Their results suggest that Schwann cell migration directionality towards the anode is a function of electric-field-mediated phenomenon whereas migration speed is an integrin- or receptor-mediated phenomenon (Forciniti et al., 2014). The group notes that other studies which conclude that Schwann cell migration was an electric-field-mediated phenomenon cannot make that claim due to the confounding factors of using composite PPy materials or co-culturing Schwann cells with neurons. For example, Quigley observed increased migration distance of Schwann cells from DRG explants after electrical stimulation on a PPy platform upon which 75:25 PLA:PLGA fibers had been wet-spun. (Quigley et al., 2009) Cell-cell interactions between neurons and Schwann cells as well as the polymer blend may have influenced Schwann cell behavior.

While there is an ever-growing body of studies indicating benefits of electrical stimulation, future *in vitro* studies should include data to elucidate the molecular mechanisms behind enhanced neural and glial cell behavior. Experiments which utilize quantitative RT-PCR, in-cell western blot analyses, and flow cytometry function to determine the targets and molecular pathways involved. It could also be informative to use siRNA to knockdown gene expression suspected to be associated with growth and migration processes. siRNA knockdown studies could help determine signal transduction pathways that may be affected by electrical stimulation. Once more comprehensive evidence of molecular mechanisms has been collected, electrical stimulation of co-cultures of neurons and glial cells could be informative to gain a systems understanding. Further, once molecular pathway targets have been identified, the exact parameters of the electrical stimulus or waveform necessary to elicit desired effects can be defined.

*In vivo* assessment of scaffold efficacy is also required to demonstrate the potential for clinical efficacy. It is critical to drive forward animal testing to gain crucial information regarding long-term physiological response to conductive materials, functional recovery of

nerves, and immune response to degradation products. In a review of peripheral nerve regeneration, Bellamkonda emphasizes several key points with regards to evaluating scaffold efficacy in animal models. First, the scaffolds in question should repair nerve defects greater than 15 mm (in rats) and be compared to control autografts. If these repairs are successful, the scaffolds should then be tested in a larger animal model with gap lengths greater than 40 mm. He asserts that in order for these interventions to be clinically translatable, it is equally important to perform electrophysiological studies to assess the functional repair of sensory and motor nerve fibers in addition to histological measurement of neuromuscular junctions (Bellamkonda, 2006). Extending these principles to *in vivo* electrical stimulation studies is essential for characterizing the efficacy of interventions using conductive scaffolds.

From the conductive scaffold design and synthesis side, fabrication techniques utilizing 3D printing and extrusion technologies may become more widespread. Mire *et. al.* embedded conductive PEDOT tracks into chitosan and HA based substrates using custom-built extrusion printing systems with programmable xyz-translation paving the way for future gel matrix based, integrated structures containing embedded conductive components, cells, and microdevices (Mire et al., 2011). Inkjet printing techniques allow for high resolution for enhanced spatial control over cell behavior when delivering electrical stimulation. (Mire et al., 2011; Weng et al., 2012) Recently, a stereolithography-based platform was used to 3D bioprint complex tissue using UV crosslinking after printing different types of materials. (Miri et al.) Our hyaluronic acid-CNT formulation could be integrated into this system, used as either a bioink or as nanofibers combined in a layer by layer approach for integration of nano- and micron- features. (Miri et al.)

## **Conclusion**

To summarize, the contributions of this dissertation research demonstrated the potential for electrically conductive HA-CNT nanofibrous substrates to elicit regenerative behavior in neural tissue cell types. To our knowledge, the data presented is the first to demonstrate electrospun methacrylated hyaluronic acid nanofibers containing carboxylated

multi-walled carbon nanotubes within the nanofiber core. The fabrication method was performed using an aqueous solution using biocompatible dispersants (1% BSA saline) to minimize aggregation. Further, an ultra-low concentration of carbon nanotubes achieved conductivity and charge capacity capable of transmitting electronic stimuli in a physiological environment while maintaining an elastic modulus relevant to peripheral nervous tissue (local Young's modulus  $\sim 200$  kPa). Moreover, this is the first report of electrochemical characterization of hyaluronic acid nanofibers demonstrating that the nanoscale fiber diameter topography alone without a conductive filler contributes to low impedance ( $6.3 \text{ k}\Omega$  at  $1 \text{ kHz}$ ) and high capacitance ( $15.3 \text{ mF/cm}^2$ ) relative to nanofibers containing CNT aggregates that disrupt the nanofiber surface (*e.g.* 0.3% CNT). Interestingly, electrical stimulation parameters of time duration and amplitude each were statistically significant drivers in increasing neurite growth and neuron viability for neurons cultured on either HA or HA-CNT nanofibers. The largest gains in neurite growth and neuron viability were observed in neurons cultured on 0.01% HA-CNT nanofibers for 60 minutes at  $150 \text{ mV/mm}$  amplitude and above. Furthermore, the enhanced neuron growth for neurons cultured on HA-CNT relative to HA can be attributed to the electrochemical properties of charge capacity. Graves et al. (2011) demonstrated that a biphasic, charge balanced AC rectangular wave of  $200 \text{ }\mu\text{A}$  amplitude induced the greatest neurite outgrowth. The cyclic voltammetry data presented in Chapter 2 give quantitative evidence that at  $150 \text{ mV/mm}$  a  $200 \text{ }\mu\text{A}$  current amplitude is achieved in the HA-CNT nanofibers, whereas  $200 \text{ mV/mm}$  is the threshold required for the HA nanofibers. In conclusion, HA nanofibers containing an ultra-low concentration of hydrophilic carbon nanotubes offer a promising conductive biomaterial for electrical stimulation biomedical applications by matching extracellular matrix properties with enhanced electronic to ionic conductive properties.

Future success in clinical translation of this early phase HA-CNT conductive nanofibrous composite material is dependent upon:



- (1) characterizing the molecular mechanisms activated by electrical stimulation that influence cell behavior
- (2) designing conductive materials that meet all the design criteria
- (3) and systematically testing efficacy in functional *in vivo* studies.

The implications of developing effective conductive biomaterials that modulate cell behavior based on mechanistic understanding extend beyond neural tissue into the broader realm of all organ systems in the tissue engineering and regenerative medicine fields. The HA-CNT conductive nanofibrous system in this work is poised to advance to the next stages of study to realize fully functional neural regeneration.

## APPENDIX A

**Table A-1. Descriptive Statistics from SPSS Output 3-way ANOVA.**

The Dependent Variable reported here is Neurite Length. See Table A4 for Descriptive Statistics for Number of Neurite-bearing neurons, taking note that the number of observations are the same and are paired to the originating neuron with a qualifying length according to inclusion criteria described in the Methods.

| Descriptive Statistics |        |       |        |                |      |
|------------------------|--------|-------|--------|----------------|------|
| Dependent Variable:    | Length |       |        |                |      |
|                        | Time   |       | Mean   | Std. Deviation | N    |
| 0                      | 0      | CNT   | 198.71 | 153.07         | 146  |
|                        |        | HA    | 139.24 | 152.90         | 51   |
|                        |        | Total | 183.32 | 154.85         | 197  |
|                        | Total  | CNT   | 198.71 | 153.07         | 146  |
|                        |        | HA    | 139.24 | 152.90         | 51   |
|                        |        | Total | 183.32 | 154.85         | 197  |
| 30                     | 150    | CNT   | 211.91 | 157.14         | 94   |
|                        |        | HA    | 135.64 | 119.79         | 76   |
|                        |        | Total | 177.81 | 146.30         | 170  |
|                        | 200    | CNT   | 273.19 | 167.05         | 83   |
|                        |        | HA    | 229.07 | 167.28         | 32   |
|                        |        | Total | 260.91 | 167.56         | 115  |
|                        | 250    | CNT   | 288.77 | 153.02         | 103  |
|                        |        | HA    | 227.07 | 225.70         | 9    |
|                        |        | Total | 283.81 | 159.59         | 112  |
|                        | Total  | CNT   | 258.35 | 161.64         | 280  |
|                        |        | HA    | 168.23 | 149.18         | 117  |
|                        |        | Total | 231.79 | 163.15         | 397  |
| 60                     | 150    | CNT   | 316.12 | 206.42         | 177  |
|                        |        | HA    | 192.59 | 132.74         | 94   |
|                        |        | Total | 273.27 | 193.17         | 271  |
|                        | 200    | CNT   | 348.40 | 194.67         | 121  |
|                        |        | HA    | 252.10 | 174.84         | 37   |
|                        |        | Total | 325.85 | 194.03         | 158  |
|                        | 250    | CNT   | 299.74 | 204.01         | 177  |
|                        |        | HA    | 234.45 | 170.01         | 55   |
|                        |        | Total | 284.26 | 198.10         | 232  |
|                        | Total  | CNT   | 318.24 | 203.06         | 475  |
|                        |        | HA    | 216.81 | 154.54         | 186  |
|                        |        | Total | 289.69 | 195.93         | 661  |
| Total                  | 0      | CNT   | 198.71 | 153.07         | 146  |
|                        |        | HA    | 139.24 | 152.90         | 51   |
|                        |        | Total | 183.32 | 154.85         | 197  |
|                        | 150    | CNT   | 279.97 | 196.85         | 271  |
|                        |        | HA    | 167.13 | 129.88         | 170  |
|                        |        | Total | 236.47 | 182.43         | 441  |
|                        | 200    | CNT   | 317.80 | 187.21         | 204  |
|                        |        | HA    | 241.42 | 170.51         | 69   |
|                        |        | Total | 298.49 | 185.82         | 273  |
|                        | 250    | CNT   | 295.70 | 186.66         | 280  |
|                        |        | HA    | 233.41 | 176.78         | 64   |
|                        |        | Total | 284.11 | 186.20         | 344  |
|                        | Total  | CNT   | 280.26 | 188.62         | 901  |
|                        |        | HA    | 189.58 | 155.07         | 354  |
|                        |        | Total | 254.68 | 184.31         | 1255 |

**Table A-2. Tests of Between-Subjects Effects from SPSS Output 3-Way ANOVA.**

| Tests of Between-Subjects Effects |                          |      |              |          |      |                    |                             |
|-----------------------------------|--------------------------|------|--------------|----------|------|--------------------|-----------------------------|
| Dependent Variable: Length        |                          |      |              |          |      |                    |                             |
| Source                            | Type III Sum of Squares  | df   | Mean Square  | F        | Sig. | Noncent. Parameter | Observed Power <sup>b</sup> |
| Corrected Model                   | 5037213.406 <sup>a</sup> | 13   | 387477.954   | 12.802   | .000 | 166.420            | 1.000                       |
| Intercept                         | 36783616.323             | 1    | 36783616.323 | 1215.258 | .000 | 1215.258           | 1.000                       |
| Time                              | 292957.639               | 1    | 292957.639   | 9.679    | .002 | 9.679              | .875                        |
| Amplitude                         | 583403.151               | 2    | 291701.575   | 9.637    | .000 | 19.274             | .982                        |
| Type                              | 930663.637               | 1    | 930663.637   | 30.747   | .000 | 30.747             | 1.000                       |
| Time * Amplitude                  | 119673.597               | 2    | 59836.799    | 1.977    | .139 | 3.954              | .410                        |
| Time * Type                       | 40315.686                | 1    | 40315.686    | 1.332    | .249 | 1.332              | .211                        |
| Amplitude * Type                  | 45977.487                | 2    | 22988.744    | .760     | .468 | 1.519              | .180                        |
| Time * Amplitude * Type           | 12210.350                | 2    | 6105.175     | .202     | .817 | .403               | .082                        |
| Error                             | 37562788.341             | 1241 | 30268.161    |          |      |                    |                             |
| Total                             | 124000385.302            | 1255 |              |          |      |                    |                             |
| Corrected Total                   | 42600001.747             | 1254 |              |          |      |                    |                             |

a. R Squared = .118 (Adjusted R Squared = .109)

b. Computed using alpha = .05

**Table A-3. Descriptive Statistics for Dependent Variable Number of Neurite-bearing Neurons on HA nanofibers.**

| Descriptive Statistics |       |                                          |                |     |
|------------------------|-------|------------------------------------------|----------------|-----|
| Dependent Variable:    |       | Neurite-bearing Neurons on HA Nanofibers |                |     |
| Amplitude              |       | Mean                                     | Std. Deviation | N   |
| 0                      | 0     | 1.70                                     | 1.860          | 30  |
|                        | Total | 1.70                                     | 1.860          | 30  |
| 150                    | 30    | 2.45                                     | 3.161          | 31  |
|                        | 60    | 6.27                                     | 5.861          | 15  |
|                        | Total | 3.70                                     | 4.541          | 46  |
| 200                    | 30    | 2.00                                     | 2.221          | 16  |
|                        | 60    | 3.08                                     | 2.999          | 12  |
|                        | Total | 2.46                                     | 2.589          | 28  |
| 250                    | 30    | .50                                      | .985           | 18  |
|                        | 60    | 4.58                                     | 5.230          | 12  |
|                        | Total | 2.13                                     | 3.884          | 30  |
| Total                  | 0     | 1.70                                     | 1.860          | 30  |
|                        | 30    | 1.80                                     | 2.605          | 65  |
|                        | 60    | 4.77                                     | 4.997          | 39  |
|                        | Total | 2.64                                     | 3.610          | 134 |

**Table A-4. Tests of Between-Subjects Effects for Two-Way ANOVA for HA.**

Between-subject effects for the dependent variable Number of Neurite-bearing Neurons on HA nanofibers considering fixed factors of Amplitude and Time

| Tests of Between-Subjects Effects |                         |                                          |             |        |      |
|-----------------------------------|-------------------------|------------------------------------------|-------------|--------|------|
| Dependent Variable:               |                         | Neurite-bearing Neurons on HA Nanofibers |             |        |      |
| Source                            | Type III Sum of Squares | df                                       | Mean Square | F      | Sig. |
| Corrected Model                   | 361.562 <sup>a</sup>    | 6                                        | 60.260      | 5.581  | .000 |
| Intercept                         | 960.615                 | 1                                        | 960.615     | 88.969 | .000 |
| Amplitude                         | 77.694                  | 2                                        | 38.847      | 3.598  | .030 |
| Time                              | 210.275                 | 1                                        | 210.275     | 19.475 | .000 |
| Amplitude * Time                  | 40.009                  | 2                                        | 20.004      | 1.853  | .161 |
| Error                             | 1371.244                | 127                                      | 10.797      |        |      |
| Total                             | 2668.000                | 134                                      |             |        |      |
| Corrected Total                   | 1732.806                | 133                                      |             |        |      |

a. R Squared = .209 (Adjusted R Squared = .171)

**Table A-6. Descriptive Statistics for the dependent variable Number of Neurite-bearing Neurons on HA-CNT nanofibers.**

| <b>Descriptive Statistics</b> |       |                                                                  |                |     |
|-------------------------------|-------|------------------------------------------------------------------|----------------|-----|
|                               |       | Dependent Variable: Neurite-bearing Neurons on HA-CNT Nanofibers |                |     |
| Amplitude                     |       | Mean                                                             | Std. Deviation | N   |
| 0                             | 0     | 4.29                                                             | 2.970          | 34  |
|                               | Total | 4.29                                                             | 2.970          | 34  |
| 150                           | 30    | 3.03                                                             | 3.125          | 31  |
|                               | 60    | 11.06                                                            | 10.063         | 16  |
|                               | Total | 5.77                                                             | 7.361          | 47  |
| 200                           | 30    | 4.15                                                             | 3.265          | 20  |
|                               | 60    | 10.08                                                            | 8.207          | 12  |
|                               | Total | 6.38                                                             | 6.241          | 32  |
| 250                           | 30    | 1.95                                                             | 5.236          | 20  |
|                               | 60    | 14.75                                                            | 8.024          | 12  |
|                               | Total | 6.75                                                             | 8.905          | 32  |
| Total                         | 0     | 4.29                                                             | 2.970          | 34  |
|                               | 30    | 3.04                                                             | 3.900          | 71  |
|                               | 60    | 11.88                                                            | 8.939          | 40  |
|                               | Total | 5.77                                                             | 6.752          | 145 |

**Table A-7. Tests of Between-Subjects Effects for Two-Way ANOVA for HA-CNT.**

Between-subject effects for the dependent variable Number of Neurite-bearing Neurons on HA-CNT nanofibers considering fixed factors of Amplitude and Time.

| <b>Tests of Between-Subjects Effects</b> |                         |                                              |             |         |      |
|------------------------------------------|-------------------------|----------------------------------------------|-------------|---------|------|
| Dependent Variable:                      |                         | Neurite-bearing Neurons on HA-CNT Nanofibers |             |         |      |
| Source                                   | Type III Sum of Squares | df                                           | Mean Square | F       | Sig. |
| Corrected Model                          | 2289.859 <sup>a</sup>   | 6                                            | 381.643     | 12.318  | .000 |
| Intercept                                | 6000.584                | 1                                            | 6000.584    | 193.674 | .000 |
| Amplitude                                | 34.476                  | 2                                            | 17.238      | .556    | .575 |
| Time                                     | 1981.848                | 1                                            | 1981.848    | 63.966  | .000 |
| Amplitude * Time                         | 187.881                 | 2                                            | 93.940      | 3.032   | .051 |
| Error                                    | 4275.631                | 138                                          | 30.983      |         |      |
| Total                                    | 11397.000               | 145                                          |             |         |      |
| Corrected Total                          | 6565.490                | 144                                          |             |         |      |

a. R Squared = .349 (Adjusted R Squared = .320)

**REFERENCES**

1. 2012. ASTM F813-07(2012), Standard Practice for Direct Contact Cell Culture Evaluation of Materials for Medical Devices. ASTM International, West Conshohocken, PA.
2. Ahn, H.-S., Hwang, J.-Y., Kim, M.S., Lee, J.-Y., Kim, J.-W., Kim, H.-S., Shin, U.S., Knowles, J.C., Kim, H.-W., Hyun, J.K., 2015. Carbon-nanotube-interfaced glass fiber scaffold for regeneration of transected sciatic nerve. *Acta Biomater.* 13, 324-334.
3. Aigner, L.C., P, 1995. Absence of persistent spreading, branching, and adhesion in GAP-43- depleted growth cones. *The Journal of Cell Biology* 128, 647-660.
4. Al-Majed, A.A., Brushart, T.M., Gordon, T., 2000a. Electrical stimulation accelerates and increases expression of BDNF and trkB mRNA in regenerating rat femoral motoneurons. *European Journal of Neuroscience* 12, 4381-4390.
5. Al-Majed, A.A., Neumann, C.M., Brushart, T.M., Gordon, T., 2000b. Brief electrical stimulation promotes the speed and accuracy of motor axonal regeneration. *Journal of Neuroscience* 20, 2602-2608.
6. Al-Majed, A.A., Tam, S.L., Gordon, T., 2004. Electrical stimulation accelerates and enhances expression of regeneration-associated genes in regenerating rat femoral motoneurons. *Cell. Mol. Neurobiol.* 24, 379-402.
7. Allen, D.M., Mao, J.J., 2004. Heterogeneous nanostructural and nanoelastic properties of pericellular and interterritorial matrices of chondrocytes by atomic force microscopy. *Journal of Structural Biology* 145, 196-204.
8. Ambegaokar, V., Halperin, B.I., Langer, J.S., 1971. Hopping Conductivity in Disordered Systems. *Phys Rev B-Solid St* 4, 2612.
9. Anderson, M., Shelke, N.B., Manoukian, O.S., Yu, X., McCullough, L.D., Kumbar, S.G., 2015. Peripheral Nerve Regeneration Strategies: Electrically Stimulating Polymer Based Nerve Growth Conduits. 43, 131-159.

10. Arora, S., Kaur, H., Kumar, R., Kaur, R., Rana, D., Rayat, C.S., Kaur, I., Arora, S.K., Bubber, P., Bharadwaj, L.M., 2015. In Vitro Cytotoxicity of Multiwalled and Single-Walled Carbon Nanotubes on Human Cell Lines. *Fullerenes Nanotubes and Carbon Nanostructures* 23, 377-382.
11. Arslantunali, D., Budak, G., Hasirci, V., 2014. Multiwalled CNT-pHEMA composite conduit for peripheral nerve repair. *Journal of Biomedical Materials Research Part A* 102, 828-841.
12. Balasubramanian, K., Burghard, M., 2005. Chemically Functionalized Carbon Nanotubes. *Small* 1, 180-192.
13. Barde, Y.-A., 1989. Trophic factors and neuronal survival. *Neuron* 2, 1525-1534.
14. Bellamkonda, R.V., 2006. Peripheral nerve regeneration: An opinion on channels, scaffolds and anisotropy. *Biomaterials* 27, 3515-3518.
15. Berlin, Y.A., Hutchison, G.R., Rempala, P., Ratner, M.A., Michl, J., 2003. Charge hopping in molecular wires as a sequence of electron-transfer reactions. *J Phys Chem A* 107, 3970-3980.
16. Bhattacharyya, S., Guillot, S., Dabboue, H., Tranchant, J.-F., Salvetat, J.-P., 2008a. Carbon Nanotubes as Structural Nanofibers for Hyaluronic Acid Hydrogel Scaffolds. *Biomacromolecules* 9, 505-509.
17. Bhattacharyya, S., Guillot, S., Dabboue, H., Tranchant, J.F., Salvetat, J.P., 2008b. Carbon nanotubes as structural nanofibers for hyaluronic acid hydrogel scaffolds. *Biomacromolecules* 9, 505-509.
18. Borgens, R.B., 1999. Electrically mediated regeneration and guidance of adult mammalian spinal axons into polymeric channels. *Neuroscience* 91, 251-264.
19. Borgens, R.B., 2000. An imposed oscillating electrical field improves the recovery of function in neurologically (vol 16, pg 639, 1999). *J. Neurotrauma* 17, 727-727.
20. Borschel, G.H., Kia, K.F., Kuzon, W.M., Dennis, R.G., 2003. Mechanical properties of acellular peripheral nerve. *J. Surg. Res.* 114, 133-139.



21. Boudou, T., Ohayon, J., Picart, C., Tracqui, P., 2006. An extended relationship for the characterization of Young's modulus and Poisson's ratio of tunable polyacrylamide gels. *Biorheology* 43, 721-728.
22. Brooks, D.N., Weber, R.V., Chao, J.D., Rinker, B.D., Zoldos, J., Robichaux, M.R., Ruggeri, S.B., Anderson, K.A., Bonatz, E., Wisotsky, S.M., Cho, M.S., Wilson, C., Cooper, E.O., Ingari, J.V., Safa, B., Parrett, B.M., Buncke, G.M., 2012. Processed nerve allografts for peripheral nerve reconstruction: A multicenter study of utilization and outcomes in sensory, mixed, and motor nerve reconstructions. *Microsurgery* 32, 1-14.
23. Brushart, T.M., Hoffman, P.N., Royall, R.M., Murinson, B.B., Witzel, C., Gordon, T., 2002. Electrical stimulation promotes motoneuron regeneration without increasing its speed or conditioning the neuron. *Journal of Neuroscience* 22, 6631-6638.
24. Brushart, T.M., Jari, R., Verge, V., Rohde, C., Gordon, T., 2005. Electrical stimulation restores the specificity of sensory axon regeneration. *Experimental Neurology* 194, 221-229.
25. Burdick, J.A., Chung, C., Jia, X., Randolph, M.A., Langer, R., 2005. Controlled Degradation and Mechanical Behavior of Photopolymerized Hyaluronic Acid Networks. *Biomacromolecules* 6, 386-391.
26. Burt, D.W., 2005. Chicken genome: Current status and future opportunities. *Genome Research* 15, 1692-1698.
27. Caliarì, S.R., Burdick, J.A., 2016. A Practical Guide to Hydrogels for Cell Culture. *Nature methods* 13, 405-414.
28. Chan, K.M., Gordon, T., Zochodne, D.W., Power, H.A., 2014. Improving peripheral nerve regeneration: From molecular mechanisms to potential therapeutic targets. *Experimental Neurology* 261, 826-835.

29. Cheng, C., Webber, C.A., Wang, J., Xu, Y., Martinez, J.A., Liu, W.Q., McDonald, D., Guo, G.F., Nguyen, M.D., Zochodne, D.W., 2008. Activated RHOA and peripheral axon regeneration. *Experimental Neurology* 212, 358-369.
30. Cho, M.R., Marler, J.P., Thatte, H.S., Golan, D.E., 2002. Control of calcium entry in human fibroblasts by frequency-dependent electrical stimulation. *Front. Biosci.* 7, A1-A8.
31. Cho, Y., Borgens, R.B., 2010. The effect of an electrically conductive carbon nanotube/collagen composite on neurite outgrowth of PC12 cells. *J Biomed Mater Res A* 95, 510-517.
32. Chow, W.N., Simpson, D.G., Bigbee, J.W., Colello, R.J., 2007. Evaluating neuronal and glial growth on electrospun polarized matrices: bridging the gap in percussive spinal cord injuries. *Neuron Glia Biology* 3, 119-126.
33. Corey, J.M., Lin, D.Y., Mycek, K.B., Chen, Q., Samuel, S., Feldman, E.L., Martin, D.C., 2007. Aligned electrospun nanofibers specify the direction of dorsal root ganglia neurite growth. *Journal of Biomedical Materials Research Part A* 83A, 636-645.
34. Cui, X., Lee, V.A., Raphael, Y., Wiler, J.A., Hetke, J.F., Anderson, D.J., Martin, D.C., 2001. Surface modification of neural recording electrodes with conducting polymer/biomolecule blends. *Journal of biomedical materials research* 56, 261-272.
35. Daly, W.T., Knight, A.M., Wang, H., de Boer, R., Giusti, G., Dadsetan, M., Spinner, R.J., Yaszemski, M.J., Windebank, A.J., 2013. Comparison and characterization of multiple biomaterial conduits for peripheral nerve repair. *Biomaterials* 34, 8630-8639.
36. Difato, F., Tsushima, H., Pesce, M., Benfenati, F., Blau, A., Chiaregatti, E., 2011. The formation of actin waves during regeneration after axonal lesion is enhanced by BDNF. *Sci Rep* 1, 10.

37. Ding, Z.Q., Zhu, Y.P., Branford-White, C., Sun, K., Um-I-Zahra, S., Quan, J., Nie, H.L., Zhu, L.M., 2014. Self-assembled transparent conductive composite films of carboxylated multi-walled carbon nanotubes/poly(vinyl alcohol) electrospun nanofiber mats. *Materials Letters* 128, 310-313.
38. Donnelly, D.F., 1994. A novel method for rapid measurement of membrane resistance, capacitance, and access resistance. *Biophysical Journal* 66, 873-877.
39. Dror, Y., Salalha, W., Khalfin, R.L., Cohen, Y., Yarin, A.L., Zussman, E., 2003. Carbon Nanotubes Embedded in Oriented Polymer Nanofibers by Electrospinning. *Langmuir* 19, 7012-7020.
40. Durgam, H., Sapp, S., Deister, C., Khaing, Z., Chang, E., Luebben, S., Schmidt, C.E., 2010. Novel Degradable Co-polymers of Polypyrrole Support Cell Proliferation and Enhance Neurite Out-Growth with Electrical Stimulation. *J. Biomater. Sci.-Polym. Ed.* 21, 1265-1282.
41. Ebendal, T., 1979. Stage-dependent stimulation of neurite outgrowth exerted by nerve growth factor and chick heart in cultured embryonic ganglia. *Developmental Biology* 72, 276-290.
42. Eva, R., Crisp, S., Marland, J.R., Norman, J.C., Kanamarlapudi, V., French-Constant, C., Fawcett, J.W., 2012. ARF6 directs axon transport and traffic of integrins and regulates axon growth in adult DRG neurons. *The Journal of neuroscience : the official journal of the Society for Neuroscience* 32, 10352-10364.
43. Fairfield, J.A., 2017. Nanostructured Materials for Neural Electrical Interfaces. *Adv. Funct. Mater.*, 1701145-n/a.
44. Feng, J.F., Liu, J., Zhang, X.Z., Zhang, L., Jiang, J.Y., Nolta, J., Zhao, M., 2012. Guided migration of neural stem cells derived from human embryonic stem cells by an electric field. *Stem Cells* 30, 349-355.

45. Firme Iii, C.P., Bandaru, P.R., 2010. Toxicity issues in the application of carbon nanotubes to biological systems. *Nanomedicine: Nanotechnology, Biology and Medicine* 6, 245-256.
46. Forciniti, L., Ybarra, J., Zaman, M.H., Schmidt, C.E., 2014. Schwann cell response on polypyrrole substrates upon electrical stimulation. *Acta Biomater.* 10, 2423-2433.
47. Frischknecht, R., Heine, M., Perrais, D., Seidenbecher, C.I., Choquet, D., Gundelfinger, E.D., 2009. Brain extracellular matrix affects AMPA receptor lateral mobility and short-term synaptic plasticity. *Nature Neuroscience* 12, 897.
48. Fung, Y.C., 1989. Connecting incremental shear modulus and Poisson's ratio of lung tissue with morphology and rheology of microstructure. *Biorheology* 26, 279-289.
49. Gao, Y., Deng, K., Hou, J., Bryson, J.B., Barco, A., Nikulina, E., Spencer, T., Mellado, W., Kandel, E.R., Filbin, M.T., 2004. Activated CREB Is Sufficient to Overcome Inhibitors in Myelin and Promote Spinal Axon Regeneration In Vivo. *Neuron* 44, 609-621.
50. Geremia, N.M., Gordon, T., Brushart, T.M., Al-Majed, A.A., Verge, V.M.K., 2007. Electrical stimulation promotes sensory neuron regeneration and growth-associated gene expression. *Experimental Neurology* 205, 347-359.
51. Ghasemi-Mobarakeh, L., Prabhakaran, M.P., Morshed, M., Nasr-Esfahani, M.H., Ramakrishna, S., 2009. Electrical Stimulation of Nerve Cells Using Conductive Nanofibrous Scaffolds for Nerve Tissue Engineering. *Tissue Eng. Part A* 15, 3605-3619.
52. Gottipati, M.K., Bekyarova, E., Brenner, M., Haddon, R.C., Parpura, V., 2014. Changes in the Morphology and Proliferation of Astrocytes Induced by Two Modalities of Chemically Functionalized Single-Walled Carbon Nanotubes are Differentially Mediated by Glial Fibrillary Acidic Protein. *Nano Lett.* 14, 3720-3727.

53. Graves, M.S., Hassell, T., Beier, B.L., Albors, G.O., Irazoqui, P.P., 2011. Electrically Mediated Neuronal Guidance with Applied Alternating Current Electric Fields. *Annals of Biomedical Engineering* 39, 1759-1767.
54. Gu, X.S., Ding, F., Williams, D.F., 2014. Neural tissue engineering options for peripheral nerve regeneration. *Biomaterials* 35, 6143-6156.
55. Guo, H.F., Li, Z.S., Dong, S.W., Chen, W.J., Deng, L., Wang, Y.F., Ying, D.J., 2012. Piezoelectric PU/PVDF electrospun scaffolds for wound healing applications. *Colloid Surf. B-Biointerfaces* 96, 29-36.
56. Gurkoff, G., Shahlaie, K., Lyeth, B., Berman, R., 2013. Voltage-gated calcium channel antagonists and traumatic brain injury. *Pharmaceuticals (Basel, Switzerland)* 6, 788-812.
57. Gutkin, B., Pinto, D., Ermentrout, B., 2003. Mathematical neuroscience: from neurons to circuits to systems. *Journal of Physiology - Paris* 97, 209-219.
58. Hamid, S., Hayek, R., 2008. Role of electrical stimulation for rehabilitation and regeneration after spinal cord injury: an overview. *European Spine Journal* 17, 1256-1269.
59. Hannila, S.S., Filbin, M.T., 2008. The role of cyclic AMP signaling in promoting axonal regeneration after spinal cord injury. *Experimental Neurology* 209, 321-332.
60. Harris, A.R., Morgan, S.J., Chen, J., Kapsa, R.M.I., Wallace, G.G., Paolini, A.G., 2013. Conducting polymer coated neural recording electrodes. *Journal of neural engineering* 10.
61. Haxaire, K., Braccini, I., Milas, M., Rinaudo, M., Pérez, S., 2000. Conformational behavior of hyaluronan in relation to its physical properties as probed by molecular modeling. *Glycobiology* 10, 587-594.
62. Heredia, A., Bui, C.C., Suter, U., Young, P., Schäffer, T.E., 2007. AFM combines functional and morphological analysis of peripheral myelinated and demyelinated nerve fibers. *NeuroImage* 37, 1218-1226.

63. Hopley, E.L., Salmasi, S., Kalaskar, D.M., Seifalian, A.M., 2014. Carbon nanotubes leading the way forward in new generation 3D tissue engineering. *Biotechnology Advances* 32, 1000-1014.
64. Hronik-Tupaj, M., Raja, W.K., Tang-Schomer, M., Omenetto, F.G., Kaplan, D.L., 2013. Neural responses to electrical stimulation on patterned silk films. *Journal of Biomedical Materials Research Part A* 101, 2559-2572.
65. Hu, H., Ni, Y., Montana, V., Haddon, R.C., Parpura, V., 2004. Chemically Functionalized Carbon Nanotubes as Substrates for Neuronal Growth. *Nano Lett* 4, 507-511.
66. Huang, J., Ye, Z., Hu, X., Lu, L., Luo, Z., 2010. Electrical Stimulation Induces Calcium-Dependent Release of NGF From Cultured Schwann Cells. *Glia* 58, 622-631.
67. Huang, Y.J., Wu, H.C., Tai, N.H., Wang, T.W., 2012. Carbon Nanotube Rope with Electrical Stimulation Promotes the Differentiation and Maturity of Neural Stem Cells. *Small* 8, 2869-2877.
68. J., L., C., M.P., S., C.W., K., T.C., Z., T.B., J.-K., K., 2007. Correlations between Percolation Threshold, Dispersion State, and Aspect Ratio of Carbon Nanotubes. *Adv. Funct. Mater.* 17, 3207-3215.
69. Jain, S., Webster, T.J., Sharma, A., Basu, B., 2013. Intracellular reactive oxidative stress, cell proliferation and apoptosis of Schwann cells on carbon nanofibrous substrates. *Biomaterials* 34, 4891-4901.
70. Jang, M.J., Namgung, S., Hong, S., Nam, Y., 2010. Directional neurite growth using carbon nanotube patterned substrates as a biomimetic cue. *Nanotechnology* 21, 235102.
71. Jin, G.Z., Kim, M., Shin, U.S., Kim, H.W., 2011a. Effect of carbon nanotube coating of aligned nanofibrous polymer scaffolds on the neurite outgrowth of PC-12 cells. *Cell Biol. Int.* 35, 741-745.

72. Jin, G.Z., Kim, M., Shin, U.S., Kim, H.W., 2011b. Neurite outgrowth of dorsal root ganglia neurons is enhanced on aligned nanofibrous biopolymer scaffold with carbon nanotube coating. *Neurosci. Lett.* 501, 10-14.
73. Jin, J., Limburg, S., Joshi, S.K., Landman, R., Park, M., Zhang, Q., Kim, H.T., Kuo, A.C., 2013. Peripheral Nerve Repair in Rats Using Composite Hydrogel-Filled Aligned Nanofiber Conduits with Incorporated Nerve Growth Factor. *Tissue Eng. Part A* 19, 2138-2146.
74. Jin, L., Xu, Q., Wu, S., Kuddannaya, S., Li, C., Huang, J., Zhang, Y., Wang, Z., 2016. Synergistic Effects of Conductive Three-Dimensional Nanofibrous Microenvironments and Electrical Stimulation on the Viability and Proliferation of Mesenchymal Stem Cells. *ACS Biomaterials Science & Engineering* 2, 2042-2049.
75. Kamber, D., Erez, H., Spira, M.E., 2009. Local calcium-dependent mechanisms determine whether a cut axonal end assembles a retarded endbulb or competent growth cone. *Experimental Neurology* 219, 112-125.
76. Kaplan, D.R., Miller, F.D., 2000. Neurotrophin signal transduction in the nervous system. *Current Opinion in Neurobiology* 10, 381-391.
77. Kaplan, H.M., Mishra, P., Kohn, J., 2015. The overwhelming use of rat models in nerve regeneration research may compromise designs of nerve guidance conduits for humans. *Journal of Materials Science: Materials in Medicine* 26, 1-5.
78. Kar, P., Choudhury, A., 2013. Carboxylic acid functionalized multi-walled carbon nanotube doped polyaniline for chloroform sensors. *Sens. Actuator B-Chem.* 183, 25-33.
79. Kawamura, D.H., Johnson, P.J., Moore, A.M., Magill, C.K., Hunter, D.A., Ray, W.Z., Tung, T.H.H., Mackinnon, S.E., 2010. Matching of motor-sensory modality in the rodent femoral nerve model shows no enhanced effect on peripheral nerve regeneration. *Experimental Neurology* 223, 496-504.

80. Kehoe, S., Zhang, X.F., Boyd, D., 2012. FDA approved guidance conduits and wraps for peripheral nerve injury: A review of materials and efficacy. *Injury-Int. J. Care Inj.* 43, 553-572.
81. Khan, S.P., Auner, G.G., Newaz, G.M., 2005. Influence of nanoscale surface roughness on neural cell attachment on silicon. *Nanomedicine : nanotechnology, biology, and medicine* 1, 125-129.
82. Kim, J.S., 2011. Evaluation of biocompatible dispersants for carbon nanotube toxicity tests. *Archives of toxicology* 85, 1499-1508.
83. Kim, Y.-t., The role of aligned polymer fiber-based constructs in the bridging of long peripheral nerve gaps. *Biomaterials* 29, 3117-3127.
84. Koch, D., 2012. Strength in the Periphery: Growth Cone Biomechanics and Substrate Rigidity Response in Peripheral and Central Nervous System Neurons. *Biophys. J.* 102, 452-460.
85. Kochlamazashvili, G., Henneberger, C., Bukalo, O., Dvoretzkova, E., Senkov, O., Lievens, P.M.J., Westenbroek, R., Engel, A.K., Catterall, W.A., Rusakov, D.A., Schachner, M., Dityatev, A., 2010a. The Extracellular Matrix Molecule Hyaluronic Acid Regulates Hippocampal Synaptic Plasticity by Modulating Postsynaptic L-Type Ca<sup>2+</sup> Channels. *Neuron* 67, 116-128.
86. Kochlamazashvili, G., Henneberger, C., Bukalo, O., Dvoretzkova, E., Senkov, O., Lievens, P.M.J., Westenbroek, R., Engel, A.K., Catterall, W.A., Rusakov, D.A., Schachner, M., Dityatev, A., 2010b. The Extracellular Matrix Molecule Hyaluronic Acid Regulates Hippocampal Synaptic Plasticity by Modulating Postsynaptic L-Type Ca(2+) Channels. *Neuron* 67, 116-128.
87. Koppes, A.N., Keating, K.W., McGregor, A.L., Koppes, R.A., Kearns, K.R., Ziemba, A.M., McKay, C.A., Zuidema, J.M., Rivet, C.J., Gilbert, R.J., Thompson, D.M., Robust neurite extension following exogenous electrical stimulation within single walled carbon nanotube-composite hydrogels. *Acta Biomater.*



88. Koppes, A.N., Nordberg, A.L., Paolillo, G.M., Goodsell, N.M., Darwish, H.A., Zhang, L.X., Thompson, D.M., 2014a. Electrical Stimulation of Schwann Cells Promotes Sustained Increases in Neurite Outgrowth. *Tissue Eng. Part A* 20, 494-506.
89. Koppes, A.N., Seggio, A.M., Thompson, D.M., 2011. Neurite outgrowth is significantly increased by the simultaneous presentation of Schwann cells and moderate exogenous electric fields. *Journal of neural engineering* 8, 13.
90. Koppes, A.N., Zaccor, N.W., Rivet, C.J., Williams, L.A., Piselli, J.M., Gilbert, R.J., Thompson, D.M., 2014b. Neurite outgrowth on electrospun PLLA fibers is enhanced by exogenous electrical stimulation. *Journal of neural engineering* 11.
91. Koppes, A.N., Zaccor, N.W., Rivet, C.J., Williams, L.A., Piselli, J.M., Gilbert, R.J., Thompson, D.M., 2014c. Neurite outgrowth on electrospun PLLA fibers is enhanced by exogenous electrical stimulation. *Journal of neural engineering* 11, 1-11.
92. Kotwal, A., Schmidt, C.E., 2001. Electrical stimulation alters protein adsorption and nerve cell interactions with electrically conducting biomaterials. *Biomaterials* 22, 1055-1064.
93. Lee, J.Y., 2013. Electrically Conducting Polymer-Based Nanofibrous Scaffolds for Tissue Engineering Applications. *Polym Rev* 53, 443-459.
94. Lee, J.Y., Lee, J.W., Schmidt, C.E., 2009. Neuroactive conducting scaffolds: nerve growth factor conjugation on active ester-functionalized polypyrrole. *Journal of the Royal Society Interface* 6, 801-810.
95. Li, R.J., Liu, Z.G., Pan, Y.M., Chen, L., Zhang, Z.X., Lu, L.J., 2014. Peripheral Nerve Injuries Treatment: a Systematic Review. *Cell Biochemistry and Biophysics* 68, 449-454.
96. Li, X., Macewan, M.R., Xie, J.D., Siewe, D., Yuan, X., Xia, Y., 2010. Fabrication of Density Gradients of Biodegradable Polymer Microparticles and Their Use in Guiding Neurite Outgrowth. *Adv Funct Mater* 20, 1632-1637.

97. Lin, D.C., 2008. Nanomechanics of polymer gels and biological tissues: A critical review of analytical approaches in the Hertzian regime and beyond. *Soft matter* 4.
98. Liu, G., Ling, Q.D., Teo, E.Y., Zhu, C.X., Chan, D.S., Neoh, K.G., Kang, E.T., 2009. Electrical Conductance Tuning and Bistable Switching in Poly(N-vinylcarbazole)-Carbon Nanotube Composite Films. *ACS Nano* 3, 1929-1937.
99. Liu, X., Yue, Z.L., Higgins, M.J., Wallace, G.G., 2011. Conducting polymers with immobilised fibrillar collagen for enhanced neural interfacing. *Biomaterials* 32, 7309-7317.
100. Luo, B.E., Huang, J.H., Lu, L., Hu, X.Y., Luo, Z.J., Li, M., 2014. Electrically induced brain-derived neurotrophic factor release from schwann cells. *J. Neurosci. Res.* 92, 893-903.
101. Luo, Y.-L., Xu, F., Feng, Q.-S., Chen, Y.-S., Ma, C., 2010. Preparation and characterization of PMAA/MWCNTs nanohybrid hydrogels with improved mechanical properties. *Journal of biomedical materials research. Part B, Applied biomaterials* 92, 243-254.
102. Lynam, C., Grosse, W., Wallace, G.G., 2009. Carbon-Nanotube Biofiber Microelectrodes. *J Electrochem Soc* 156, P117-P121.
103. Maksymiuk, K., 2006. Chemical reactivity of polypyrrole and its relevance to polypyrrole based electrochemical sensors. *Electroanal* 18, 1537-1551.
104. Marklein, R.A., Burdick, J.A., 2010. Controlling Stem Cell Fate with Material Design. *Adv Mater* 22, 175-189.
105. Martin, J.H., McGraw-Hill Professional eBook Library - Medical: Primary, C., 2012. *Neuroanatomy: text and atlas*, 4th ed. McGraw-Hill, New York.
106. Mathie, A., Kennard, L.E., Veale, E.L., 2003. Neuronal ion channels and their sensitivity to extremely low frequency weak electric field effects. *Radiation Protection Dosimetry* 106, 311-316.

107. McCaig, C.D., Rajniecek, A.M., Song, B., Zhao, M., 2002. Has electrical growth cone guidance found its potential? *Trends Neurosci* 25, 354-359.
108. McCaig, C.D., Rajniecek, A.M., Song, B., Zhao, M., 2005. Controlling Cell Behavior Electrically: Current Views and Future Potential. *Physiological Reviews* 85, 943-978.
109. Meng S, R.M., and Zhang Z, 2011. Applied Biomedical Engineering: Electrical Stimulation in Tissue Regeneration, in: Gargiulo, G. (Ed.). InTech.
110. Mire, C.A., Agrawal, A., Wallace, G.G., Calvert, P., 2011. Inkjet and extrusion printing of conducting poly (3, 4-ethylenedioxythiophene) tracks on and embedded in biopolymer materials. *J. Mater. Chem.* 21, 2671-2678.
111. Miri, A., Nieto, D., Iglesias, L., Goodarzi, H.H., Maharjan, S., Ruiz-Esparza, G.U., Khoshakhlagh, P., Manbachi, A., Dokmeci, M.R., Chen, S., Shin, S.R., Zhang, Y.S., Khademhosseini, A., Microfluidics-Enabled Multimaterial Maskless Stereolithographic Bioprinting. *Adv Mater* 0, 1800242.
112. Mokarram, N., Dymanus, K., Srinivasan, A., Lyon, J.G., Tipton, J., Chu, J., English, A.W., Bellamkonda, R.V., 2017. Immunoengineering nerve repair. *Proceedings of the National Academy of Sciences*.
113. Mow, V.C., Gibbs, M.C., Lai, W.M., Zhu, W.B., Athanasiou, K.A., 1989. BIPHASIC INDENTATION OF ARTICULAR-CARTILAGE .2. A NUMERICAL ALGORITHM AND AN EXPERIMENTAL-STUDY. *Journal of Biomechanics* 22, 853-861.
114. Mukhatyar, V., Tissue Engineering Strategies Designed to Realize the Endogenous Regenerative Potential of Peripheral Nerves. *Advanced materials (Weinheim)* 21, NA-NA.
115. Neubauer, D., Graham, J.B., Muir, D., 2010. Nerve grafts with various sensory and motor fiber compositions are equally effective for the repair of a mixed nerve defect. *Experimental Neurology* 223, 203-206.

116. Onuma, E.K., Hui, S.W., 1988. Electric field-directed cell shape changes, displacement, and cytoskeletal reorganization are calcium dependent. *The Journal of Cell Biology* 106, 2067-2075.
117. Ouasti, S., Donno, R., Cellesi, F., Sherratt, M.J., Terenghi, G., Tirelli, N., 2011. Network connectivity, mechanical properties and cell adhesion for hyaluronic acid/PEG hydrogels. *Biomaterials* 32, 6456-6470.
118. Oyen, M.L., Cook, R.F., 2009. A practical guide for analysis of nanoindentation data. *J. Mech. Behav. Biomed. Mater.* 2, 396-407.
119. Park, S.Y., Park, J., Sim, S.H., Sung, M.G., Kim, K.S., Hong, B.H., Hong, S., 2011. Enhanced differentiation of human neural stem cells into neurons on graphene. *Adv Mater* 23, H263-H267.
120. Patel, N., Poo, M.M., 1982. Orientation of Neurite Growth by Extracellular Electric-Fields. *Journal of Neuroscience* 2, 483-496.
121. Patel, S., Kurpinski, K., Quigley, R., Gao, H.F., Hsiao, B.S., Poo, M.M., Li, S., 2007. Bioactive nanofibers: Synergistic effects of nanotopography and chemical signaling on cell guidance. *Nano Lett.* 7, 2122-2128.
122. Peppas, N.A., Bures, P., Leobandung, W., Ichikawa, H., 2000. Hydrogels in pharmaceutical formulations. *European Journal of Pharmaceutics and Biopharmaceutics* 50, 27-46.
123. Petroski, H., 1992. *To Engineer Is Human: The Role of Failure in Successful Design*. New York: Vintage Books.
124. Pires, F., Ferreira, Q., Rodrigues, C.A.V., Morgado, J., Ferreira, F.C., 2015. Neural stem cell differentiation by electrical stimulation using a cross-linked PEDOT substrate: Expanding the use of biocompatible conjugated conductive polymers for neural tissue engineering. *Biochimica Et Biophysica Acta-General Subjects* 1850, 1158-1168.

125. Prestwich, G.D., Marecak, D.M., Marecek, J.F., Vercruyssen, K.P., Ziebell, M.R., 1998. Controlled chemical modification of hyaluronic acid: synthesis, applications, and biodegradation of hydrazide derivatives. *Journal of controlled release : official journal of the Controlled Release Society* 53, 93-103.
126. Quigley, A.F., Razal, J.M., Thompson, B.C., Moulton, S.E., Kita, M., Kennedy, E.L., Clark, G.M., Wallace, G.G., Kapsa, R.M.I., 2009. A Conducting-Polymer Platform with Biodegradable Fibers for Stimulation and Guidance of Axonal Growth. *Adv Mater* 21, 4393-+.
127. Razal, J.M., 2008. Carbon Nanotube Biofiber Formation in a Polymer-Free Coagulation Bath. *Adv. Funct. Mater.* 18, 61-66.
128. Richardson-Burns, S.M., Hendricks, J.L., Martin, D.C., 2007. Electrochemical polymerization of conducting polymers in living neural tissue. *Journal of neural engineering* 4, L6.
129. Rodriguez, L.L., Schneider, I.C., 2013. Directed cell migration in multi-cue environments. *Integr. Biol.* 5, 1306-1323.
130. Royo-Gascon, N., Winger, M., Scheinbeim, J., Firestein, B., Craelius, W., 2013. Piezoelectric Substrates Promote Neurite Growth in Rat Spinal Cord Neurons. *Ann Biomed Eng* 41, 112-122.
131. Rutka, J.T., Apodaca, Gerard, Stern, Robert, Rosenblum, Mark, 1988. The extracellular matrix of the central and peripheral nervous systems: structure and function. *Journal of neurosurgery* 69, 155-170.
132. Schizas, N., Rojas, R., Kotala, S., Andersson, B., Pettersson, J., Hilborn, J., Hailer, N.P., 2014. Hyaluronic acid-based hydrogel enhances neuronal survival in spinal cord slice cultures from postnatal mice. *Journal of Biomaterials Applications* 28, 825-836.
133. Schmidt, C.E., Shastri, V.R., Vacanti, J.P., Langer, R., 1997. Stimulation of neurite outgrowth using an electrically conducting polymer. *Proceedings of the National Academy of Sciences of the United States of America* 94, 8948-8953.

134. Schnell, E., Klinkhammer, K., Balzer, S., Brook, G., Klee, D., Dalton, P., Mey, J., 2007. Guidance of glial cell migration and axonal growth on electrospun nanofibers of poly-epsilon-caprolactone and a collagen/poly-epsilon-caprolactone blend. *Biomaterials* 28, 3012-3025.
135. Sebastian, R., Lund, F., Javier, B., Humberto, P., 2018. About the relevance of waviness, agglomeration, and strain on the electrical behavior of polymer composites filled with carbon nanotubes evaluated by a Monte-Carlo simulation. *Materials Research Express*.
136. Seggio, A.M., Ellison, K.S., Hynd, M.R., Shain, W., Thompson, D.M., 2008. Cryopreservation of transfected primary dorsal root ganglia neurons. *J Neurosci Meth* 173, 67-73.
137. Seidlits, S.K., Khaing, Z.Z., Petersen, R.R., Nickels, J.D., Vanscoy, J.E., Shear, J.B., Schmidt, C.E., 2010. The effects of hyaluronic acid hydrogels with tunable mechanical properties on neural progenitor cell differentiation. *Biomaterials* 31, 3930-3940.
138. Seil, J.T., Webster, T.J., 2010. Electrically active nanomaterials as improved neural tissue regeneration scaffolds. *Wiley Interdiscip. Rev.-Nanomed. Nanobiotechnol.* 2, 635-647.
139. Serrano, M.C., Gutiérrez, M.C., del Monte, F., 2014. Role of polymers in the design of 3D carbon nanotube-based scaffolds for biomedical applications. *Progress in Polymer Science* 39, 1448-1471.
140. Shapiro, S., 2014. A Review of Oscillating Field Stimulation to Treat Human Spinal Cord Injury. *World Neurosurgery* 81, 830-835.
141. Shapiro, S., Borgens, R., Pascuzzi, R., Roos, K., Groff, M., Purvines, S., Ben Rodgers, R., Hagy, S., Nelson, P., 2005. Oscillating field stimulation for complete spinal cord injury in humans: a Phase 1 trial. *J Neurosurg-Spine* 2, 3-10.

142. Sharp, J., Bouazza-Marouf, K., Noronha, D., Gaur, A., 2017. Tissue type determination by impedance measurement: A bipolar and monopolar comparison. *Saudi Journal of Anaesthesia* 11, 15-20.
143. Shi, G., Rouabhia, M., Meng, S., Zhang, Z., 2008. Electrical stimulation enhances viability of human cutaneous fibroblasts on conductive biodegradable substrates. *Journal of Biomedical Materials Research Part A* 84, 1026-1037.
144. Shin, J., Choi, E.J., Cho, J.H., Cho, A.-N., Jin, Y., Yang, K., Song, C., Cho, S.-W., 2017. Three-Dimensional Electroconductive Hyaluronic Acid Hydrogels Incorporated with Carbon Nanotubes and Polypyrrole by Catechol-Mediated Dispersion Enhance Neurogenesis of Human Neural Stem Cells. *Biomacromolecules* 18, 3060-3072.
145. Smeds, K.A., Grinstaff, M.W., 2001. Photocrosslinkable polysaccharides for in situ hydrogel formation. *Journal of Biomedical Materials Research* 54, 115-121.
146. Song, M., Uhrich, K.E., 2007. Optimal micropattern dimensions enhance neurite outgrowth rates, lengths, and orientations. *Ann Biomed Eng* 35, 1812-1820.
147. Song, Q., Jiang, Z.Y., Li, N., Liu, P., Liu, L.W., Tang, M.L., Cheng, G.S., 2014. Anti-inflammatory effects of three-dimensional graphene foams cultured with microglial cells. *Biomaterials* 35, 6930-6940.
148. Spearman, B.S., Desai, V.H., Mobini, S., McDermott, M.D., Graham, J.B., Otto, K.J., Judy, J.W., Schmidt, C.E., 2017. Tissue-Engineered Peripheral Nerve Interfaces. *Adv. Funct. Mater.*, 1701713-n/a.
149. Steel, E.M., Sundararaghavan, H.G., 2016. Electrically Conductive Materials for Nerve Regeneration, in: Zhang, L.G., Kaplan, D.L. (Eds.), *Neural Engineering: From Advanced Biomaterials to 3D Fabrication Techniques*. Springer International Publishing, Cham, pp. 145-179.
150. Sundararaghavan, H.G., Burdick, J.A., 2011. Gradients with Depth in Electrospun Fibrous Scaffolds for Directed Cell Behavior. *Biomacromolecules* 12, 2344-2350.

151. Sung, J.H., Kim, H.S., Jin, H.J., Choi, H.J., Chin, I.J., 2004. Nanofibrous membranes prepared by multiwalled carbon nanotube/poly(methyl methacrylate) composites. *Macromolecules* 37, 9899-9902.
152. Suri, S., Schmidt, C.E., 2010. Cell-Laden Hydrogel Constructs of Hyaluronic Acid, Collagen, and Laminin for Neural Tissue Engineering. *Tissue Eng. Part A* 16, 1703-1716.
153. Thompson, B.C., Moulton, S.E., Gilmore, K.J., Higgins, M.J., Whitten, P.G., Wallace, G.G., 2009. Carbon nanotube biogels. *Carbon* 47, 1282-1291.
154. Thompson, D.M., Koppes, A.N., Hardy, J.G., Schmidt, C.E., 2014. Electrical Stimuli in the Central Nervous System Microenvironment. *Annual Review of Biomedical Engineering*, Vol 16 16, 397-430.
155. Tyler, S.E.B., 2017. Nature's Electric Potential: A Systematic Review of the Role of Bioelectricity in Wound Healing and Regenerative Processes in Animals, Humans, and Plants. *Frontiers in Physiology* 8.
156. Valipour, A., Moghaddam, P.N., Mammedov, B.A., 2012. Some aspects of chemical procedures & application trends of polyaniline as an intrinsically conductive polymer. *Life Sci. J.* 9, 409-421.
157. Varma, A.K., Das, A., Wallace, G., Barry, J., Vertegel, A.A., Ray, S.K., Banik, N.L., 2013. Spinal Cord Injury: A Review of Current Therapy, Future Treatments, and Basic Science Frontiers. *Neurochemical research* 38, 895-905.
158. Vivo, M., Puigdemasa, A., Casals, L., Asensio, E., Udina, E., Navarro, X., 2008. Immediate electrical stimulation enhances regeneration and reinnervation and modulates spinal plastic changes after sciatic nerve injury and repair. *Experimental Neurology* 211, 180-193.
159. Wallace, J., Erickson, B., Les, C., Orr, B., Banaszak Holl, M.M., 2010. Distribution of type I collagen morphologies in bone: relation to estrogen depletion. *Bone* 46, 1349-1354.



160. Wang, K., Fishman, H.A., Dai, H., Harris, J.S., 2006. Neural Stimulation with a Carbon Nanotube Microelectrode Array. *Nano Lett.* 6, 2043-2048.
161. Wang, S., 2009. Characterization of rhythmic Ca<sup>2+</sup> transients in early embryonic chick motoneurons: Ca<sup>2+</sup> sources and effects of altered activation of transmitter receptors. *The Journal of neuroscience* 29, 15232-15244.
162. Wang, Y., Ural, A., 2018. Mineralized collagen fibril network spatial arrangement influences cortical bone fracture behavior. *Journal of Biomechanics* 66, 70-77.
163. Weng, B., Liu, X., Shepherd, R., Wallace, G.G., 2012. Inkjet printed polypyrrole/collagen scaffold: A combination of spatial control and electrical stimulation of PC12 cells. *Synth. Met.* 162, 1375-1380.
164. Wenjin, W.J., Liu, W.C., Zhu, H., Li, F., Wo, Y., Shi, W.D., Fan, X.Q., Ding, W.L., 2011. Electrical Stimulation Promotes BDNF Expression in Spinal Cord Neurons Through Ca<sup>2+</sup>- and Erk-Dependent Signaling Pathways. *Cell. Mol. Neurobiol.* 31, 459-467.
165. Whitehead, T.J., 2017. An Enhanced Nerve Conduit Combined With Exercise To Improve Functional Recovery After Peripheral Nerve Injury. Dissertation, Wayne State University, Detroit, Michigan.
166. Whitehead, T.J., Avila, C.O.C., Sundararaghavan, H.G., 2018. Combining growth factor releasing microspheres within aligned nanofibers enhances neurite outgrowth. *Journal of Biomedical Materials Research Part A* 106, 17-25.
167. Wrobel M, S.H., 2013. Directed Migration in Neural Tissue Engineering. *Tissue Engineering: Part B*.
168. Wrobel, M.R., 2017. Biomaterials Approaches For Utilizing The Regenerative Potential Of The Peripheral Nerve Injury Microenvironment. Dissertation, Wayne State University, Detroit, Michigan.

169. Wrobel, M.R., Sundararaghavan, H.G., 2014. Directed Migration in Neural Tissue Engineering. *Tissue Engineering Part B-Reviews* 20, 93-105.
170. Wu, Y., Wang, L., Guo, B., Ma, P.X., 2017. Interwoven Aligned Conductive Nanofiber Yarn/Hydrogel Composite Scaffolds for Engineered 3D Cardiac Anisotropy. *ACS Nano* 11, 5646-5659.
171. Xia, R., Berger, F., Piallat, B., Benabid, A.L., 2007. Alteration of hormone and neurotransmitter production in cultured cells by high and low frequency electrical stimulation. *Acta Neurochir.* 149, 67-73.
172. Xie, J.W., MacEwan, M.R., Li, X.R., Sakiyama-Elbert, S.E., Xia, Y.N., 2009a. Neurite Outgrowth on Nanofiber Scaffolds with Different Orders, Structures, and Surface Properties. *Acs Nano* 3, 1151-1159.
173. Xie, J.W., MacEwan, M.R., Willerth, S.M., Li, X.R., Moran, D.W., Sakiyama-Elbert, S.E., Xia, Y.N., 2009b. Conductive Core-Sheath Nanofibers and Their Potential Application in Neural Tissue Engineering. *Adv. Funct. Mater.* 19, 2312-2318.
174. Yi, W., Chaoyang, C., Zhaoying, F., Yong, X., Chengpeng, Z., Nirul, M., John, C., Mark Ming-Cheng, C., 2015. A flexible and implantable microelectrode arrays using high-temperature grown vertical carbon nanotubes and a biocompatible polymer substrate. *Nanotechnology* 26, 125301.
175. Yu, W.W., Jiang, X.Q., Cai, M., Zhao, W., Ye, D.X., Zhou, Y., Zhu, C., Zhang, X.L., Lu, X.F., Zhang, Z.Y., 2014. A novel electrospun nerve conduit enhanced by carbon nanotubes for peripheral nerve regeneration. *Nanotechnology* 25.
176. Zhang, H.L., 2011. Effects of electrospinning parameters on morphology and diameter of electrospun PLGA/MWNTs fibers and cytocompatibility in vitro. *J. Bioact. Compat. Polym.* 26, 590-606.
177. Zhang, X., Chen, Y., Wang, C., Huang, L.-Y.M., 2007a. Neuronal somatic ATP release triggers neuron-satellite glial cell communication in dorsal root ganglia. *Proceedings of the National Academy of Sciences* 104, 9864-9869.

178. Zhang, Z., Rouabhia, M., Wang, Z.X., Roberge, C., Shi, G.X., Roche, P., Li, J.M., Dao, L.H., 2007b. Electrically conductive biodegradable polymer composite for nerve regeneration: Electricity-stimulated neurite outgrowth and axon regeneration. *Artif Organs* 31, 13-22.
179. Zheng, F., Zhou, X., Luo, Y., Xiao, H., Wayman, G., Wang, H., 2011. Regulation of Brain-Derived Neurotrophic Factor Exon IV Transcription through Calcium Responsive Elements in Cortical Neurons. *PLoS ONE* 6, e28441.

**ABSTRACT****ENGINEERING HYALURONIC ACID-CARBON NANOTUBE NANOFIBERS:  
A PERIPHERAL NERVE INTERFACE TO ELECTRICALLY STIMULATE REGENERATION**

by

**ELISABETH MARIE STEEL****August 2018****Advisor:** Dr. Harini G. Sundararaghavan**Major:** Biomedical Engineering**Degree:** Doctor of Philosophy

Traumatic peripheral nerve injuries affect 50,000 patients annually with USD 7 billion in healthcare costs. Current treatments like the gold standard autograft and commercially available nerve guide conduits (NGC) are insufficient to repair long gap peripheral nerve injuries. Autografts have a severe size mismatch limitation resulting in incomplete functional recovery further confounded by harvest site co-morbidities. NGCs can aid recovery but lack key microenvironment cues that promote nerve regeneration over long gap injuries. We hypothesized that providing topographical, mechanical, and electrical guidance cues into a nanofibrous composite biopolymer would result in improve neuron growth metrics in an *in vitro* model. We embedded hydrophilic carbon nanotubes (CNT) within hyaluronic acid (HA) nanofibers by electrospinning. The aims of this study were (1) to define the topographical, nanomechanical, and electrochemical material properties of HA-CNT nanofibers and (2) to determine the electrical stimulus parameters required to elicit increased neurite outgrowth on our nanofibrous scaffold.

HA-CNT topography was visualized as smooth nanofibers, nanoscale in diameter, with CNTs contained within the nanofiber core, as characterized by scanning electron microscopy and tunneling electron microscopy. Mechanical properties were evaluated under physiological conditions by hydrating nanofibers to equilibrium, then testing samples fully immersed in electrolyte buffer. A reduced elastic modulus was obtained by fitting

quantitative nanomechanical mapping data to the Sneddon model using atomic force microscopy imaging in fluid. Local modulus was measured to The electrochemical characterization performed was electrical impedance spectroscopy (EIS) and cyclic voltammetry (CV). EIS resulted in a decreased resistance to current flow by a factor of 1.7 at 20 Hz and 1.2 at 1kHz. CV revealed a 2.1-fold increase in specific capacitance ( $\text{mF}/\text{cm}^2$ ) of HA-CNT relative to HA nanofibers.

Chick dorsal root ganglia neurons grown on HA or HA-CNT substrates for 24h were either unstimulated or stimulated at 20Hz for 30min or 60min using a bi-phasic 150, 200, or 250mV/mm square wave. Significant effects of fiber type and stimulus amplitude and time were observed when measuring neuron viability and neuron outgrowth after 72 h. Neuron outgrowth was significantly longer on HA-CNT substrates electrically stimulated for 60min at all stimulus amplitudes versus all other groups ( $p < 0.01$  3-Way ANOVA,  $\alpha$ ). This study demonstrates the potential of combining electrical stimulation with material based repair strategies for neural regeneration. Further, the results contribute to defining the electrical stimulus parameters necessary for regeneration in the peripheral nerve environment. Incorporating well-dispersed hydrophilic CNTs in HA nanofibers significantly enhances neural regeneration following electrical stimulation. Future work encompasses characterizing glial responses to electrical stimulation including electrophysiological calcium imaging assays to elucidate the governing molecular mechanisms for both neuronal and glial behavior.

## AUTOBIOGRAPHICAL STATEMENT

**Elisabeth M. Steel**

### **EDUCATION**

---

**Wayne State University**, Detroit, Michigan

2018 PhD, Biomedical Engineering

2013 Master of Science, Biomedical Engineering

**The University of Toledo**, Toledo, Ohio

2007 Bachelor of Science, Bioengineering

### **SELECTED PUBLICATIONS AND CONFERENCE PROCEEDINGS**

---

1. M. DeNies, L.K. Rosselli-Murai, V.L. Murray, **E.M. Steel**, A.P. Liu. (2018). Proximity Biotinylation for Studying G Protein-Coupled Receptor Dimerization. Receptor-Receptor Interactions in the Central Nervous System. K. Fuxe and D. O. Borroto-Escuela. New York, NY, Springer New York: 251-263.
2. **Steel EM**, Sundararaghavan HG. "Electrically Conductive Materials." Neural Engineering: from Advanced Biomaterials to 3D Fabrication Techniques. Ed: Zhang LG, Kaplan D. Springer. 2016.
3. **Steel EM**, Murray VL, Liu AP (2014). Multiplex Detection of Homo- and Heterodimerization of G Protein-Coupled Receptors by Proximity Biotinylation. PLoS ONE 9(4):e93646. doi:10.1371/journal.pone.0093646.
4. **Steel EM**, Sundararaghavan HG. "Directing Cell Behavior through Conductive CNT Hyaluronic Acid Composite Nanofibers." 10<sup>th</sup> World Biomaterials Congress. New Frontiers Symposium: *Bioelectrical field: From petri dish to tissue regeneration*. May 22, 2016. Montreal, Quebec, Canada. (podium)
5. **Steel EM**, Pechey CL, Ruehlman, D, MacLeay JM, Turner AS, Fyhrie DP, Yeni Y, Les CM. The Relationship Between Material Stiffness and Fracture Toughness in Ovine Compact Bone at High Displacement Rates is Lost with OVX and is Rescued with Estrogen Replacement. 2012 58<sup>th</sup> Annual Meeting of the Orthopaedic Research Society.
6. Pechey CL, **Michels EM**, Fang M, MacLeay JM, Turner AS, Banaszak-Holl M, **Les CM**. Histologic and Mineralization Correlates of Estrogen Depletion-related Changes in Ovine Bone Collagen I D-spacing. 2011 57<sup>th</sup> Annual Meeting of the Orthopaedic Research Society. (Podium)
7. Jayasuriya AC, **Michels EM**, Ebraheim NA. Demineralized Bone Matrix Incorporated PLGA Matrices. Proceedings of ASME International Mechanical Engineering Congress and Exposition 2006. (Technical Publication, Podium)

### **HONORS AND DISTINCTIONS**

---

- Wayne State University 3 Minute Thesis Winner, 2018
- College of Engineering 3 Minute Thesis Winner, 2017
- Graduate Research Assistantship (2017-2018)
- Graduate Teaching Assistantship (2016-2017, 2015-2016, 2013-2014)
- Graduate Student Professional Travel Award, 2014, 2016, 2018
- Wayne State University Graduate School Summer Dissertation Fellowship, 2016
- Rumble Fellowship, Wayne State University, 2014-2015

### **SPECIALTY TRAINING**

---

TESCAN: GAIA Focused Ion Beam/SEM for ion lithography, Detroit, MI, 2014

Center for human Embryonic Stem Cell Research: Culture Techniques, Ann Arbor, MI, 2013

Invitrogen: Attune Acoustic Focusing Flow Cytometer, Ann Arbor, MI 2013

Licor: Odyssey quantitative traditional and on-cell western blotting, Ann Arbor, MI, 2012

Bruker: Atomic Force Microscopy Biological Applications, Santa Barbara, CA, 2010

Instron: Mechanical Testing 8800 W/MMI Operator's Course, Norwood, MA, 2008